

# POLITECNICO DI TORINO

CORSO DI LAUREA MAGISTRALE IN INGEGNERIA MECCANICA (MECHANICAL ENGINEERING)

## Master degree Thesis



**Politecnico  
di Torino**

## Filtration performance of innovative fibrous media

**Supervisor**

Prof. Paolo Tronville

**Candidate**

Yu Xiao

A.A 2023-2024



<b>1. ABSTRACT</b> .....	<b>3</b> -
<b>ACKNOWLEDGEMENT</b> .....	<b>4</b> -
<b>2.INTRODUCTION</b> .....	<b>5</b> -
2.1 FILTRATION PERFORMANCE TESTING .....	7 -
2.11 <i>Test standards and measurement</i> .....	7 -
2.12 <i>Equivalent size and particle sensing instruments</i> .....	8 -
2.2 FILTRATION PERFORMANCE OF FIBROUS MEDIA .....	11 -
2.21 <i>Electrostatic fibrous media</i> .....	11 -
2.22 <i>Depth filtration and surface filtration</i> .....	11 -
2.23 <i>Energy cost of air filters</i> .....	12 -
2.24 <i>Electrospun nanofibers</i> .....	13 -
2.3 AIM OF WORK .....	14 -
2.4 LITERATURE REVIEW .....	17 -
2.41 <i>Particle capture and removal efficiency</i> .....	17 -
2.42 <i>Particle loading</i> .....	20 -
<b>3. METHODOLOGY</b> .....	<b>21</b> -
3.1 TEST RIG CHARACTERIZATION .....	21 -
3.11 <i>Sample preparation</i> .....	22 -
3.12 <i>Main components and control</i> .....	24 -
3.2 AIR RESISTANCE TEST .....	26 -
3.21 <i>Calibration of Test rig with TEXTEST</i> .....	28 -
3.22 <i>Permeability of mosquito net</i> .....	30 -
3.3 PARTICLE REMOVAL EFFICIENCY TEST .....	31 -
3.31 <i>Optical particle sizer and spectrometer</i> .....	33 -
3.32 <i>Aerosol generation system</i> .....	35 -
3.33 <i>Aerosol sampling system</i> .....	36 -
3.34 <i>Test procedures</i> .....	38 -
3.4 PARTICLE LOADING TEST .....	42 -
3.41 <i>Working principle of 8130A</i> .....	43 -
3.42 <i>Relative Humidity during tests</i> .....	45 -
3.43 <i>Scanning Mobility Particle Sizer</i> .....	47 -
3.44 <i>Test media and filtration velocity</i> .....	51 -
3.45 <i>Test procedure</i> .....	53 -
3.46 <i>Penetration test results</i> .....	54 -
3.47 <i>Gravimetric test results</i> .....	56 -
3.48 <i>Particle size distribution</i> .....	58 -
3.5 CHARACTERIZATION OF TEST RIG FOR RH CONTROL .....	60 -
3.51 <i>Description of test rig</i> .....	62 -
3.52 <i>Atomizer</i> .....	67 -
3.53 <i>Neutralizer EAN 581</i> .....	69 -
3.54 <i>Operating parameters of neutralization</i> .....	71 -
3.55 <i>Tested fibrous flat sheet media</i> .....	72 -



<b>4. RESULTS AND DISCUSSION</b>	<b>- 73 -</b>
4.1 PRESSURE DROP OF NANOFIBER MEDIA	73 -
4.11 <i>Test results</i>	73 -
4.12 <i>Discussion</i>	76 -
4.13 <i>Theoretical model</i>	77 -
4.2 PARTICLE REMOVAL EFFICIENCY	80 -
4.21 <i>OPS3330</i>	80 -
4.22 <i>LAS3340A vs OPS3330</i>	84 -
4.23 <i>MPPS and minimum efficiency</i>	90 -
4.24 <i>Discussion</i>	93 -
4.3 LOADING TEST	94 -
4.31 <i>Loading curve</i>	95 -
4.32 <i>Linear regression of surface loading</i>	97 -
4.33 <i>Comparison of two media</i>	98 -
4.4 FILTER MEDIA TESTED WITH RH CONTROLLED	101 -
4.41 <i>Characterization of clean Ahlstrom media</i>	101 -
4.42 <i>Parameter tuning for neutralization</i>	102 -
<b>5. CONCLUSION</b>	<b>- 104 -</b>
<b>REFERENCES</b>	<b>- 106 -</b>



# 1. Abstract

Air filtration using fibrous air filter is common solution used in (Heating Ventilation Air conditioning) HVAC systems for reducing particle matter contamination inside building. Indoor environment with strictly particle control at different levels is required by diverse applications. Filtration performance of air filters is characterizing factors for usages, it includes air resistance, particle removal efficiency, and service life, regarding respectively energetic and economic perspective, functionality, and life cycle. The filtration performance of air filters can be tested on product level, or on material level as flat sheet fibrous filter media. Latter is concerned as main purpose of this study.

Ideally high efficiency and low air resistance are expected for better quality of fibrous filter media. Filtration performance of fibrous filter media can be improved by optimizing filtration characteristics of fibers, which includes fiber size, solid volume fraction, thickness, and charges. Electrospinning technology allows to produce fiber in nanometer scale. Theoretically finer fibers lead to higher air resistance by taking advantages of higher particle removal efficiency at finer particle size range. Increasing of pressure drop can be compensated by slip effect as fiber diameters approaching mean free path of air molecules which provides better tradeoff between two aspects. Standardized experimental tests is effective way for investigate real behavior of such filter media, providing reliable results with good level of accuracy. Electrospun nanofiber media as PAN (Polyacrylonitrile), PANCO (Polyacrylonitrile + Caster oil), PAN15CNC (Polyacrylonitrile + Caster oil + Cellulose nanocrystals), PANCO15CNC (Polyacrylonitrile + Castor oil + Cellulose nanocrystals), PAN0.4CNF (Polyacrylonitrile + Cellulose nanofibrils) and PANCO0.4CNF (Polyacrylonitrile + Caster oil + Cellulose nanofibrils), are firstly tested on air resistance and efficiency of clean media. Air resistance of clean samples are tested at different filtration velocities, from 0.01m/s to 0.15m/s. Fractional particle removal efficiency at fixed filtration velocity 0.1m/s are then tested, using two types of optical particle counters which have different detecting range of particle size, 0.3 $\mu$ m to 10 $\mu$ m, and 90nm to 10  $\mu$ m respectively. Wider detecting range is essential for studying most penetrating particle size (MPPS) and minimum efficiency of nanofiber samples.

The second part is studying loading behavior of several types of filter media, using two types of test machine. One of them is standardized mask test machine TSI 8130A in comparison to another test rig with relative humidity and temperature control. Loading test enabling assessment of service life of fibrous filter media. First tests are performed on TSI 8130A, using neutralized ultrafine NaCl solid particles to charge filter media at fixed flow rate. Particle size distribution from aerosol generator is studied using scanning mobility particle sizer whose detecting range from 10nm to 1000nm. Relative humidity is monitored during tests as it impacts loading behavior of filter media. Second tests are performed on test rig with relative humidity control for the preliminary characterization of working status of machine components. Studies on aerosol atomizer and neutralizer are performed to find technical solutions for reliable result of loading test on the test rig.



## **Acknowledgement**

This project was carried out under the continuous guidance and encouragement of my tutor Prof. Paolo Tronville, to whom I would like to express my deepest gratitude, for enlightening me into field of aerosol science and technology by his lectures. Furthermore, he motivates me and gives me this unique opportunity for performing experimental study in laboratory as concluding work of master's degree.

Also, I own my thanks to all people who helped me during my study on this topic, especially to Ing. Emanuele Norata for giving me technical supports whenever I encounter difficulties, and for transferring me lots of practical knowledge regarding experimental procedure.

I'm very grateful to have had this unforgettable and interesting laboratory experience in my life.



## 2.Introduction

With development of industry, air pollution is now becoming serious problem that human must deal with. These pollutants can originate from natural sources, such as wildfires, volcanic eruptions, and biological processes, as well as human activities, including industrial processes, transportation, agriculture, and energy production. Among all kinds of pollutants, particulate matter, which consists of tiny solid or liquid particles suspended in the air. Those particles range vary in size, from few nanometers to millimeters, as classified in Figure 1, with fine particles (PM2.5) and coarse particles (PM10) being the most commonly measured, regarded as important indicators of air quality. Those particles pose serious risks to human health, especially ultrafine particles (PM0.1), due to large number present in ambient air, affecting respiratory function, cardiovascular health, and overall quality of life[1]. These outdoor PM2.5 can enter indoor environments by means of natural ventilation, infiltration, or mechanical ventilation.[2], [3] It is crucial to reduce indoor exposure to PM2.5, since people spend most of their time for indoor activities[4]. WHO (world health organization) has proposed guidelines for assessment air qualities and defining thresholds of concentration of PM2.5 and PM10. Current guidelines suggest that annual average concentration of indoor PM2.5 should not exceed  $5\mu\text{g}/\text{m}^3$ , while 24-hour average exposures should not exceed  $15\mu\text{g}/\text{m}^3$  more than 3-4 days per year.[5]

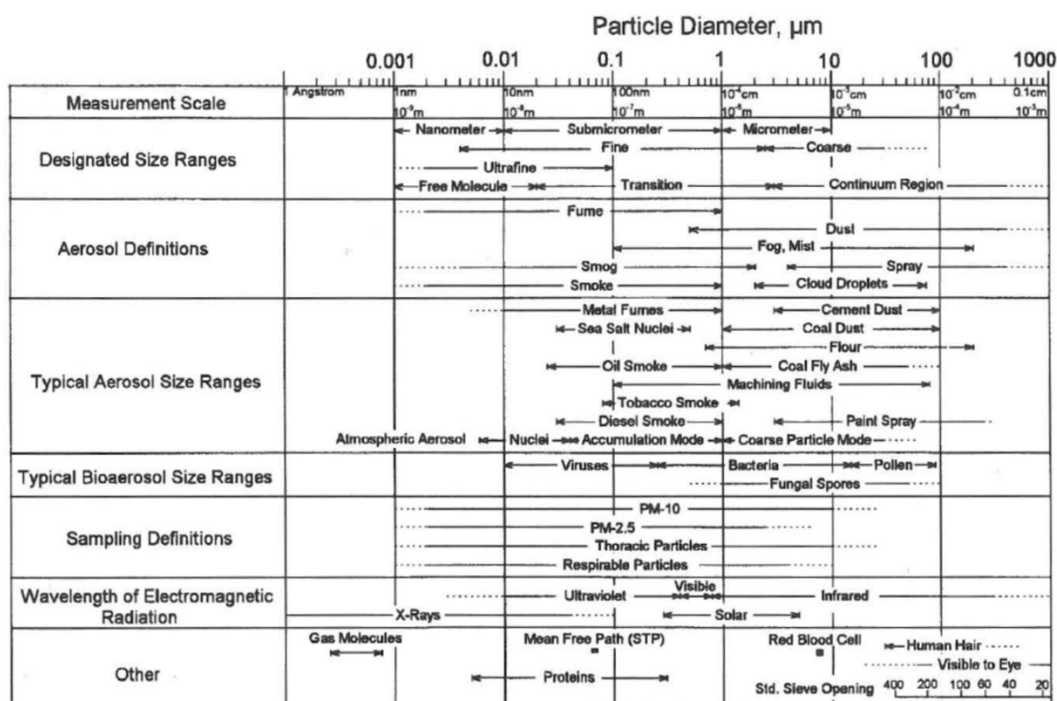


Figure 1 Particle size range of different substances[6]



To achieve good level of indoor air quality, air filtration plays crucial role in removing particles from environment, ensuring clean air for living and production, safeguarding public health and maintaining optimal operating conditions in manufacturing processes, those aspects are mainly concerned for developing well performed air filtration system while reducing energy consumption and costs. Fibrous air filters are commonly used among diverse range of air filtration technologies, for their ability to efficiently capture particles across a wide range of sizes, offering a cost-effective way for various applications, from HVAC systems (Heating, Ventilation and Air conditioning system) and automotive engines to medical devices and cleanroom environments etc. The filtration performances are key factors to categorize air filters into numerous fields of application.

From manufacturer's point of view, produce fibrous air filters with materials with reduced cost, while maintaining highest possible performance, is key point to make profits from market. As a common sense, there are always a tradeoff between one and another. So as the performances of fibrous filter media, higher capability in removing particles usually comes with higher air resistance, which have different implication for usage. An example is in ventilation systems, higher air resistance means reduced air flow rate. While maintaining constantly air flow rate to fulfill requirements of fresh air, more energy is providing by ventilators. Another example assessment of masks quality, thresholds is set by standards for both filtering ability and air resistance. Useful masks should, not only effectively block infectious agents, but also allow people to normally breath. Commonly, quality factor is defined as ratio between filtration capability to air resistance, used as indicator to compare different filter media considering both two aspects.

Another point about performance of filter media, is its life cycle as products. Particles collected by filters will clog media during usage, eventually increase pressure drop across filters. This is typically an issue for ventilation systems due to their long-time service. Firstly, higher energy consumption is induced by increasing pressure drop, accurate prediction of behavior of filters clogging is required for better energy modeling. Secondly costs of energy, maintenance, and disposal for assessing total cost of filters necessitate well estimation of life cycle of filters.

An application for reducing cost is that, in HVAC systems is installed HEPA (High Efficiency Particulate Air) filter along with a prefilter. Due to high initial cost of HEPA filter, a less efficient but cheaper air filter is positioned at upstream, to filter amount of particles before HEPA, thus protecting HEPA from rapid clogging. Clogged prefilter should be replaced to reduce overall energy consumption. This exemplifies that precisely knowing filtration performance of filters allowing better cost management and predictive maintenance.



## 2.1 Filtration performance testing

### 2.11 Test standards and measurement

As a matter of testing performance of air filter, standard test apparatus and procedures are defined according to their applications. Some common guidelines: ASHRAE (American Society of Heating, Refrigeration and Air-Conditioning Engineers) sets ASHRAE standard 52.2 specifying test methods for determining the efficiency of air filters and includes criteria for evaluating the pressure drop across the filters and includes criteria for evaluating the pressure drop across the filter, which is related to its permeability.[7] So as other standards, (International Organization for standardization) ISO 16890 provides guidelines for classification of air filters based on their efficiency in removing particulate matter from air.[8], [9] ISO 29463 series specifies test methods for determining the efficiency and pressure drop of high-efficiency air filters. ASTM (American Society for Testing and Materials) develops standards for materials and products, including air filters. ASTM D737 specifies test methods for measuring the air flow resistance of porous materials, which can be used to evaluate the permeability of air filter media. (European Norm) EN standards are developed by European Committee for Standardization (CEN) and provide guidelines for various products and materials. EN 779 and EN 1822 are standards for evaluating the performance of air filters including criteria for pressure drop and filtration efficiency. Industry-Specific Standard for certain industries such as automotive, aerospace, and healthcare, may have specific standards or requirements for air filtration systems. These standards may include criteria for permeability to ensure optimal performance and compliance with industry regulations. It's essential to consider these standards and guidelines to ensure that chosen material meet the required performance criteria for the specific application.

The pressure drop is measured by static pressure tap inside test duct, at upstream and downstream of test filter media. A differential pressure transducer or manometer is providing the reading directly. While for particle removal efficiency test, the results are provided measuring particle concentration upstream and downstream respectively and calculated by taking ratio of them.

As for particle removal efficiency, standardized methods of measuring particle concentration are fundamental to provide reliable results. Due to microscopic nature of particles, it is hard to give direct measurement of their physical sizes. Equivalent size of particles is introduced based on techniques of measuring.



## 2.12 Equivalent size and particle sensing instruments

An example is aerodynamic diameter of particles, such as PM<sub>2.5</sub>, PM<sub>10</sub>. As reference method indicated by US Federal Reference Method (FRM) 40 CFR[10], [11] particle numbers at different sizes can be directly measured in their mass collected by size selective impactor, by means of gravimetric test. And measured mass concentration is based on particle's aerodynamic properties when pass through each stage of impactors. The design of impactors is rigorously defined by standard for not altering the aerodynamic behavior of particles, thus guarantee the accuracy. An alternative is measuring particle sizes based on their optical properties, by correlating scattered light intensity to give information about size, defined as optical diameter. In this case measurement accuracy is influenced by chemical composition, reflection index and light source instead of aerodynamic behavior. Due to advantages such as cheaper devices and finer time resolution using optical sensors to measure particle concentration respect to reference method, optical measuring device is commonly adopted in laboratories for measuring filter media efficiency. To make results from optical measurements comparable with reference method, 40 CFR Part 53[12] defined procedure to calibrate optical reading against reference methodology through indirect measurement, including appliances and techniques. So that the users can regard the measurements equivalent to reference equipment the accuracy is within band of 25% from reference if periodic calibration is performed. The measurements using optical devices is defined as Federal Equivalent Method (FEM) in the standards.[13] Detecting range of optical counters and impactors, with other particle sensing devices as shown in Figure 3.



Figure 2 An example of optical particle counters TSI OPS3330 for size range 0.3-10 micrometers[14]

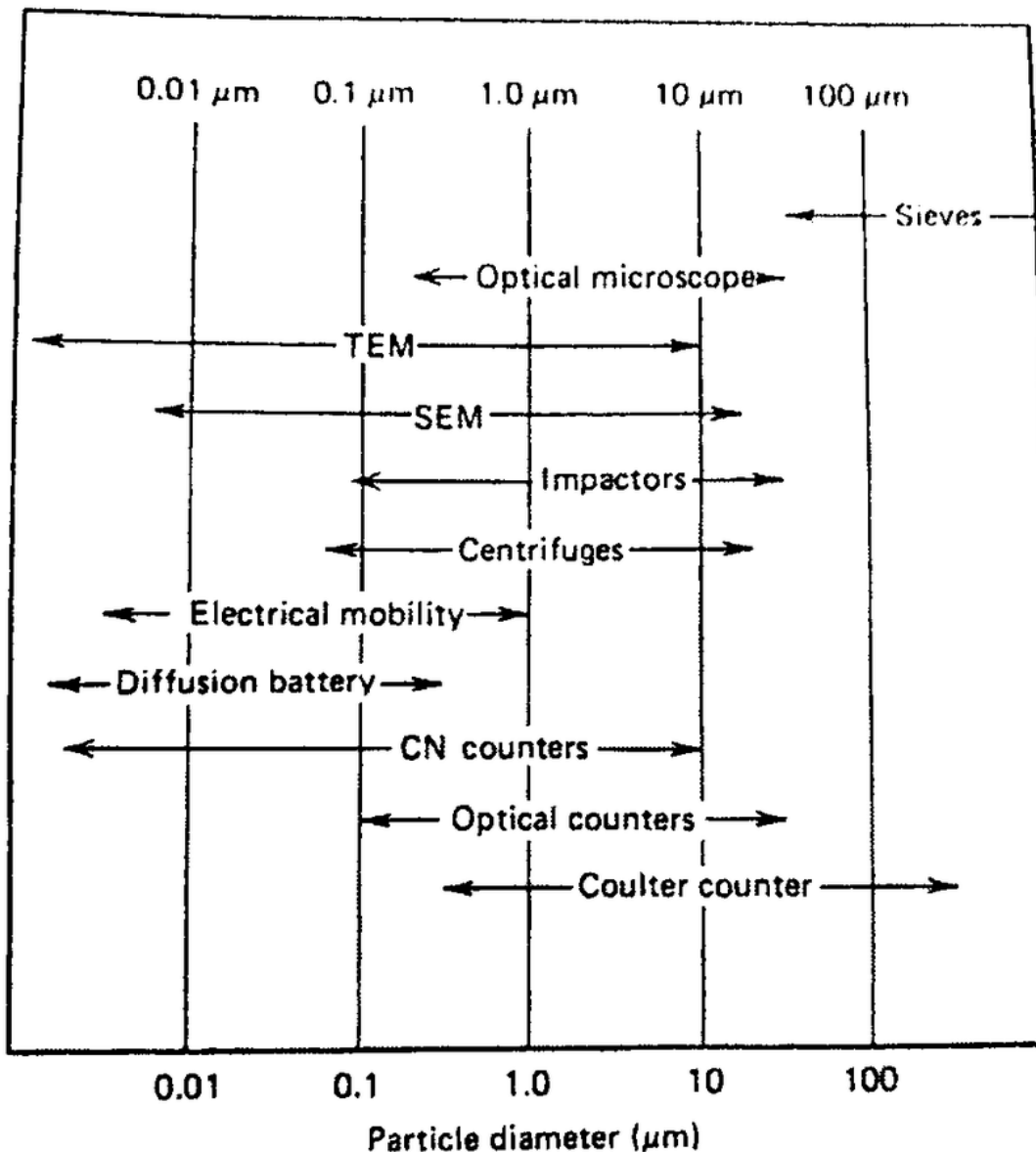


Figure 3 Particle counters based on their sizes[6]

Being detection range of particle size, from  $0.1\mu\text{m}$  to over  $10\mu\text{m}$ , using optical measuring devices. For studying finer particles than  $0.1\mu\text{m}$ , others particle equivalent diameter should be considered. DMA (Differential Mobility analyzer) is much more useful for sensing ultrafine particles by their electrical mobility, which is the ability of charged particles to move under the influence of an electrical field.

In this application, aerosol particles are passed through neutralizer which is used to impart a net charge on particles, so the charge distribution resulting in Boltzmann type, with known fractions of particles with single charge or multiple charges.

The DMA consists of two electrodes typically a cylindrical inner electrode and surrounding outer electrode. An electric field is applied between two electrodes. As aerosol particles pass through the DMA, they are subjected to a combination of electrical and aerodynamic forces.



The electrical mobility of particles depends on particle's physical size and charge they carry. Under effect of flow and electrical field imposed by electro classifier, only particles with certain mobility allowed to pass eventually to monodisperse aerosol outlet, other particles will be collected on electrodes. By adjusting the voltage of electrodes DMA can select target sized monodisperse aerosol to outlet. A particle counters at downstream is needed to count particles from such outlet.

DMA is often used in conjunction with other instruments such as condensation particle counters (CPC), also known as Condensation Nucleus (CN) counters, detecting range listed in Figure 3. The combination of two devices is so called scanning mobility particle sizers (SMPS) to measuring concentration of smaller particles from 1nm to 1000nm. In this thesis work both optical counters and SMPS is used for testing filtration performance of filter media for different size range of particles at upstream. Figure 4 shows SMPS used.



Figure 4 SMPS model 3938 consists of DMA and CPC for detecting electrical mobility of particles from 10nm to 1000nm



## 2.2 Filtration performance of fibrous media

As defined by ASHARE, media for a fibrous-type air cleaner, is that part of device that is actual dust-removing agent. Webs of spun fiberglass and papers are examples of air-filter media.[7] Fibrous media can be categorized into non-woven and woven type based on their structure and manufacturing process.

### 2.21 Electrostatic fibrous media

Some fibrous media have electrostatic charges that can be either naturally charged or imposed on the media during manufacturing.[7] Such charged fibrous media will enhance the efficiency on filtering particles by electrostatic force, without increasing the air resistance respect to non-charged one. However, during service, charge level on the fibers is decreasing, thus special maintenance is needed for those type of media.

### 2.22 Depth filtration and surface filtration

Depends on how particles deposits on air filters, deep filtration and surface filtration are commonly observed during aging process of air filters and are defined as two sequential stages. Depth filtration process often refers to thicker media of multiple layers of media forming a tortuous path to retain particles. When particles passing through layers of fibrous media, they are captured by fibers through-thickness with efficiency based on size of particles.

Larger particles that cannot pass the tortuous path are collected on the surface, forming layer structures so called 'particle cake'. This formation refers to surface filtration. Basic difference between functionality of non-woven and woven fibers media is whether their filtering ability is based on surface filtration or depth filtration. Woven media is working based on surface filtration, by means of sieving particles without deposition on tortuous path. Larger particles will retain on surface forming particle cake while smaller particle passes through media. Layer formed by particles increases air resistance clogging filter media, but it is removable by vibration or inverse air flow.

For non-woven media, both surface filtration and deep filtration take place. Nominally rated media are the most common on market and usually cheaper than depth media, being initially less efficient in capturing particles with targeted size range but while particle cake is forming, it increases filtering efficiency up to 100% with higher air resistance is caused by particle cake.

Instead, for depth media whose efficiency close to hundred percent at beginning of use and the effect of the surface on filtration rate is only a portion of overall filtration efficiency, thus air resistance does not increase much for surface loading. Depth media are usually regarded as high-performance air filter media.



## 2.23 Energy cost of air filters

Air filters were first developed in 1930s for forced-air heating systems and were initially designed to reduce the risk of building fires by protecting the systems' heating elements from dust. Since 1940s, they began to be used more for HVAC systems for protecting cooling coils from dust preventing fouling. Till 1980s and 1990s not only for HVAC protection but also for concerning over indoor air quality, air filters also used for clean air stream for building occupants.[15] As the advent of ASHRAE standard 52.2, MERV (minimum Efficiency Reporting Value) became indicator accepted by North America for comparing filtration efficiency.

Air filtration is evolving continuously with aim of achieving better energetic performance, since filters are regarded as component which absorbs electrical energy providing by fans. Total cost of purchasing filters includes initial cost which links to manufacturing processes and raw materials, and a large portion of energy cost for operation. In Table 1 lists some filters with their breakdowns to clearly show how much energy cost is in portion of total cost.

	Initial Cost	Energy Cost	Initial Cost % of total	Energy Cost % of total
MERV 6-11 Pleated Filter	\$4	\$46	8%	92%
MERV 11-15 Rigid Box Filter	\$70	\$304	19%	81%

Table 1 Breakdown of filters[15]

For both energetic and economic aspects, developing innovative filter media with lowest possible air resistance while satisfies needs of applications is a straightforward way for future technological advancement regarding sustainable and affordable energy.

## 2.24 Electrospun nanofibers

Recently developed electrospinning technique allowing producing nonwovens nanofibers media whose fiber diameter comparable to mean free path of air molecules.[16], [17], [18] Theoretically keeping same volume fraction, pressure drop increases as fiber diameter  $d_f$  decreases. [19], [20] Another aspect is slip effect when fiber diameter approaching mean free path of air molecules  $\lambda$ , leads to large Knudsen number defined as  $Kn = \frac{2\lambda}{d_f}$ , which indicates how air flow through fibers affecting by slip effect. Large Knudsen number means that significant slip effect reduces drag force induced by air flow, so pressure drop is lowered by introducing slip correction. [20], [21]

As for particle collection, most penetrating particle size (MPPS) decreases, and minimum efficiency increases as fiber diameter decreases.[20], [22] Interception collection are enhanced for smaller fiber diameter. Overall nanofibers media might provide good particle removal efficiency with low air resistance. Nanofiber filter media could be better solution for producing new generation of air filters reducing energy consumption and costs.

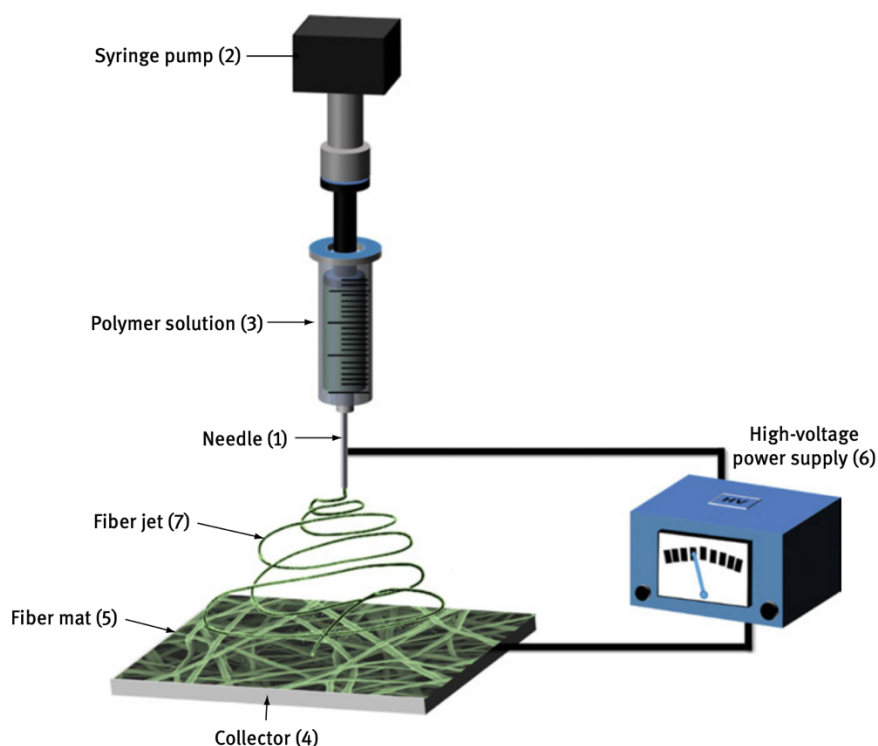


Figure 5 Schematic and set up of electrospinning[17]

Characterizing filtration performance of nanofibers filter media with standardized test methods is way for better assessing this new type of filter media, enabling comparison with others fibrous filter media that are available on current market.

## 2.3 Aim of work

First activities of this thesis work are to test the filtration performance of six types of nanofiber flat sheet filter media, classified based on their composition as shown in Figure 6, each type includes 6 samples. Standardized test method and innovative method are used for assessing air resistance and filtration efficiency of those media.



Figure 6 Test samples of nanofiber flat sheet media and their composition

Thirty-six samples of those nanofiber flat sheet media being tested, are provided by Federal University of São Carlos. Measured physical properties of sample media are provided in Table 2. Those measurements of fibrous media are used to calculate theoretical air resistance and MPPS and efficiency of clean filter media using models developed in previous studies to compare with experimental results. As activities in collaboration, test results of filtration performance are feeding back for correlating data from experiments to the measurements, enabling further corrections.

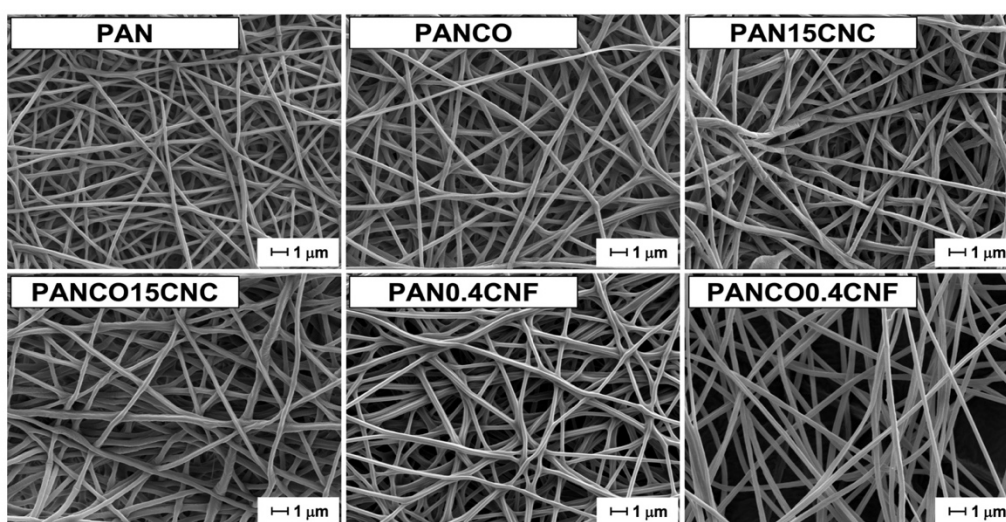
**Table 2** Physical properties of PAN electrospun membranes.

Sample ID <sup>a</sup>	Average fiber diameter $\pm$ SD (nm)	Average thickness $\pm$ SD ( $\mu$ m)	Average basis weight $\pm$ SD ( $g\ m^{-2}$ )	Average bulk density $\pm$ SD ( $g\ cm^{-3}$ )	Estimated porosity $\pm$ SD (%)
PAN	249 $\pm$ 50	157 $\pm$ 4	13.3 $\pm$ 1.5	0.08 $\pm$ 0.01	92.8 $\pm$ 0.8
PANCO	321 $\pm$ 56	154 $\pm$ 3	11.3 $\pm$ 1.5	0.07 $\pm$ 0.01	93.8 $\pm$ 0.9
PAN15CNC	353 $\pm$ 63	147 $\pm$ 6	11.3 $\pm$ 1.2	0.08 $\pm$ 0.01	93.2 $\pm$ 0.9
PANCO15CNC	379 $\pm$ 65	144 $\pm$ 2	9.7 $\pm$ 1.2	0.07 $\pm$ 0.01	94.1 $\pm$ 0.6
PAN0.4CNF	310 $\pm$ 67	152 $\pm$ 10	5.0 $\pm$ 1.0	0.03 $\pm$ 0.01	97.2 $\pm$ 0.5
PANCO0.4CNF	378 $\pm$ 56	133 $\pm$ 4	8.7 $\pm$ 0.6	0.065 $\pm$ 0.002	94.5 $\pm$ 0.2

<sup>a</sup>Membrane acronyms are composed of the name of the polymer/matrix (PAN), name of the compatibilizing agent (CO), content of cellulose (15 wt% or 0.4 wt%) and form of cellulosic fibers (CNC or CNF).

Table 2 Physical properties of PAN electrospun nanofiber media

As SEM (Scanning Electron Microscope) shown in Figure 7, it is clear to have view of nonwovens structure of nanofiber media of each type and scale of fibers diameter.



Acronyms formed by: PAN + CO (castor oil) + wt% CNC or CNF (cellulose nanocrystal or cellulose nanofibrils, respectively)

Figure 7 Scanning Electron Microscope (SEM) of samples from each nanofiber type

Tests are conducted at AEROSOLTECH laboratory in DENERG department of Politecnico di Torino. Air resistances are tested using accurate test machine TEXTEST and results are compared with empirical models. Particle removal efficiency tests are performed using two type of optical particle counters of different detecting size range. Spectral efficiencies for particle size range from 0.3 micrometers to 10 micrometers measured using OPS3330 which is commonly recommended by many standards. And that of particle size range from 0.09 micrometers to 10 micrometers using another optical counter LAX3340 allowing to identify most penetrating particle size (MPPS), which is usually in the range of 0.1 micrometers to 0.3 micrometers for common fibrous filter media. MPPS is a function of filtration velocity, so tests are performed at fixed air flow rate for all type of samples.

After testing air resistances and fractional particle removal efficiencies, the second part of work is related to loading test of flat sheet media, using turnkey machine 8130A and test rig with relative humidity control of test air flow. Since latter is prototype, specific functional tests for



characterization of test rig status are performed.

Loading tests are way to study service life of air filter media from pressure drop increases. After efficiency tests some loading tests are performed on others type of flat sheet media instead of nanofiber samples. That is because, at low filtration velocity, precise control of aerodynamic behavior of air flow inside ducts is difficult. Secondly, time requiring for conducting tests covering whole stages of loading using ultrafine particles is long. So, aim of this part of work is to study loading behavior using commercial masks test machine 8130A, verifying functionality of aerosol generator whether it gives constant production of aimed particle sizes. This is done by using SMPS to check particle size distribution of upstream air, identifying characteristic of ultrafine particles is needed for photometer measuring. This part of work is more focusing on solving technical issues for better accuracy of results.

At the end, study of influences of relative humidity (RH) on loading process by controlling variables at different RH levels is performed. Using solid particles to charge the filter media means that electrostatic charge distribution should be carefully studied to reduce uncertainty as much as possible. Tests on test rig for RH control equipped with aerosol generators to give different particle concentrations, and neutralizer to reduce electrostatic effect of produced particles by corona discharge particles into Boltzmann distribution. Tests on those components are performed to tuning the operating conditions. Those works could be regarded as preliminary work for further study of loading behavior of nanofiber media in order to find better technical solution for designing experimental procedures to provide reliable and repeatable solutions.



## 2.4 Literature review

### 2.41 Particle capture and removal efficiency

Modern filtration theories are developed through theoretical and experimental studies with contributions of many aerosol scientists. Models for predict particle filtration performance of clean fibrous filter media are well developed and detailly documented by Brown (1993), Hinds (1999) and Lee and Mukund (2001).[20] The classical filtration theory is based on particle collection by isolated single fiber. Five main mechanisms are considered for capturing particles: diffusion, interception, inertial impaction, gravitation, electrostatic.[6] The single fiber theory assuming five mechanisms works without interference with each other, which are not in realistic case. For improving accuracy of analytical expressions, interception of diffusing particles is then considered.

Interception is defined for particle which follows a streamline is deposited on fiber, in such way that center of particle is within one radius from fiber surface. The single fiber efficiency of interception is expressed in Kuwabara flow field:[23]

$$\eta_{inter} = \frac{1 + R}{2Ku} [2\ln(1 + R - 1 + \alpha + \left(\frac{1}{1 + R}\right)^2 \left(1 - \frac{\alpha}{2}\right) - \frac{\alpha}{2}(1 + R)^2]$$

Where R is ratio of particle diameter to fiber diameter  $d_p/d_f$ , Ku is Kuwabara hydrodynamic factor,  $\alpha$  is solidity of filter. The relationship shows interception efficiency depends on particle sizes and fiber diameters.

Diffusion mechanism is related to particles are captured by hitting fiber due to brownian motion, the expression for single fiber efficiency of diffusion is given:[23]

$$\eta_{diff} = 2.58 \left(\frac{1 - \alpha}{Ku}\right)^{\frac{1}{3}} Pe^{-\frac{2}{3}}$$

Where Pe is Peclet number defined as  $d_f U_0 / D$ , in which  $U_0$  is filtration velocity, D is diffusion coefficient of particles defined as  $kTC_c / 3\pi\mu d_p$ .

The validity for this expression:  $0.05 < \alpha < 0.2$ ,  $10^{-3} < U_0 < 2m/s$ ,  $0.1 < d_f < 50\mu m$ .

Considering interference between interception and diffusion, which is also important for study most penetrating particle size and the expression for single fiber efficiency for this effect:[6]

$$\eta_{ar} = \frac{1.24R^{2/3}}{(KuPe)^{1/2}}$$



Inertial impaction describes that particles are captured due to inertial force, its single fiber efficiency depends on stokes number of particles.[21] This effect is relevant for larger particles, or at high filtration velocity. The accurate quantification of this mechanism is still difficult at low stokes number, due to intervention of other predominant mechanisms.

Gravitational capture due to settling of the particles under gravity force. Air flow direction and settling velocity of particles are influencing in this case. Again, it is only relevant for larger particles.[6]

Electrostatic collection is negligible for the case of non-charged fiber with neutralized particles.

Overall single fiber efficiency is combining approximately in following expression while neglecting possible interaction of inertial impaction with interception, which is hard to quantify.

$$\eta_{\Sigma} \approx 1 - (1 - \eta_{inter})(1 - \eta_{impac})(1 - \eta_{dr})(1 - \eta_{diff})(1 - \eta_{elec})(1 - \eta_{grav})$$

Total efficiency for filtration media is calculable from single fiber efficiency:[6]

$$\eta = 1 - P = 1 - \exp\left(-\eta_{\Sigma}\alpha\frac{4}{\pi(1-\alpha)d_f}t\right)$$

Where t is thickness of media.

In Figure 8 shows that at low filtration velocity as 10cm/s, dominants mechanisms are diffusion and interception for most penetrate particle size. The interception efficiency is increasing with increasing of particle size, while diffusion efficiency decreases. At this velocity experiments are performed for efficiency test because low flow rate is required to test flat sheet media for low tenacity of nanofibers.

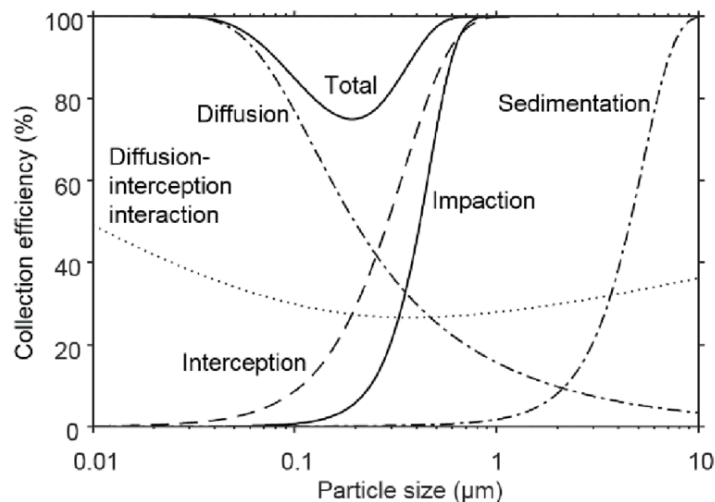


Figure 8 Theoretical efficiency as function of particle size at 10cm/s, fiber diameter =2μm, t=1mm[6]

As fiber diameter decreases, the fractional efficiency curve of interception will translate towards smaller particle because of interception ratio R increases. Such that most penetrating



particle size will move towards left and increases the minimum of overall efficiency for finer fibers as shown in Figure 9.

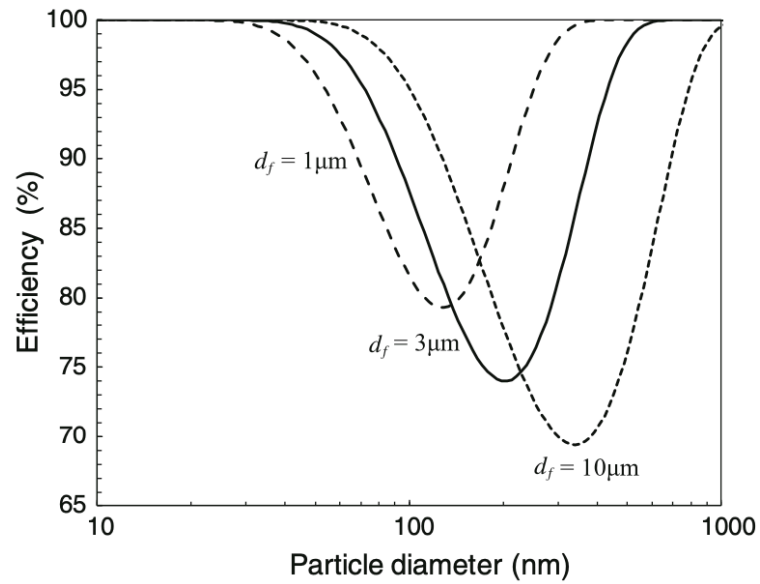


Figure 9 Fractional efficiency for different fiber diameters at same solidity 0.05 and velocity 0.2m/s[20]



## 2.42 Particle loading

Single fiber theory is conceptual basis for study loading behavior. Previously described particle removal efficiency refers to clean media with no prior particle deposited and assuming that particle collected during efficiency test are negligible, which is reasonable if loading time during efficiency test is relatively short. In fact, particles deposit continuously onto previously collected particles forming agglomerates or more compact structure.[19] Solid particles adheres onto fibers and particles mainly through van der Waals force, with probability of detachment and resuspension, which decreases particle deposition rate in dynamic regime. Single fiber theory is useful for study particle deposition rate as function in time. As another aspect to collection efficiency which is developed by single fiber theory, structure of collected particles is change based upon the filtration parameters such as Stokes number, Peclet number and interception ratio.[24] Regarding nanoparticle filtration, particle shapes also influence particle collection and capture mechanism at same filtration parameters.[25]

As in macroscopic level, overall loading process of filter media is divided into three sequential regimes, regards depth loading, transition loading and surface loading. In depth loading and surface loading regimes, pressure drop across filters increase linearly as mass loaded. Instead transition phase in between those two stages showing nonlinear growth of pressure drop. The concept is particles deposit on fibers forming dendrite structure, those structure grows and entangle with each other forming single structure. The dendrite growth represents depth regime, and entanglement and growth of single structure forms the basis of nonlinear transition from depth loading to surface loading.[26] After transition period, pressure drop will increase linearly as mass loaded with same slope using same monodisperse aerosol regardless of media type, this stage refers to surface loading.[27] Being nonlinear behavior at transition regime, there is no distinct boundaries for each regime.

Loading process of fibrous filter media is influenced by factors, not only for these introduced in filtration theory, but also particle types, their materials, surface roughness, hygroscopicity, and relative humidity which affects adhesion forces. The state of art is study loading process on various factors, through analytical approach, computational approach, and experimental approach.[28] Analytical approach aim to assess loading behavior on wide spectrum of influencing factors, but accuracy rely on the simplification of assumption. Computational model allows to investigate microscopically the loading process and complex geometry in relatively inexpensive way, but its accuracy is limited by development of theory. Experimental approach provides ability to correlate data for quantitatively assess difficult processed avoiding errors introduced by simplification, but cost and time requiring are the most, and inherent difficulties present when encounter anomalies. The research gap is identified as that, accuracy of current models still needs to improve thus it needs more data, which becomes motivation of present study to investigate realistic loading behavior using experimental approach.

## 3. Methodology

### 3.1 Test rig characterization

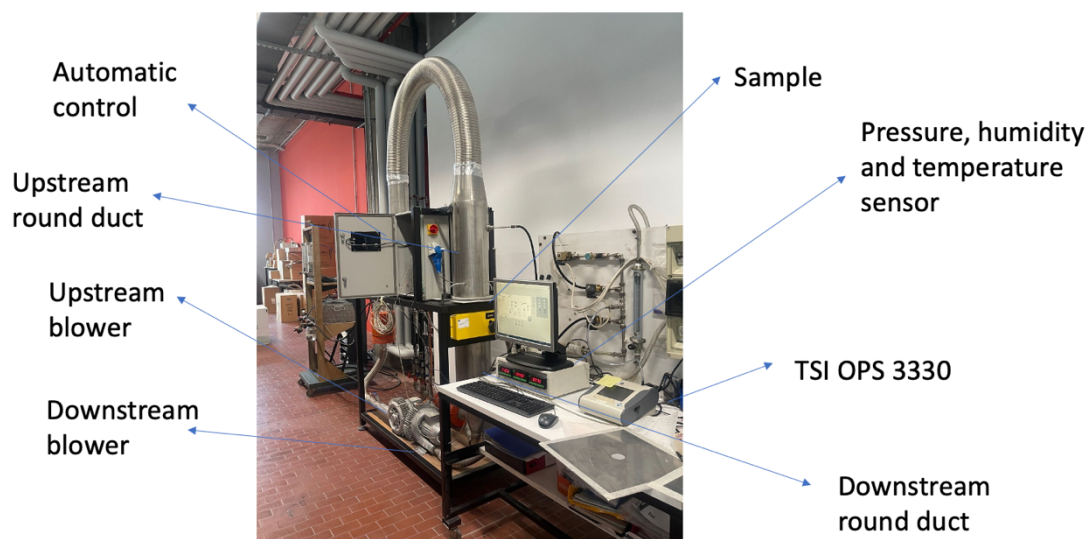


Figure 10 Test rig for spectral particle removal efficiency

The test rig has upstream blower and downstream compressor, rotating speed of two fans is electronically controlled through inverters. In this way air flow rate and overpressure inside duct is controlled by regulating speed of fans. It is observed during tests that upstream fan is more sensitive for overpressure controlling and downstream fan is mainly used for air flow rate controlling but providing negative pressure respect ambient pressure. Overpressure inside ducts is essential during test for preventing ambient particles getting inside test ducts, which induces error. So, two fans should be regulated together to provide stable air flow, by means of readings from flowmeters within variational range 5%, for the aim of stable filtration velocity and constant production of aerosol during tests.

The test rig is electrically grounded with ducts which has a smooth interior finish and rigid enough to avoid deformation at operation pressure according to requirement of standards. The up-round duct is sealed by aluminum tape to prevent air leakage during test, this check is done along tests by sensing air flow with hands if there are large amount of aerosol leaks which induces error.

### 3.11 Sample preparation

Figure 10 indicates main components of test rig used for assessment of spectral particle removal efficiency and air resistance of flat sheet media. Samples to be tested is contained by two layers of mosquito net to prevent mechanical breaking during test and sealed with tapes at boundary to prevent in-plane air flow. Figure 11 show an example of tested sample. Samples prepared are then installed between two perforated plates with a central hole of 5cm diameter, an example is showed in Figure 12. Tapes are necessary for fixing position of samples and plates. Finally perforated plates with sample clamped in between filter holders.

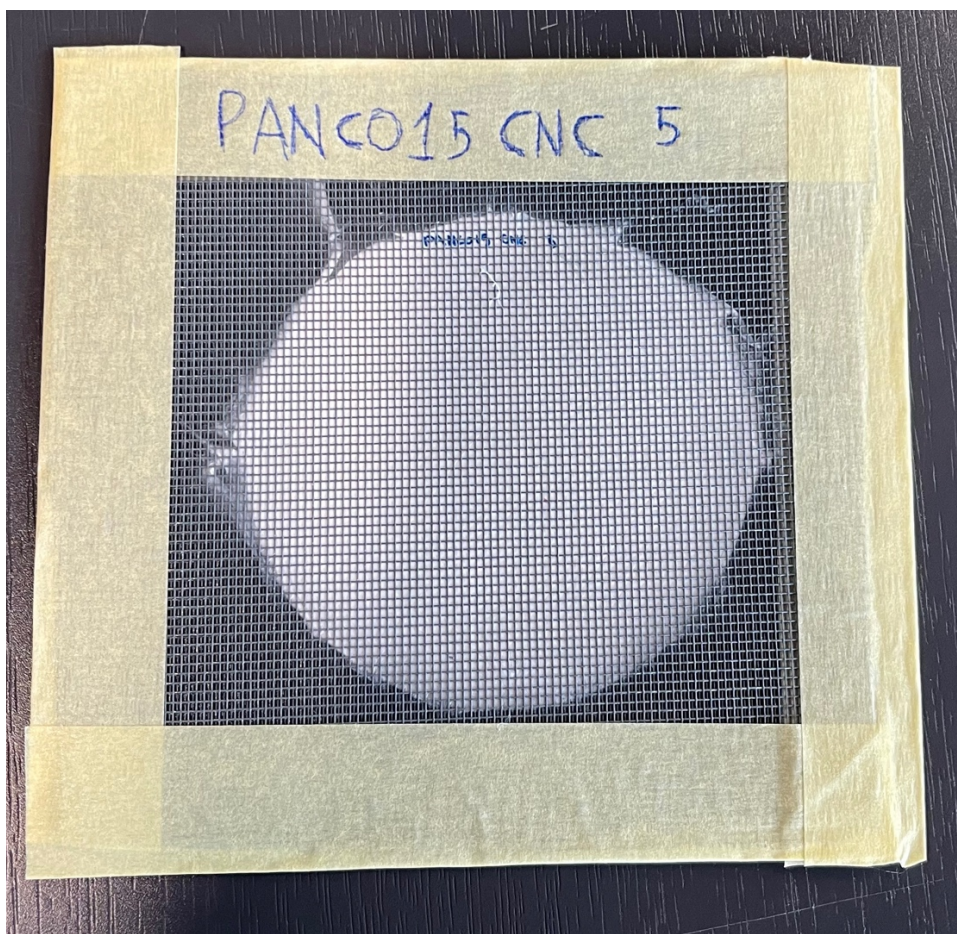


Figure 11 Sample within 2 layers of mosquito net sealed by tapes

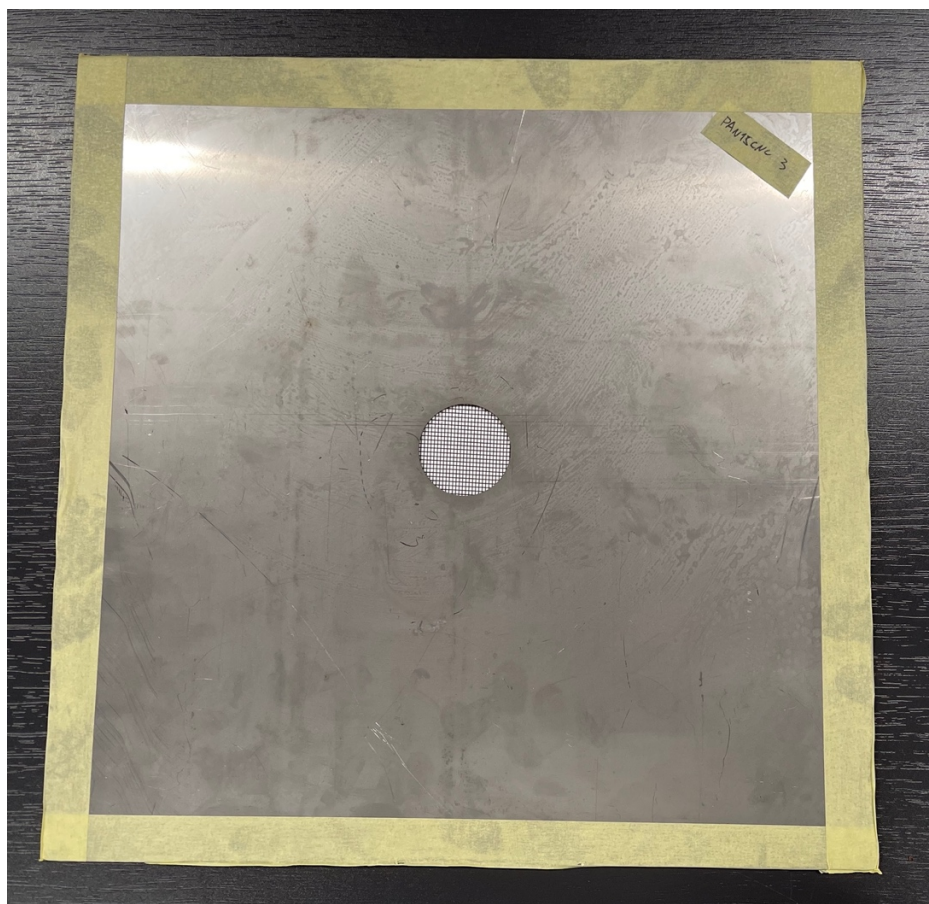


Figure 12 Perforated plates contains sample with central hole diameter 5cm

Samples are labeled with tapes for distinguishing from each other. Six pairs of perforated plate are available for testing in sequence 6 samples without dissemble them from plates.

### 3.12 Main components and control

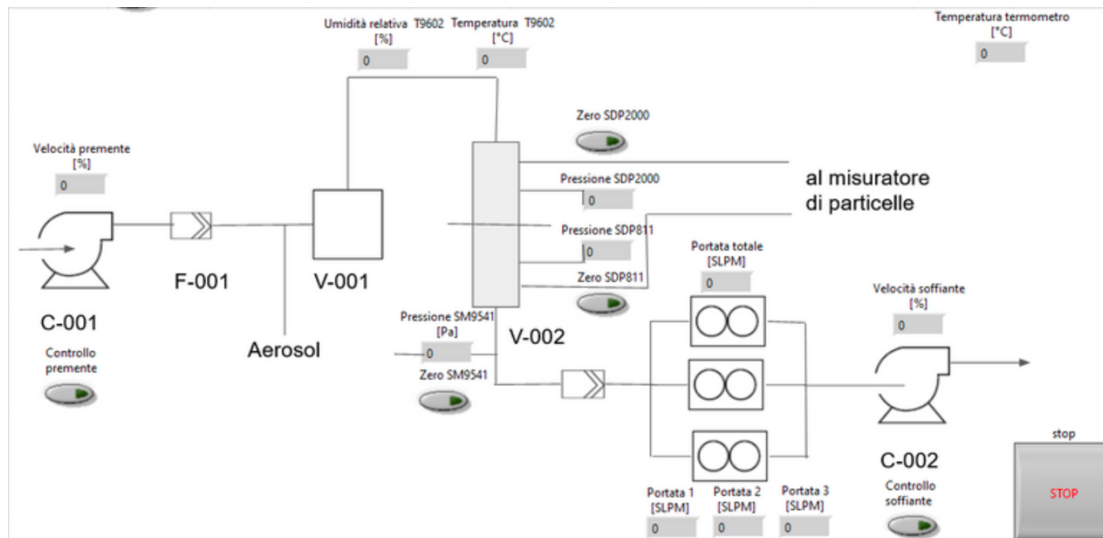


Figure 13 Interface for automatic control of air flow

Figure 13 provides clear schematic representation of the test rig. The LabView interface allowing inputs parameters for controlling air flow in two modes: 1) automatic mode, inputting parameters of overpressure and flowrate, rotating speed of fans is regulated automatically by PID controlling system, receiving reading of flowmeters at downstream duct as feedback. 2) manual mode, for specific need, inputs parameters are rotating speed of two fans directly feed into inverters. Manually checking whether aiming air flow rate and overpressure from sensors reading is archived is necessary.

F-001 and F-002 (after V-002) in Figure 13 indicated two HEPA filters inside ducts. F-001 is upstream HEPA filter to prevent particle contamination of ambient air from upstream fan, which shows in Figure 26 as orange cylinder. Instead, F-002 is HEPA at downstream of filter holder (V-002), filtering aerosol particles during tests, in Figure 14 represented as an orange cylinder same as before.

V-001 is representing a plenum of 600x600x600mm to guarantee an adequate control volume to mix the generated aerosol with intake airflow. It is essential condition of uniformity of aerosol charging the samples along tests, for accurate results.

Environmental conditions of laboratory such as barometric pressure, temperature, and relative humidity readings of mixed air flow, at upstream duct are provided by sensors, those readings allow correcting the air flow rate in LPM (Liter Per Minute) into standard environmental condition in SLPM (Standard Liter Per Minute). Before test, face velocity is calculated by taking ratio of standard air flow rate and sample area.

Air resistance of samples is measured by two static pressure taps at upstream and downstream of filter holder. Two pressure transducers in Figure 13, SDP2000 and SDP811 provides differential pressure simultaneously for different measuring ranges. Another pressure



transducer SM9541 reads overpressure value inside duct. Zeroing of pressure transducers and flowmeters is carefully done at each single test.



Figure 14 Mechanical valves for air flow adjustment and upstream and downstream fans

In Figure 14 is possible to see mechanical valves for regulating air flow. This operation is especially necessary when aim air flow cannot be archived by simply inputting parameters. As an implement operation, either for aim air flow rate is too small by regulation of fans speed, for overpressure is too low or even negative at minimum flow rate, and for avoiding too high back pressure at upstream of sample due to high air resistance of itself otherwise optical counter OPS3330 will showing error.



### 3.2 Air resistance test

Tests of air resistance of nanofiber media are conducted with samples at face velocities range from 1cm/s up to 15cm/s, with resolution of 1cm/s, by regulating air flow corresponding to each velocity. Theoretically pressure drop will increase linearly with increasing face velocity according to Darcy law of fluid passing through porous media, states that pressure gradient across samples is linear function of volumetric flow rate:

$$Q = \frac{k * A}{\mu} * \frac{\Delta P}{L}$$

Where k is permeability of media, A is sample area,  $\mu$  is viscosity of air,  $\frac{\Delta P}{L}$  is pressure gradient across sample, Q is volumetric air flow rate. This formula is valid for fluid field with low Remolds number so that inertial effect for air stream is negligible. This condition is valid for clean flat sheet media in this case because of low filtration velocity is used. As results of test, the slope of correlating pressure drop at different velocities will directly give permeability of samples knowing sample area and viscosity of air.

The accuracy of pressure drop is important for assessment of samples. For this reason, more accurate test equipment is used to measuring air resistance of samples. For the purposes of calibrating test rig and provide results accurately as possible. As a matter of fact, during tests on test rig is noted that pressure drop across sample is varying when overpressure changes at fixed velocity, that means not accurate readings. This might be caused by turbulence effect at static pressure taps. Preliminary air resistance tests are conducted on filter media between perforated plates with different central hole diameters, 220mm, 100mm, 40mm respectively, aiming to checking turbulence effect. Results was also compared with TEXTEST showing in Figure 15, which measures the air permeability of all kinds of flat materials as well as foam cubes and recently calibrated by manufacturer, so the results are regarded as most accurate.

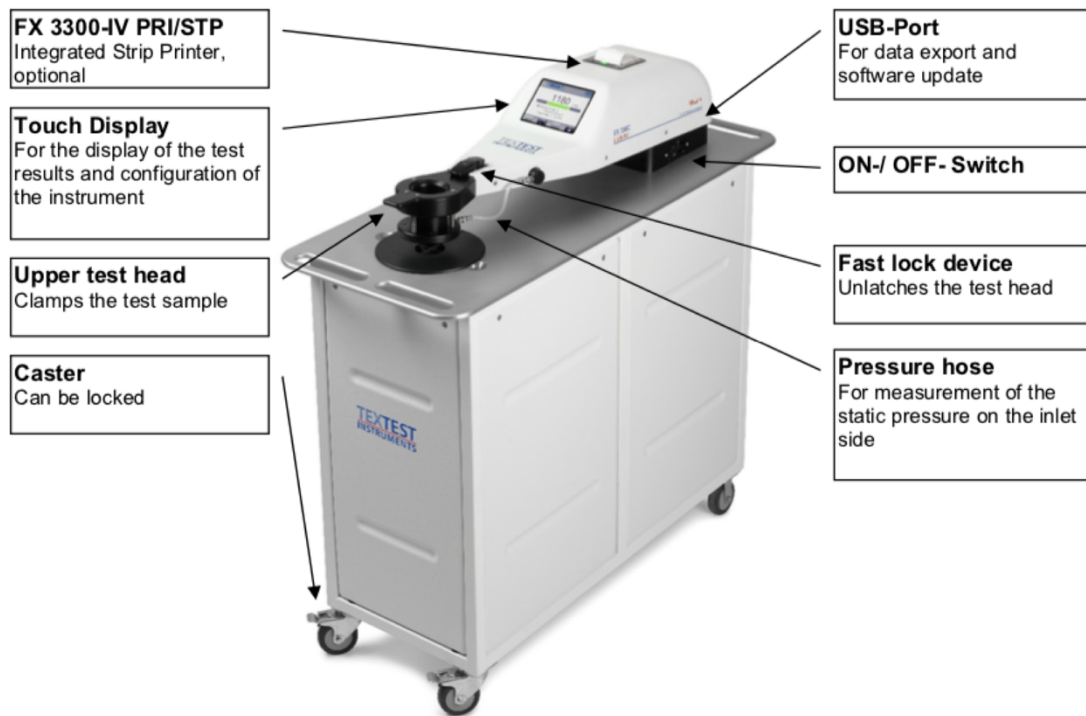


Figure 15 Function blocks of TEXTEST FX-3300 LABAIR

Before tests using TEXTEST, calibration of air flow is checked following instruction, this is essential for stable air flow for test and accurate measurement. Specific details of TEXTEST FX-3300 LABAIR refers to working manual provided by manufacturer.[29]



### 3.21 Calibration of Test rig with TEXTEST

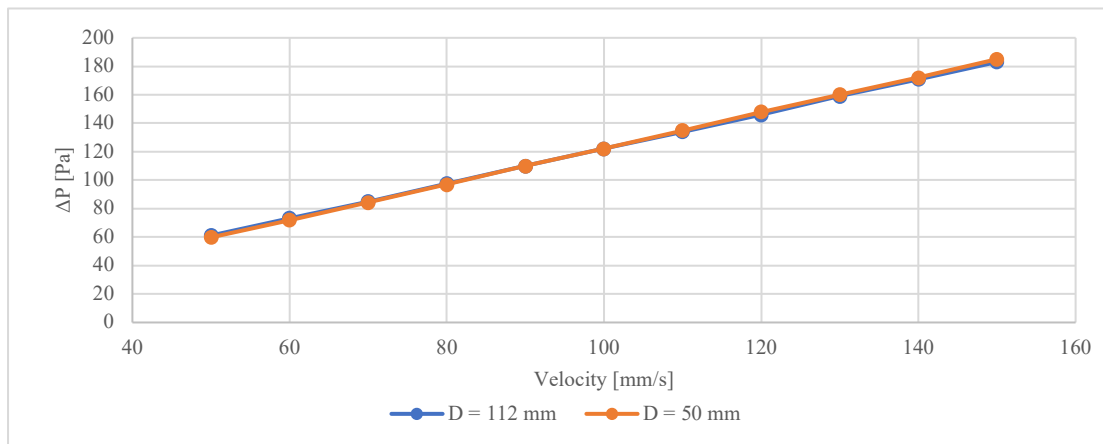


Figure 16 Pressure drops at different sample area TEXTEST

Firstly, checks for air resistance of FCR filter media is done on TEXTEST with different sample area, with diameter 112mm and 50mm, for face velocity from 5cm/s to 15cm/s, results are plotted on Figure 16. Two superimposing plot lines shows accurate measurement on TEXTEST, verifies that pressure drop is not affected by sample area.

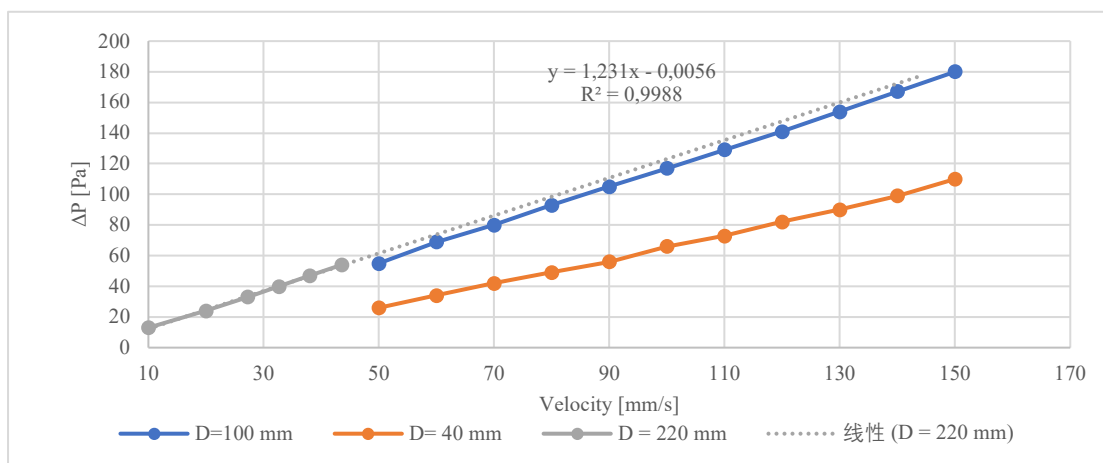


Figure 17 Pressure drops at different sample area Test rig

Then tests are done on test rig, for central hole diameter 100mm and 40mm, face velocity is regulated from 5cm/s to 15cm/s. Instead for 220mm, face velocity is set at lower range from 1cm to 4cm/s and interpolated linearly up to 15cm/s. This is because airflow rate reaching same face velocity for large diameter is outside of adjustable range of fans. From results of test rig shown in Figure 17, it is clear to see that for larger diameters, 100mm and 220mm, pressure drops not affected by sample area. Instead for 40mm, pressure drop is lower because of turbulent effect introduced by stronger restriction of flow area in this case.

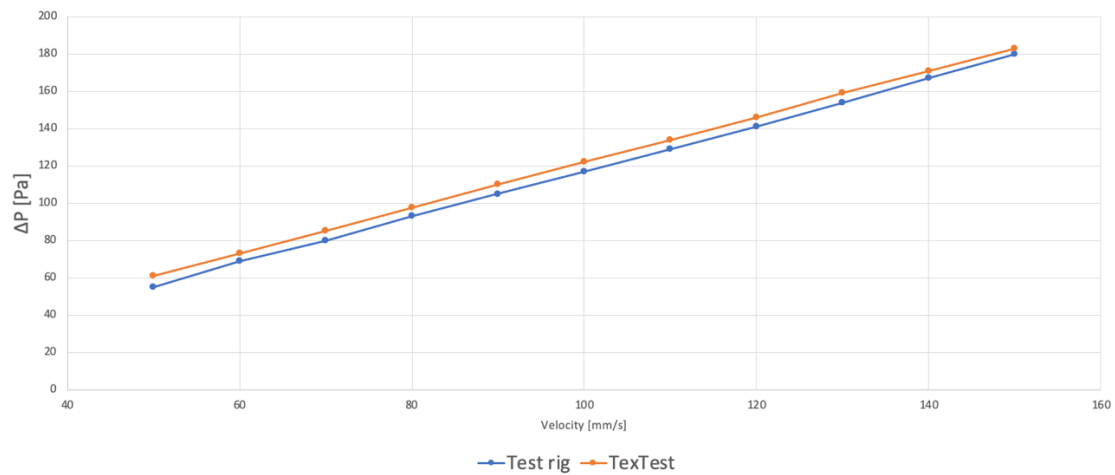


Figure 18 Test rig vs TEXTEST at diameter 100mm

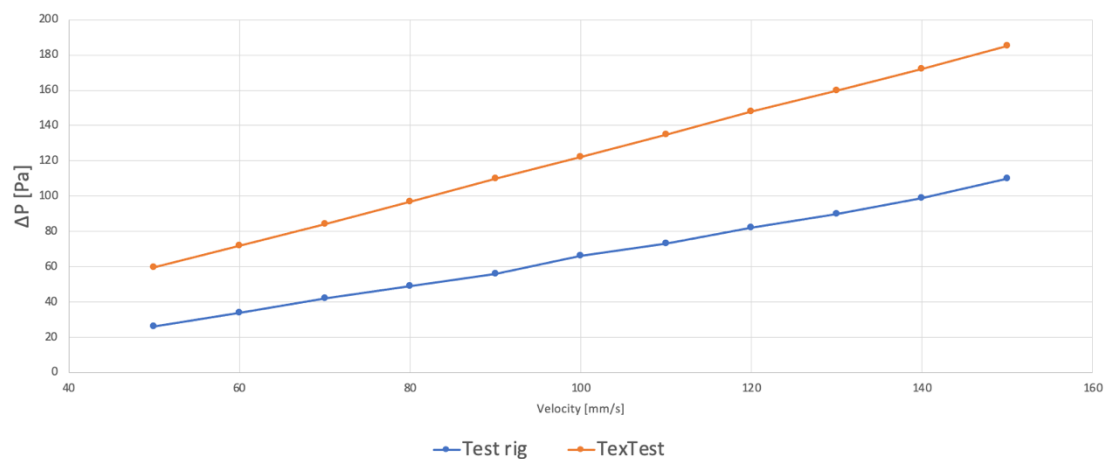


Figure 19 Test rig vs TEXTEST at diameter 40mm

Comparing results from test rig and TEXTEST showing in Figure 18 and Figure 19, concludes that for the case of study, using 5mm diameter perforated plates to test nanofiber samples, test rig will not give accurate reading of pressure drops at different face velocities as TEXTEST do. So, for air resistance tests, only results from TEXTEST are reported later in discussion section.



### 3.22 Permeability of mosquito net

For testing air resistance of nanofiber samples, with the configuration as shown in Figure 11, samples are kept at central position of 5cm diameter test head provided with TEXTEST, avoiding that inhomogeneity of sample affects the result. Considering that permeability of mosquito net might affect accuracy of result, permeability test is done by manufacturer of TEXTEST to check effect of mosquito net.

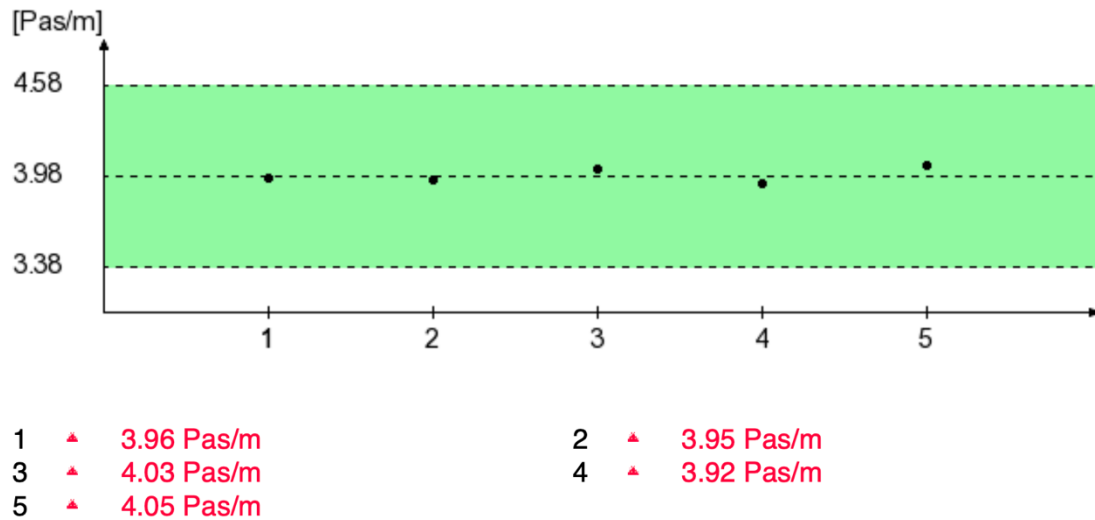


Figure 20 Permeability test of mosquito net

According to results provided, pressure drop introduced by mosquito net at 15cm/s is calculated by multiplying permeability by velocity, resulting 0.6 Pa, so it is negligible.



### 3.3 Particle removal efficiency test

Fibrous filtration efficiency is a function of particle size and other parameters.[21] As previously introduced, equivalent methods for measuring particle removal efficiency based on equivalent size are preferred because of conveniences on time and cost of instruments, respect to reference method. Optical particle counters or SMPS enabling detecting single particle based on its size, and particle counts is accumulated at size ranges and provided as histogram whose bin width indicates particle size range and bin height indicates frequency of particle numbers counted at each size channel. An example in Figure 21. By taking ratio of measured histogram at downstream of filter media to that of upstream provides efficiencies at each size range, and the results are represented together in single graph defined as fractional efficiency or spectral efficiency. Providing fractional efficiency as result of test allowing comprehensive assessment of filter media since particle size distribution is implicitly known. Test methods using optical spectrometers are commonly defined by standards such as ISO16890, ASHRAE 52.2, EN779 for filter media of HVAC systems.

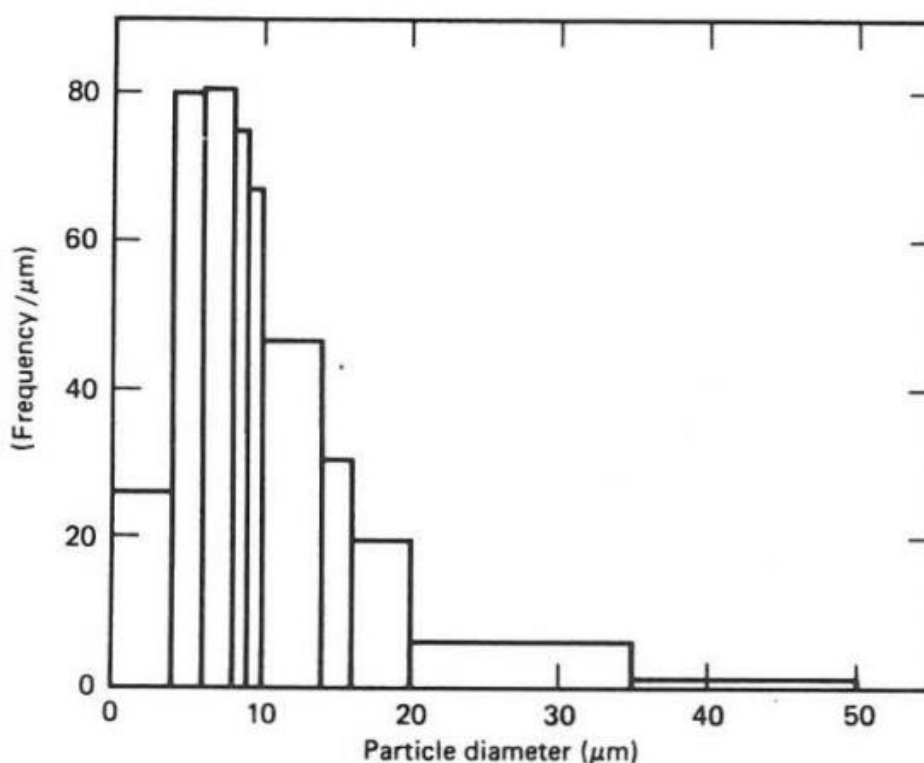


Figure 21 Histogram of frequency normalized by width of intervals vs. particle size[6]

Unlike optical spectrometers, photometers are another type of optical detector, which senses scattered light intensity from a cluster of particles together instead of single particle at time. Measurement obtained this way is total number of particles covering all size ranges available from aerosol generator, total penetration or overall efficiency is calculable by taking ratio of upstream reading to downstream reading of vice versa. In this case particle size distribution at upstream of filter is strictly required for comparing results from other methods. In other words,



total penetration obtained for filter media can be compared with benchmark if generated particle size distribution is same as defined by standards. For example, the National Institute for Occupational Safety and Health (NIOSH) published Guide to the Selection and Use of Particulate Respirators Certified under 42 CFR 84 (Code of Federal Regulations Part 84) indicates that selection of filter efficiency depends on the maximum filter penetration that can be accepted, and states that for N-series filters must be tested against a mildly degrading aerosol of NaCl with count median diameter (CMD) of  $0.075 \pm 0.020$  micrometers and geometric standards deviation (GSD) less than 1.86.[30] The specific model TSI 8130A with photometers for penetration test of masks under this regulation is used for purpose of loading test will be introduced at later section.

Ultrafine solid particles which have CMD lower than 100nm better represents accumulation mode in typical urban atmospheric aerosol which has highest contribution to total numbers in long ranges.[31] As shown in Figure 22 both for number and surface distribution represented with single mode. This size distribution of particles poses severe effects for health and for simulating aging HVAC filters under most common conditions.

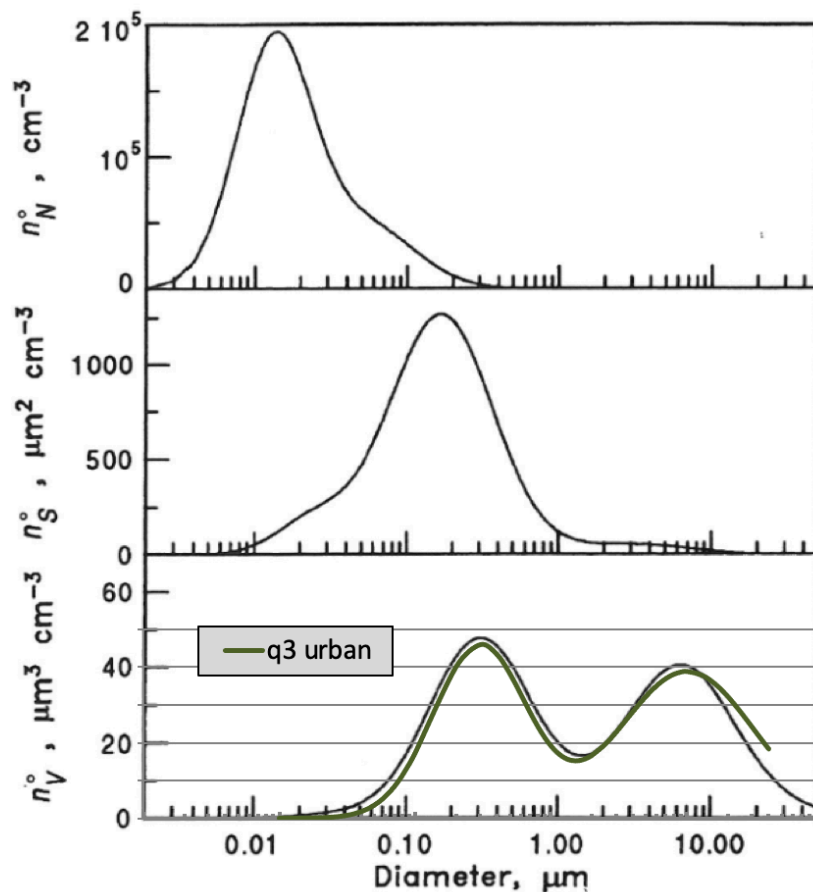


Figure 22 Typical urban aerosols: number, surface, volume distribution[31]

### 3.31 Optical particle sizer and spectrometer

For more comprehensive assessment of performance of nanofiber flat sheet media, tests are performed with models of optical spectrometers with different particle sensing range to provide fractional efficiency. First one is TSI OPS3330 in Figure 2 which measures particle at optical size ranges from 0.3 to 10 micrometers, as specified by ISO16890, liquid phase aerosol particles generated from untreated and undiluted DiEthylHexylSebacate (DEHS) by Laskin nozzle, is used to challenge samples.[32] Advantages using liquid aerosol compares to solid particle aerosol for performing spectral particle removal efficiency test is, negligible loading effects of particles during experiment, without needs to neutralize generated aerosol. Additionally, particle bouncing only takes place when using solid particle and those leads to inaccuracy.

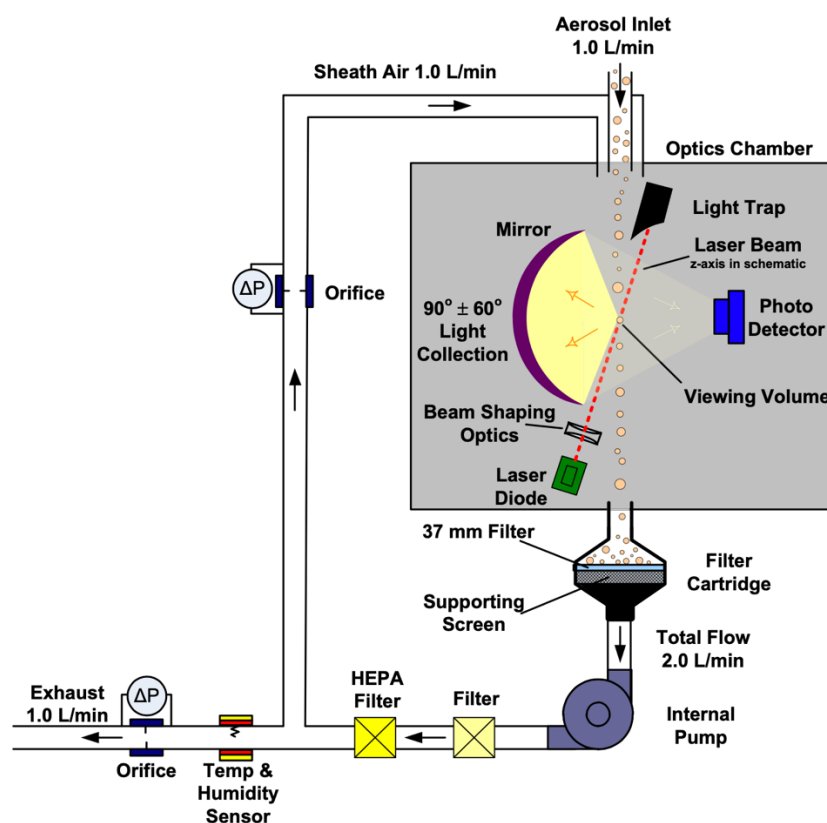


Figure 23 Sample flow path in OPS 3330[14]

Figure 23 shows sample flow path in OPS3330, sample flow rate is fix at 1 liter per minute, and light source consists of 638nm wavelength laser emitted by long life laser diode.[14]

Second model is (Laser Aerosol Spectrometers) LAS 3340A in Figure 24, which measures particles from 90nm to 7.5 micrometers, with a range of sampling flow rate from 0.01 to 0.1 liter per minute. Light source is 633nm wavelength Helium-Neon gas laser of intracavity power higher than 1W. Two detectors working together for smallest and largest particles: Avalanche Photo Diode (APD) for detecting the smallest particles with high-gain, while pair of low-gain

PIN photodiode for detection of upper size range of the instrument, such way that detecting smallest particles as 90nm with 50% efficiency, the resolution is calculable thus providing user-defined particle size channel numbers up to 100.[33] Two detection circuits shown in Figure 25. Those are main differences of two models. However, size sensitivity of system is limited at smaller size range due to noise source as photon shot noise on the detected molecular scatter from background gas since particles are small enough closing to dimension of molecules along with other technique noises such like Johnson noise of photodiode.



Figure 24 LAS 3340A[33]

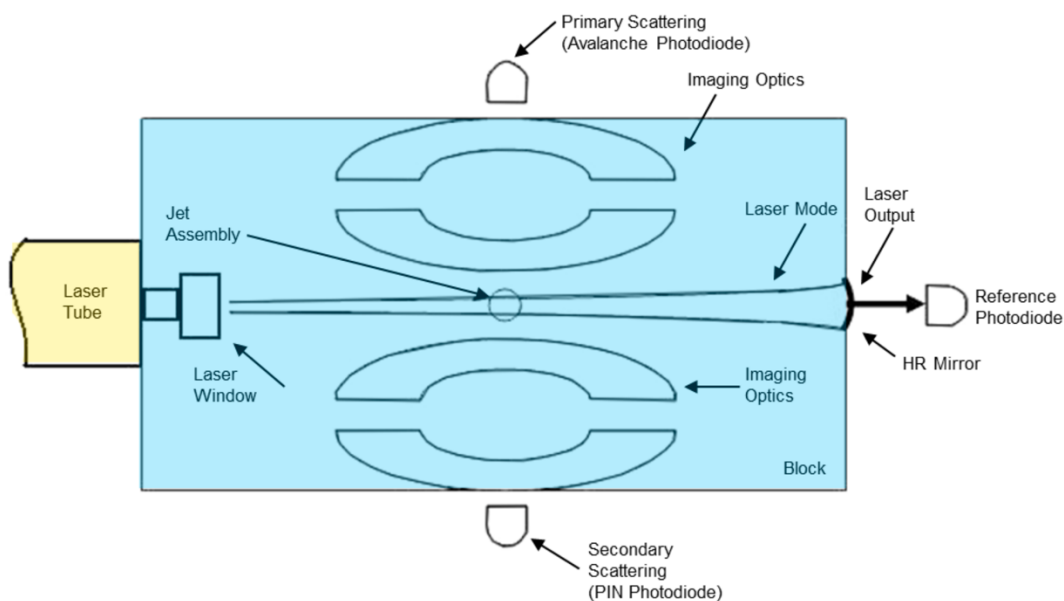


Figure 25 Two optical sensing circuits for detecting small and large particle respectively[33]

### 3.32 Aerosol generation system



Figure 26 Liquid aerosol DEHS (DiEthylHexylSebacate) generator

In Figure 26 showing arrangement of liquid DEHS aerosol generator, a Laskin nozzle with specific design according to requirements of ISO16890 which produces spherical particles with particle size distributions with one or more log-mean modes, Count Median Diameter or CMD from 0.2 to 0.8 micrometers.[32], [34] Such aerosol is intended for measuring filter efficiency from 0.3 to 3.0 micrometers, and it can be extended up to 10 micrometers.[8], [9] Valve on the left of aerosol generator controls opening of the clean compressed air which feeds Laskin nozzle submerged beneath free surface of liquid, at pre adjusted pressurized level yielding enough particles in the test filter airflow to meet requirement of standards.

Vaporized DEHS into liquid particles moves through pipe at right side. The number distribution of particles is fixed by pressure of intaking compressed air, covering range of particle size needed for tests. The number concentration of particles should be at approximately 30% of maximum reading threshold of particle counters to avoid overload of particle counters, this can be adjusted by regulating compressed air flow rate before test. Once this has been done, it will take like 30 minutes to restore stability of aerosol production into new level of concentration, continuously monitoring of readings from particle counters at upstream duct is essential in this condition. Because ISO16890 is intended for fully assembled filters, in case of flat sheet media is tested keeping at same face velocity at operational condition of filters, but concentration of particles is significantly lower because of lower volume flow rate as indicated by standards.[32]



### 3.33 Aerosol sampling system

Aerosol sampling system of test rig consists of sampling probes of 9mm diameter installed at upstream and downstream ducts, connected respectively by PTFE tubes to a three-way valve allowing commuting sampling sequence from upstream sampling, downstream sampling, and white area for filtered air.

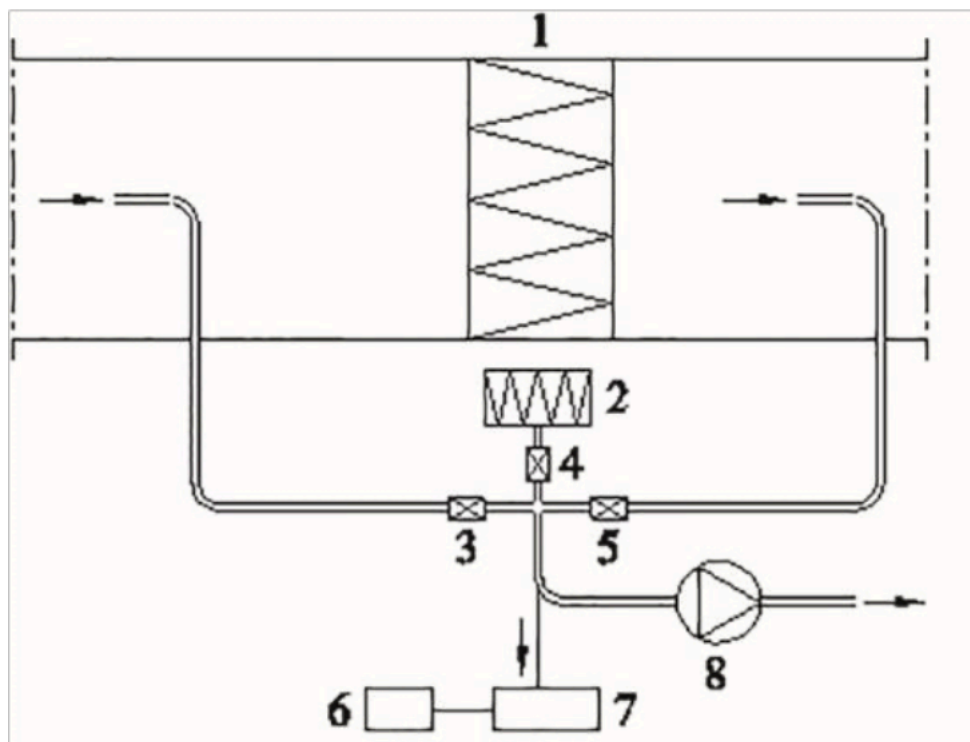


Figure 27 Aerosol sampling system with three-way valve for commuting sampling sequences

In schematic representation of sampling system shown in Figure 27, there are components:

1. Sample of flat sheet filter media to be tested
2. White area: HEPA filter that filters intake air from ambient
3. Upstream sampling line valve
4. White area valve
5. Downstream sampling line valve
6. Computer for automatic commuting and data processing
7. Optical Particle counters
8. Auxiliary pump for suction of sampling flow



Geometric designing of duct and sampling probe is essential for providing reliable test result, reducing loss factors due to transport, diffusion, and sampling. Isokinetic sampling is important to ensure that the sample of particles directed towards the measurement instrument is representative of the particles in the duct without having a size bias requiring identical velocity of air entering the sampling probe to the velocity of air in the duct.[32] And this condition is verified as equal ratios of probe flow to probe cross section area and duct flow to duct cross area so that velocities are equal for air entering both probe and duct or within 10% similitude is required by standards for isokinetic sampling. Axis of probes is parallel to that of sampling duct toward incoming air stream. And positioning of probes should at center of duct as well as sample area of flat sheet media, due to velocity profile in case of laminar flow of air stream. As required by standards, air velocity uniformity in the test duct across 9 points and aerosol uniformity should be done biannually.[7]

Commutation between valves is controlled by automatic program available on computer, by setting primarily sampling cycle time, sampling cycle numbers, purge time, sampling flow parameters, particle counters type and aerosol type before each test. The computer program proceeds as predefined sequences during test. It is necessary to check same setting on particle counters as that of program.



### 3.34 Test procedures

Following procedures are done daily or changing test setting as required by standards,

#### 1) Setting particle size channel of particle counters

Channel	Lower limit [ $\mu\text{m}$ ]	Upper limit [ $\mu\text{m}$ ]	Geometric mean [ $\mu\text{m}$ ]
1	0.09	0.10	0.09
2	0.10	0.12	0.11
3	0.12	0.15	0.13
4	0.15	0.20	0.17
5	0.20	0.25	0.22
6	0.25	0.30	0.27
7	0.30	0.40	0.35
8	0.40	0.55	0.47
9	0.55	0.70	0.62
10	0.70	1.00	0.84
11	1.00	1.30	1.14
12	1.30	1.60	1.44
13	1.60	2.20	1.88
14	2.20	3.00	2.57
15	3.00	4.00	3.46
16	4.00	5.50	4.69
17	5.50	7.00	6.20
18	7.00	10.00	8.37

Table 3 Particle size channels setting for tests



As lists specifically in Table 3, for OPS3330 particle size channel is set prescribed by ISO 1690-2:2016, which consists of twelve logarithmically spaced particle size channels. For LAS3340A 6 channels are added for particle size ranges from 90nm to 300nm.

## 2) Zero particle test

In this step, one empty perforated plat is used at sampling section, optical particle counter is monitoring continuously the particle as sequences: white area → upstream → downstream, until each step particle detected lower than 10 for cycles ensuring background particles are purged

## 3) Correlation ratio

Once second step is checked, correlation ration is done keeping same configuration as efficiency test, after opening aerosol generator valve and waiting aerosol generation stabilized. This is for correcting upstream reading and downstream for efficiency tests, reducing error introduced by commutation. This test should be done daily or after filtration velocity is changed. Ideally this ratio should approximately one, and a range for check referring standards.

- ◆ 0.30-1.0 micrometers: 0.90% to 1.10%
- ◆ 0.30-1.0 micrometers: 0.80% to 1.20%
- ◆ 3.0-10 micrometers: 0.70% to 1.30%

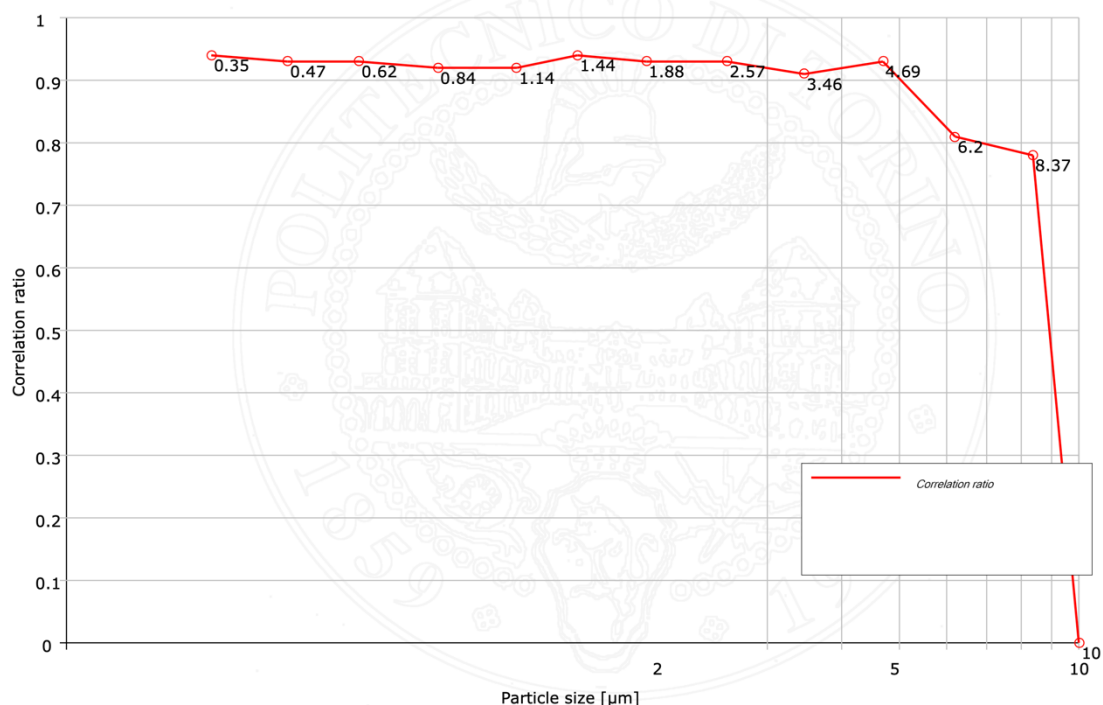


Figure 28 Example of results from correlation ratio test

## 4) Efficiency test



After results of step 3 are reported, samples are replacing the perforated plate. In this step, total particle number concentration generated decreases due to air resistance presented by flat sheet media samples. So proper adjustments on compressed air flow rate is usually needed to have enough particles for accurate particle sensing. Once aerosol stabilized after adjustment, test starts with following set up for testing nanofiber samples:

- ◆ Filtration velocity = 10cm/s for ease of stabilized air flow
- ◆ Sample cycles number = 6, one cycle consists of upstream sampling interval and downstream sampling interval, and purge time before each sampling interval for clean particles in ducts from last cycle. As lists in Table 4. Fractional efficiency is calculated automatically by program when finishing of downstream sampling. At the end of sixth cycle, additional purge and upstream sampling are performed to take average with previous upstream reading, and final fractional efficiency value is calculated as average result of six cycles with uncertainty not greater than 10%, ideally lower than 5% at each size channel. Otherwise, test should be repeated increasing cycle time.
- ◆ Time for sampling and purge = 45s as default, in case of uncertainty >10%, time should be increased to 60s and repeat the test. Minimum cycle time required by standards is 30s for having time to sense enough number of particles of each size channel
- ◆ Total time intervals are 26 for efficiency test, 4 intervals for each cycle, and additional two at the end of test. That of correlation ration test is 24 intervals without last two.

All test procedures and set up parameters are same for both tests using OPS3330 and LAS3340A, except sampling flow rates and OPC sound diameter.

- ◆ OPS3330 – 1L/min with sampling nozzle D=5mm
- ◆ LAX3340A – 0.095L/min with sampling nozzle D=2mm

	Cycle 1	Cycle 2	Cycle 3	Cycle 4	Cycle 5	Cycle 6	
U	P S	P S	P S	P S	P S	P S	P S
D	P S	P S	P S	P S	P S	P S	

Table 4 Sampling Sequences

- ◆ U: Upstream
- ◆ D: Downstream
- ◆ P: Purge



- ◆ S: Sampling
- ◆ Efficiency at each cycle  $E = 1 - \frac{\text{Downstream counts}}{\text{Upstream counts}}$
- ◆ Sampling counts iterates by taking average with previous counts i.e., Upstream sampling at third cycle =  $\frac{N_3 + \frac{N_1 + N_2}{2}}{2}$ , where N is number of particles counted for sampling intervals
- ◆ Efficiency values at each cycle is recorded, as results, average efficiencies of all cycles and uncertainties are reported

### 3.4 Particle loading test

For studying mass loading behavior of flat sheet media, model TSI 8130A is used. This model is widely available on market, generally used for the purpose of testing masks under regulation of EN143:2007, ISO 16900-3, 42 CFR 84, GB 2626. According to different specifications of standards, special designed atomizers are available to produce aerosol particles with type and size distribution, lists in Figure 29.

<b>Specifications – Aerosol Generation</b>				
	<b>EN 143:2007</b>	<b>ISO 16900-3</b>	<b>42CFR part 84</b>	<b>GB 2626</b>
<b>Oil Test</b>	<b>Paraffin</b>	<b>Paraffin</b>	<b>DOP</b>	<b>Paraffin or DOP</b>
Equipment	Atomizer	Atomizer	Atomizer	Atomizer
Equipment	Light scattering photometer (scattering at 45°)	Light scattering photometer (forward scattering, max 45°)	Suitable light scattering photometer or equivalent instrumentation	Defined by concentration range and precision accuracy
Test Flow Rate	95 L/min	to be recorded in report	85 ± 4 L/min (42.5 ± 2 L/min if used in pairs)	85 ± 4 L/min
Aerosol Concentration	20 ± 5 mg/m <sup>3</sup>	15 to 35 mg/m <sup>3</sup>	≤ 200 mg/m <sup>3</sup>	50 - 200 mg/m <sup>3</sup>
Count Median Diameter	0.16 µm	0.16 to 0.21 µm	0.185 ± 0.020 µm	0.185 ± 0.020 µm
Geometric Std. Deviation	≤ 2	≤ 1.4 to 1.8	≤ 1.60	≤ 1.60
Temperature	Ambient (24 ± 8 °C)	Ambient (16 to 32 °C)	Ambient (25 ± 5 °C)	Ambient (25 ± 5 °C)
Humidity (rH)	not defined	50 ± 30 %	30 ± 10 %	30 ± 10 %
	<b>EN 143:2007</b>	<b>ISO 16900-3</b>	<b>42CFR part 84</b>	<b>GB 2626</b>
<b>Salt Test</b>	<b>NaCl (Sodium Chloride)</b>	<b>NaCl (Neutralized)</b>	<b>NaCl (Neutralized)</b>	<b>NaCl (Neutralized)</b>
Equipment	Atomizer	Atomizer	Atomizer	Atomizer
Equipment	Flame scattering photometer (equivalency shown for 8130)	Flame scattering photometer (equivalency shown for 8130)	Suitable light scattering photometer or equivalent instrumentation	Defined by concentration range and precision accuracy
Test Flow Rate	95 L/min	to be recorded in report	85 ± 4 L/min (42.5 ± 2 L/min if used in pairs)	85 ± 4 L/min
Aerosol Concentration	8 ± 4 mg/m <sup>3</sup>	8 to 35 mg/m <sup>3</sup>	≤ 200 mg/m <sup>3</sup>	≤ 200 mg/m <sup>3</sup>
Count Median Diameter	0.06 µm	0.06 to 0.1 µm	0.075 ± 0.020 µm	0.075 ± 0.020 µm
Geometric Std. Deviation	1.9	≤ 1.4 to 1.8	≤ 1.86	≤ 1.86
Humidity (rH)	60%	<40 % at 23 °C (± 3 °C)	30 ± 10 %	30 ± 10 %

Figure 29 Specifications on particle generation and operational range for different standards[35]

In case of studying mass loading process of fibrous filter media using ultrafine particles, solid particle of NaCl with specific particle size range as required by 42CFR part 84 is chosen for doing experiments. So, salt aerosol generator NIOSH 8118A is used, shown in Figure 30.



Figure 30 Aerosol generator NIOSH 8118A



Purposes of study includes:

- ◆ Verifying operational range of relative humidity (RH), whether within required range  $30 \pm 10\%$  and how it changes with different environmental RH
- ◆ Verifying output of aerosol generator, whether it within required range, for photometers particle size distribution upstream filter media is important for accuracy of penetration
- ◆ Study of loading behavior of media, verifying loading characteristic curve that pressure increases as function of mass loaded, whether it is the same if maintaining other variables

### 3.41 Working principle of 8130A

This type of aerosol generator filled with 3 liters of 2% NaCl solution, made by distilled water and 98% purity of NaCl. For avoiding severe degradation of solution, it should be used not exceed 24 operating hours according to user manual.[36] Special designed atomizer jet works in the same principle as Laskin nozzle described previously. Inlet of generator is connected to filter tester 8130A through compressed air line. A size selective impactor at outlet removes large droplet produced, outlet is connected to mixture manifold, so that produced aerosol particles are properly mixed with sheath flow to meet required volume flow rate. Before that, exhausting droplets pass through a heater for drying into solid particles, then neutralized by neutralizer.

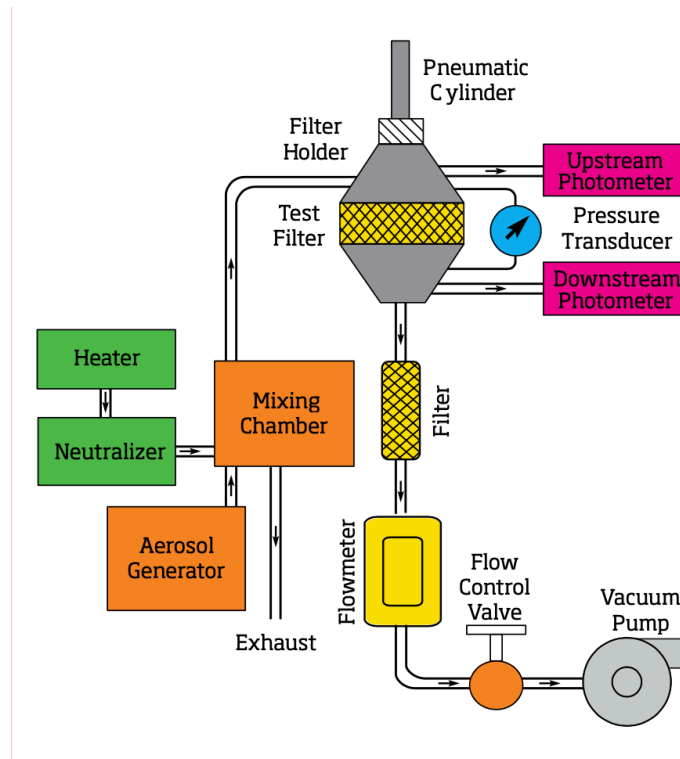


Figure 31 Schematic representation of 8130A[36]

As shown in Figure 31, the measurement of penetration is provided by a pair of photometers,



as previously mentioned, photometers do not count particle. Instead, light intensity scattered by a cluster of particles is converted into voltage signal by photometer, and penetration value is calculated as ratio of downstream voltage to upstream voltage, the precision of penetration is up to 99.9999%. Sensitivity of two photometers is different, because concentration of particles at downstream is usually order of magnitude lower respect to that of upstream. More sensitive photometer is used at downstream. Correcting voltage level of two photometers is needed before calculation of penetration, correlation factor (CF) is calculated when filter media is absent:

$$CF = \frac{\text{Downstream voltage} - \text{Downstream background voltage}}{\text{Upstream voltage} - \text{Upstream background voltage}}$$

Penetration is calculated when filter media is presented:

$$\text{Penetration} = \frac{\text{Downstream voltage}}{\text{Upstream voltage} * CF}$$

While measuring penetration, pressure transducer and flowmeter provides reading of air resistance in mmH<sub>2</sub>O and volumetric flow rate respectively. This configuration is essential for mass loading process, for logging pressure and penetration values in function of time.

◆ Machine warm up

8130A should be properly warmed up about 10 minutes before commencing of tests, to increase temperature of heater up to 55°C. This is for stable production of aerosol. During this phase, operational parameters such as filter holder pressure 40 psi, aerosol generator inlet pressure 30 psi and make up air flowrate 70 l/min are set according to protocol. Valves in Figure 32.



Figure 32 Valves for adjust pressure and flowrate

### 3.42 Relative Humidity during tests

Relative humidity reading is not given by machine during tests, so external relative humidity sensor could be helpful to monitor relative humidity changes under different environmental condition. Theoretically it is feasible to monitor from exhaust shown in Figure 31, assuming that relative humidity of exhaust air flow after being dried by heater is same as the air flow go through filter holder. At outlet of 3 meters long PTFE exhaust tube, two configurations of sensor arrangement are considered for RH measuring.

- 1) In Figure 33 left part showing first configuration, using low-cost sensor nova fitness SDS011 equipped with MKR ENV shield which provides RH reading continuously every 2 seconds as programed during tests. However, results are strongly affected by mixing of flow, so no meaningful readings are made.



Figure 33 Measurement configurations: Left Nova fitness SDS011 with MKR ENV shield, Right RIP 02/02 temperature and RH probe inside tube

- 2) In Figure 33 right part showing another sensor arrangement for measuring RH, with detecting probe plugged in the outlet of tube. This configuration gives reliable measurement as if no mixing of flow takes place inside tube, but cannot provide continuous readings as first configuration, instead, readings are made every 15 minutes during test.
- 3) Comparison between two configurations is made during test. In Figure 34 showing measured trend of RH and PM2.5 concentration of 2 hour after starting loading test. Environmental RH reading is 41% and trend of RH read by low-cost sensor is quite stable around 40% during test. While RIP 02/02 gives RH reading of 29%. Those readings confirm that measurement of SDS011 is strongly affected by mixing of the outlet flow with environmental air.
- 4) Only reading of RIP 02/02 is considered. However, RH of exhaust is still not accurate since it is affected by temperature change along the exhaust tube. Better solution to give more accurate reading is to measure RH at filter holder section using hygrometer with specific dimension which is not available for now.

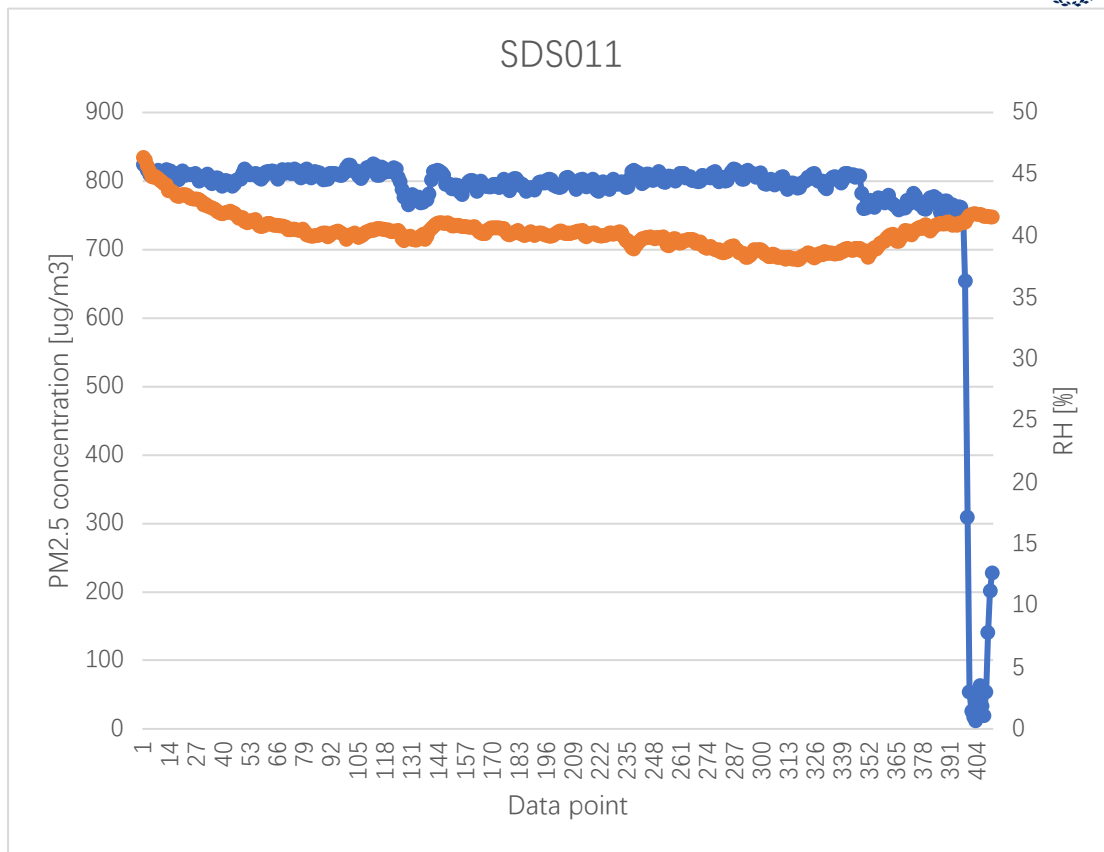


Figure 34 Continuous reading of two hours using low-cost sensor during test, RH in orange, PM2.5 in blue. Each data point represents average reading in 20 seconds.

As detected by RIP 02/02 probe during tests under different environmental condition, results are listed in Table 5. The RH during operation of 8130A is stable within range.

Test	Temperature [°C]	Environmental RH [%]	Barometric Pressure [kPa]	RH at Exhaust [%]
1	23.3	42.3	997	29.6
2	22.8	13.6	987	29
3	20.1	32.6	983	31
4	19.8	34.6	977	31

Table 5 RH readings under different environmental condition

### 3.43 Scanning Mobility Particle Sizer

For checking particle size distribution at upstream of filter media, Scanning Mobility Particle Sizer (SMPS) model TSI 3938 is used for count particle number from 10nm to 1000nm based on electrical mobility of particles. In left part of Figure 35 showing arrangement of 8130A with SMPS. The cylindrical sampling shell is placed between filter holds, with 4 sampling outlets symmetrically and equally spaced at wall of shell connected with inlet of DMA. This arrangement is for uniform sampling of aerosol in all flow direction. Such operation is done at the begin and end of each loading test.

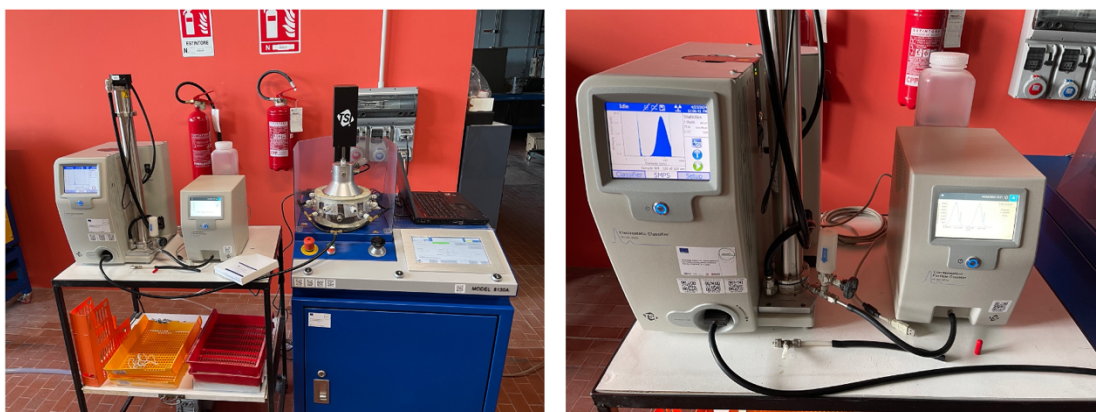


Figure 35 Left: Arrangements to sample upstream aerosol Right: Connection between DMA (Differential Mobility Analyzer) and CPC (Condensation Particle Counter)

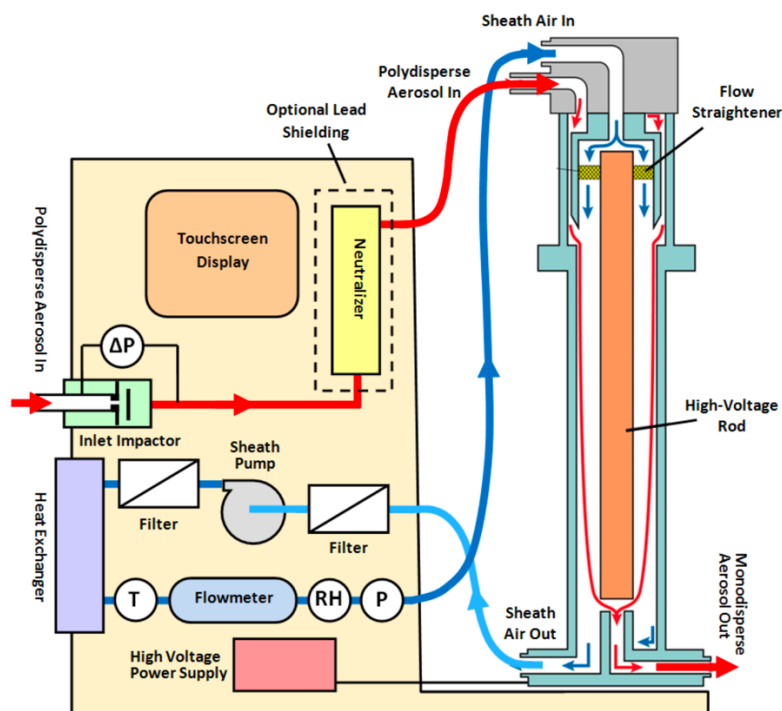


Figure 36 Schematic of electrostatic classifier (left part) and DMA (right part)[37]



Working principle of SMPS is briefly introduced before, more detailed information refers to working manual[37]. Here some technical issues are concerned on sampling and measuring. Refers to schematic of electrostatic classifier and DMA in Figure 36, impactor is useful for measuring inlet air flow and allow connection with tube. Its nozzle size selection is based on sampled aerosol air flow (Table 6) for better accuracy and determine the upper bound of detection range. In the case of study, aerosol inlet flow is 1L/min so the nozzle size 0.0508cm is selected (Figure 37 left). To be coupled with impactor, an equalizer (Figure 37) is used to adjust flow rate of CPC so that DMA can work in lower flow rate that CPC. The equalizer is adjusted so that CPC works in 1L/min.

Aerosol Inlet Flow Range(L/min)	Nozzle Size (cm)
0.2 to 0.8	0.0457
0.3 to 1.0	0.0508
0.6 to 2.1	0.071

Table 6 Impactor selection[37]

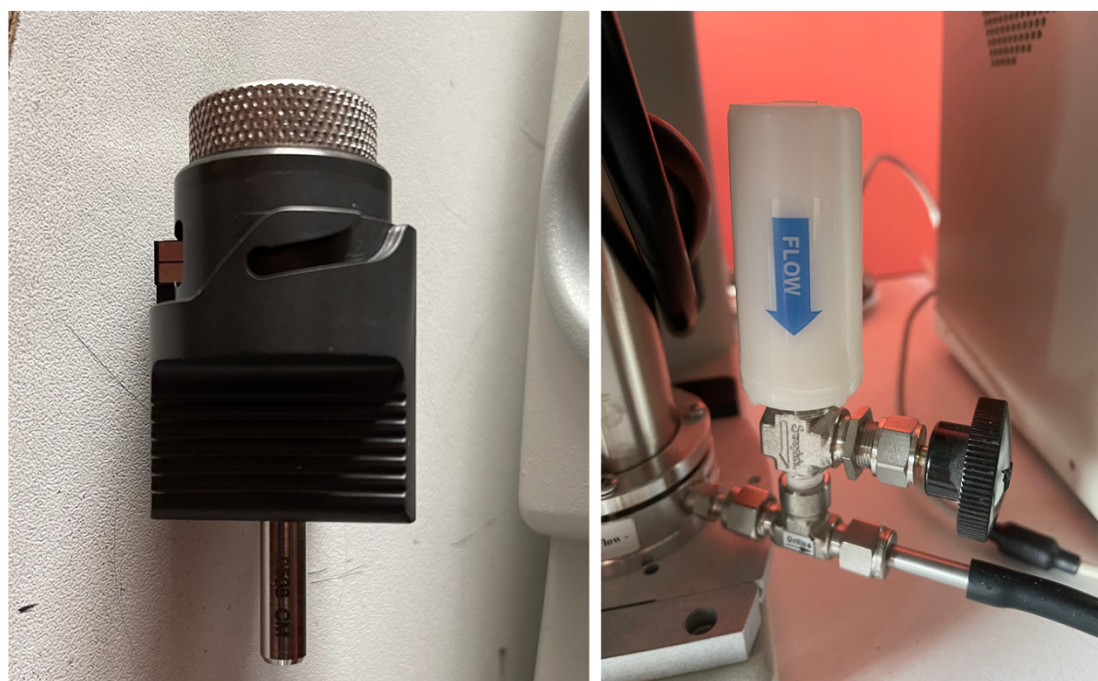


Figure 37 Left Impactor selected Right Equalizer

Health flow is important for assessing aerodynamic behavior of particles for accurate measuring. As suggest by instruction, 10L/min of health flow is set because with 10:1 heath to



aerosol ration, SMPS measuring particles within 5% accuracy.

Overpressure of sampled aerosol flow is crucial for avoiding damages of DMA. Without precisely knowing how large overpressure is, it is better to use a three-way junction (Figure 38) to release pressure of sampled air before impactor inlet as suggested by technician. However, with T junction might introduces error when measuring.



Figure 38 T junction

For verifying whether T junction affects measurement of particles and whether overpressure of sampled air is over limit of SMPS. A test is carefully done with direct connection of sampling tube with impactor inlet. It turns out that even without T junction, SMPS works properly, and the results shows that T junction strongly affects measurement of particles.



Figure 39 Left: without T junction Right: with T junction



For clear comparison of results showing in Figure 39, main statistical parameters detected in two cases are listed:

---

	Number concentration [#/cm <sup>3</sup> ]	CMD [nm]	GSD
With T	8.90e03	54.3	2.27
Without T	6.64e06	81.5	1.92

---

Table 7 Comparison of SMPS reading with T junction and without

For sure that with T junction not only pressure is released but also sampled aerosol particles will be mixing with air introducing errors.



### 3.44 Test media and filtration velocity

Sample area of filter holder is 100cm<sup>2</sup> with measured diameter of 11.3cm. During loading test volume flow rate is set at 85L/min as prescribed by protocol. After warming up of machine, adjustment of flow rate is performed to stabilize it close as possible to set value. Thus, filtration velocity is calculated 14cm/s.

Two type of filter media is used for loading test, instead of nanofiber samples tested before, in order to not waste them. First media (Figure 40) is standard media sheets provided with aerosol generator, which should be used for verifying penetration data against prescribed limit at certain pressure drop, so that normal functionality of 8130A is checked. Another media is FCR filter media in the laboratory (Figure 41).



Figure 40 First filter media: Left package with information of media type Right clean media



Figure 41 Second filter media: Left roll of filter media Right pieces of media cut from roll



For second type of filter media, considering inhomogeneity of surface, all cut pieces is taken from center part of roll media.

In case of loading test, filter media are directly clamped within filter holder, without mosquito net used before. Because for fiberglass type media mechanical resistance is enough higher than nanofiber media, so protection is not necessary. Besides, mosquito net will affect loading results.

Before each test, clean samples are weighted by Sartorius balance (Figure 42) with precision up to two digits after decimal point of milligram as required by 8130A for gravimetric test. FCR media pieces are cut in way that it can be put inside balance.

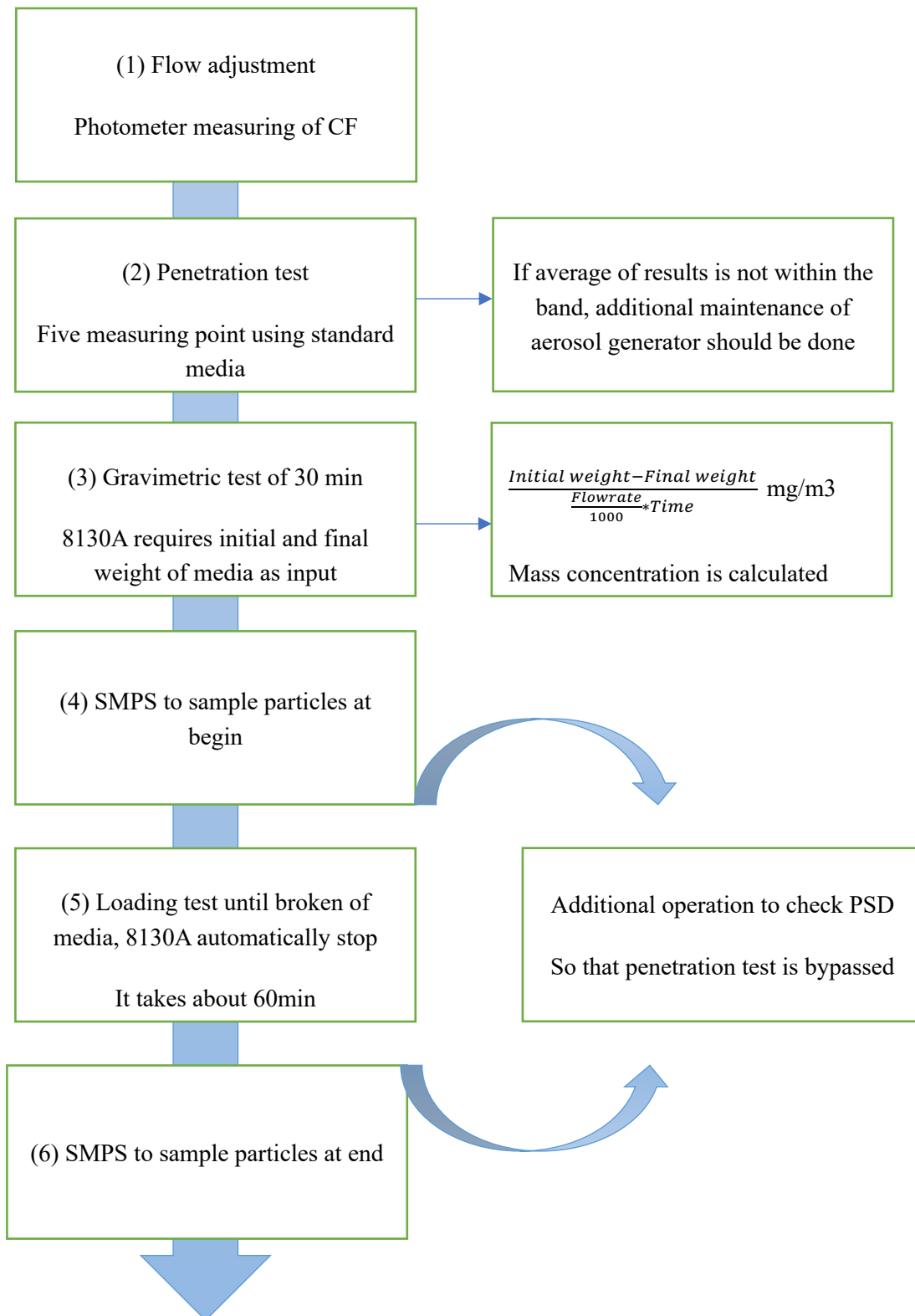


Figure 42 Sartorius balance with its precision



### 3.45 Test procedure

Following flow chart describe operational procedure after 8130A being warmed up.





### 3.46 Penetration test results

Penetration test is measuring particles penetrate media  $P = \frac{\text{downstream concentration}}{\text{upstream concentration}}$ , regardless upstream particle size distribution (PSD). So, it is important to do five penetrating tests and comparing data point with provided band to check upstream PSD. As following graphs. Data points are shifted toward higher resistance with lower penetration because loading effect of solid particles (Figure 43).

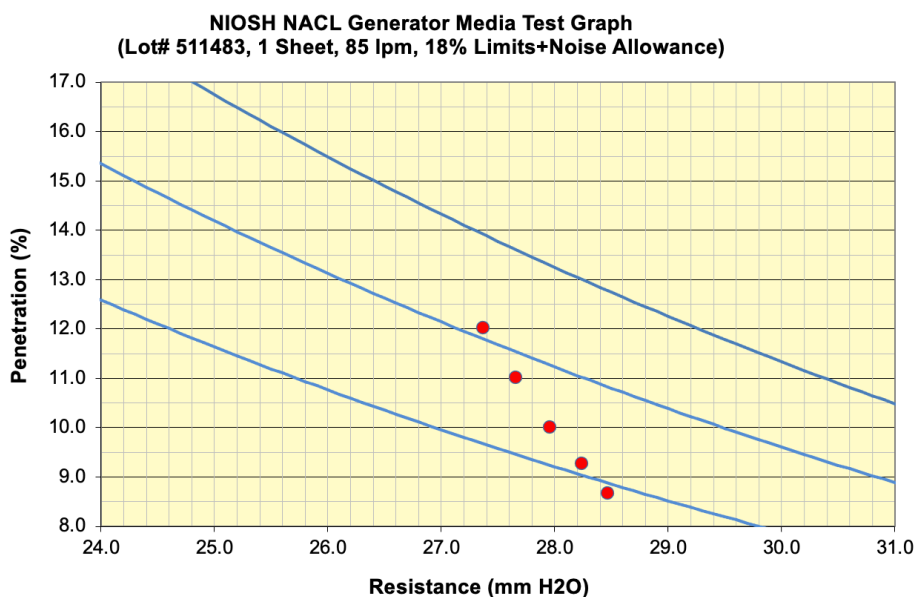


Figure 43 Penetrating test results plotted against band provided

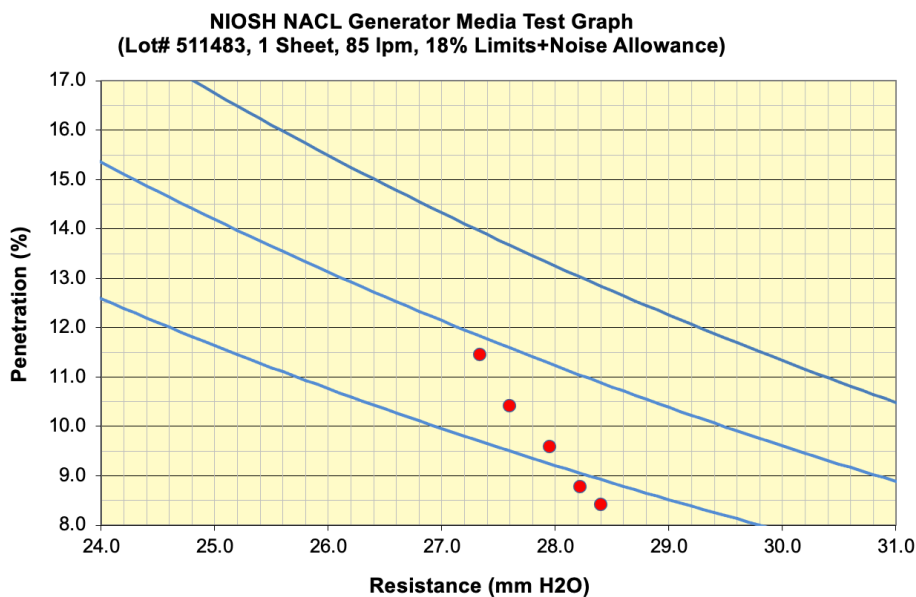


Figure 44 Five data points are shifted while consuming NaCl solution



Comparing Figure 43, Figure 44 and Figure 45, while salt solution is consuming during operation, results point of penetration test are moving downwards so that penetration test is no more passed (Figure 45) even operating hours do not exceed 24h. Those data mean that aerosol particle size distribution at upstream is altered. More large particles produced leads to lower penetration because large particles are more easily captured. And particle clogging faster lead to higher resistance detected. This explanation can also be checked with gravimetric test results later.

Figure 46 shows data points moving upwards after changing the solution and refilled up to 3L.

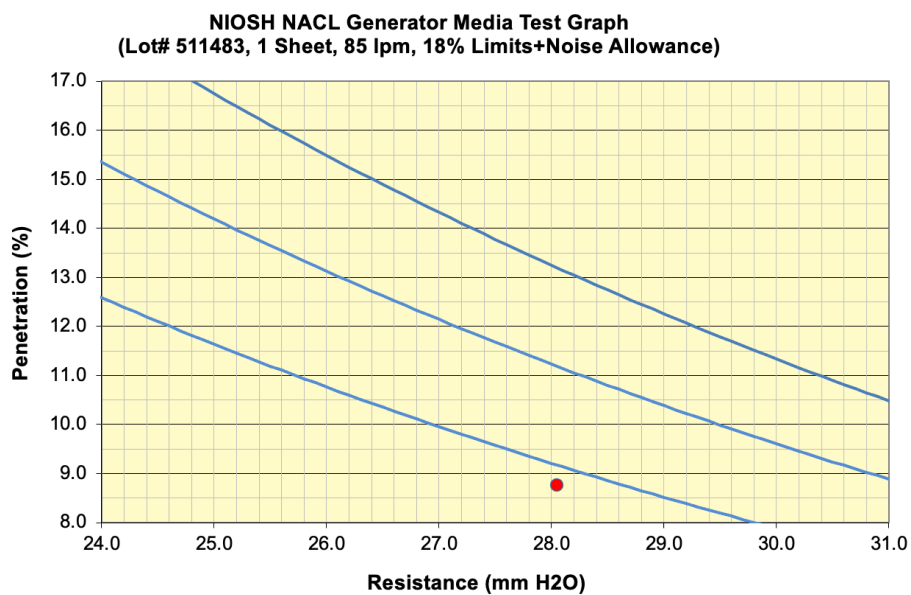


Figure 45 Five data points are out of range because solution is consumed too much

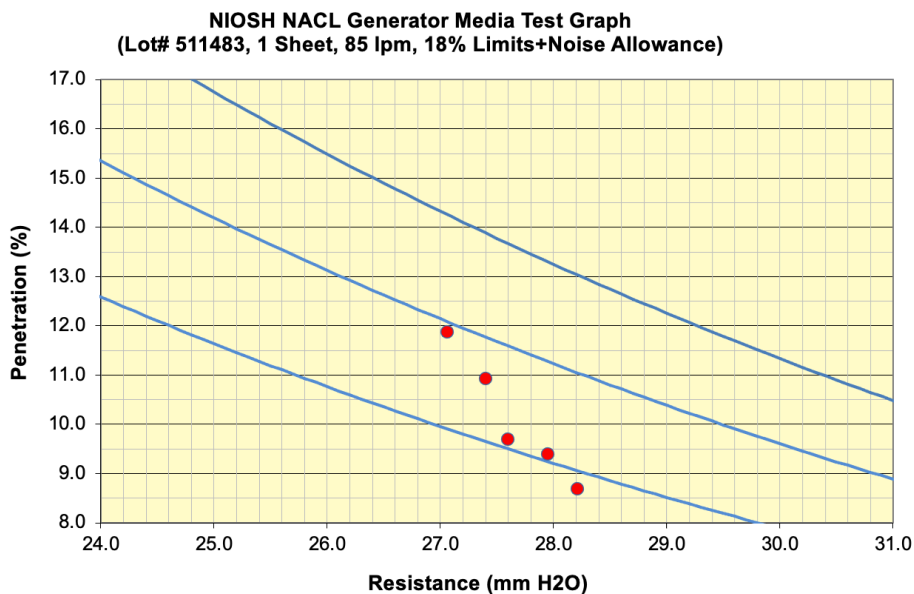


Figure 46 After change and refilling the solution, data points are moving upwards



### 3.47 Gravimetric test results

Gravimetric test measures mass concentration, by weighting tested media at the begin and end. Mass of particle captured is influenced by particle size distribution as penetration do. Although mass concentrations are detected within the indicated range  $20 \pm 5 \text{ mg/m}^3$ . It is observed from the results listed in Table 8, mass concentration is increased while solution is consuming, so more large particles are captured. As assuming particle size distribution is log normal, this means higher geometric standard deviation is induced by lowering of solution level. After refilling solution in generator up to maximum level, mass concentration is restored in lower value.

Test	Penetration test	Average Resistance [mmH <sub>2</sub> O]	Average Penetration [%]	Mass Concentration [mg/m <sup>3</sup> ]
1	Passed	27.4	10.818	16.455
2	Passed	27.9	10.196	17.969
3	Passed	27.9	9.728	17.911
4	Not passed	28.6	7.580	18.388
5	Passed	27.6	10.110	16.534

Table 8 Results of penetration test and gravimetric test

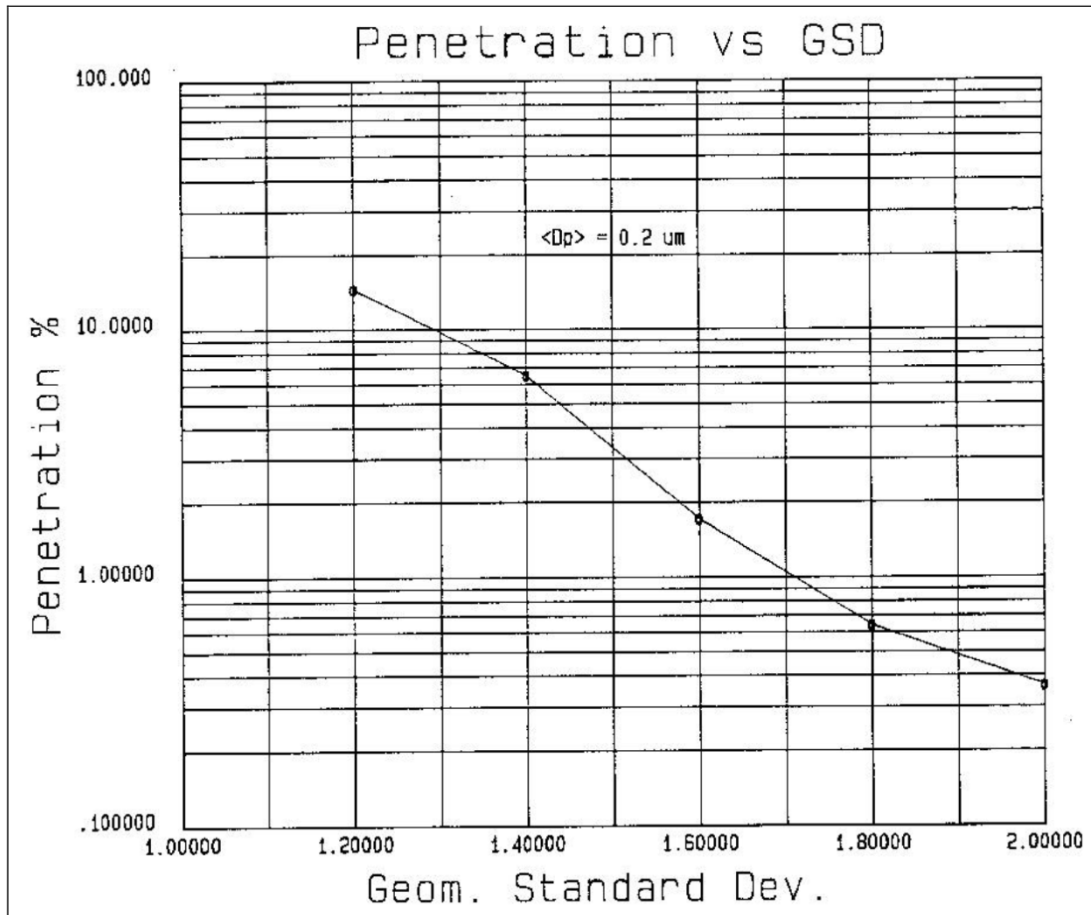


Figure 47 Penetration as function of geometric standard deviation[36]

In service manual of 8130A is providing a relation between penetration value and GSD of particle size distribution, without indicating the cause of variation of GSD or effect of decreasing liquid level of solution. For reaching the conclusion that mass concentration is decreased because of changes on GSD or lower production of particles, study of particle size distribution during tests at different liquid level is needed.

### 3.48 Particle size distribution

SMPS is used to check the alteration of PSD. With impactor nozzle size of 0.0508cm the cut off size is 230nm as shown in Figure 48. Particles larger than cut off size is excluded, but detected spectrum is almost complete and similar to lognormal distribution. So, count median diameter and geometric standard deviation are approximately same to that of full spectrum of aerosol produced by generator. Possible solution for improving this issue is combining SMPS with OPC to detect large particle simultaneously, but some technical issues for aerosol sampling are present.

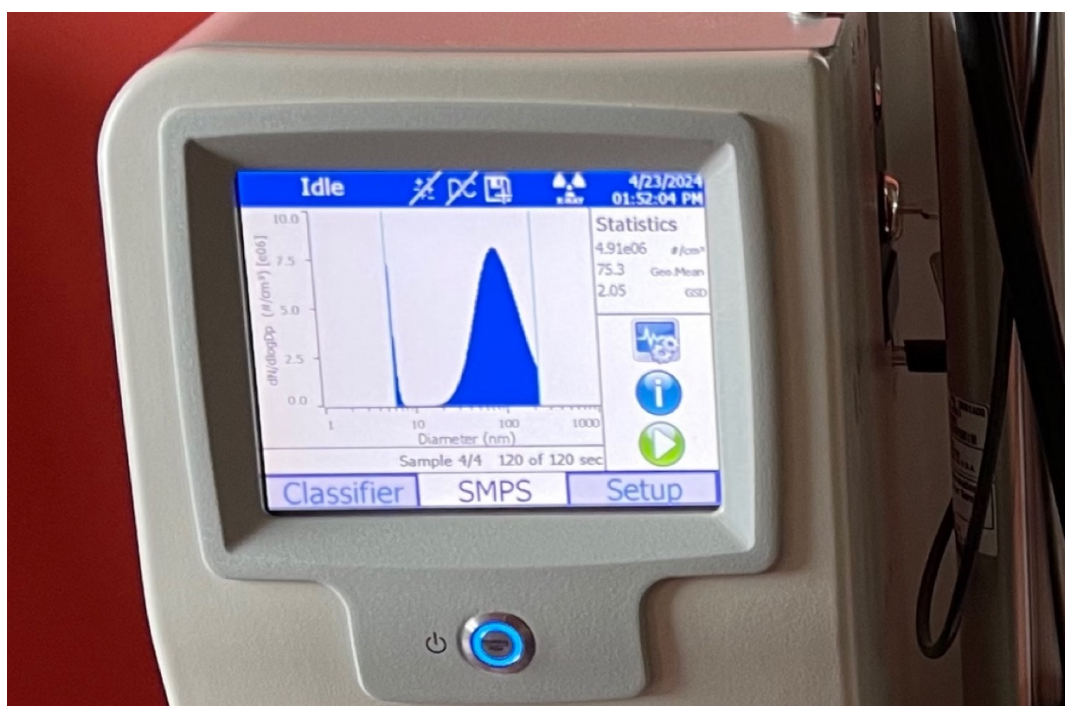


Figure 48 Detected size distribution of particles with statistical parameters

At begin and end of each loading test, measuring of PSD is done with 4 sampling cycles and 120s for each cycle. Results are reported as average of 4 cycles. For each test, average is taken of results at begin and end.

For better visualization of detected results, statistical parameters for each test are reported in Table 9 and used for tuning full spectrum of PSD so that results are compared graphically in Figure 49.



Test	1	2	3	4	5	6	7	8	9
CMD [nm]	82.7	80.0	81.3	77.3	74.8	78.7	74.4	76.5	77.4
GSD	1.85	1.90	1.91	1.94	2.07	1.82	2.09	2.00	1.99
Concentration [10 <sup>6</sup> #/cm <sup>3</sup> ]	5.04	4.97	4.98	5.72	5.02	5.30	4.71	4.34	3.94

Table 9 Statistical parameters for each test

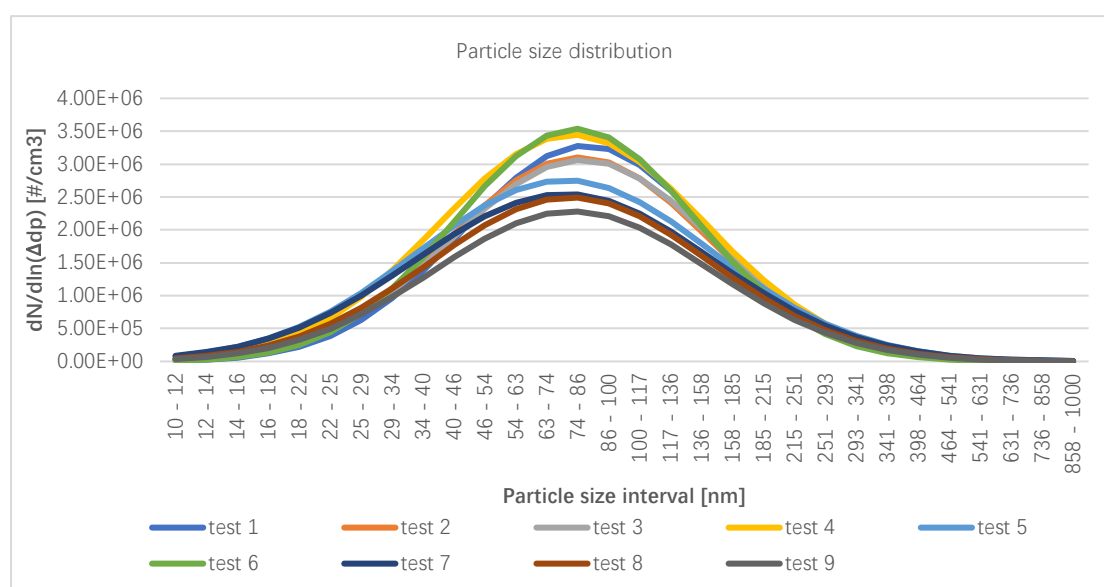


Figure 49 Particle size distribution for each test

It is concluded that count median diameter is verified within prescribed range of  $75 \pm 20$  nm, with GSD slightly higher than indicated threshold 1.86. From gravimetric test results, mass concentration decreasing as solution consuming, GSD shows similar trend but changes in small value. For number concentration, it decreases along tests. In Figure 49 curve of each test is ordered chronically, and each test represents 2 hours of operation. After being substituted the solution and refilled into maximum liquid level, the number concentration of PSD increased to highest level at test 4. The conclusion of those tests is that, constantly change the solution maintaining highest liquid level is essential for repeatable production of particles with desired PSD. Those test result can be used as indications of how PSD changes with operating hours so that solution need to be substituted if PSD is out of range.



### 3.5 Characterization of test rig for RH control

The objective of this part is to study the method for doing loading test under specific air flow conditions. Apart from air flow rate control, which is already a functionality of first test rig, the second test rig (Figure 50) controls also the temperature and relative humidity. As required by client, Ahlstrom filter media should be tested at fixed air flow velocity 10cm/s and at 23°C and 42.5% RH. The whole characterization procedure includes initial air resistance and efficiency, particle loading behavior of media and filtration performances after being loaded.



Figure 50 Test rig for RH control

Air resistance of media is not affected by temperature and RH, so there is nothing different with tests already done. The first test rig does not provide accurate pressure readings during tests because of turbulent effect especially in case of small hole size being used. For avoiding the turbulent effect, perforated plates with large hole diameter 160mm are used in case of testing Ahlstrom filter media since dimension of media is larger than nanofiber media. At air flow of



10cm/s, the air flow rate using 160mm hole is calculated around 121SLPM. The results of test rig are than compared to the results of TEXTEST for calibration.

Efficiency test is sensible to RH according to particle capture theory, so initial efficiency test and loaded efficiency test should be kept on same condition as loading test. For efficiency test, solid salt particles are used for charging the filter media. To have PSD inside detecting range of OPS3330, 20% KCl solution is used to have submicron particles for tests. Instead for loading test, 2% KCl is used for having ultrafine particles charging the filter media, this is similar to the case of 8130A. Two atomizers are used for producing particles with different range of number concentration. For having enough particles to perform efficiency test without exceeding maximum reading limit of OPS3330, TSI 3079A is used because it produces moderate number of particles. Another atomizer available is Topas ATM 230, it is more suitable for loading test for producing higher number concentration of particles thus reducing time requiring for loading. Different models of atomizer might produce different PSD, so it is essential to monitor PSD constantly during tests. The number concentration of particles produced by atomizers are regulatable on inlet flow rate, but is not indicated in relationship of inlet airflow, so the first step is to tuning proper inlet air flow for test purpose.

After particles being atomized, the charge distribution is not known. For minimizing the electrostatic effect on particle removing efficiency and loading behavior, neutralization of particles is needed. Neutralizer EAN 581 is used for this purpose, with adjustable ionization current and voltage level, and inlet air flow. Since the charge distribution of particles is unknown, the procedure is to tuning the operating parameters of EAN 581 so that filter media shows minimum efficiency using discharged particles because columbic force is minimized, in other word, particle charge state is in Boltzmann distribution so that fraction of particles with zero charge or single charge can be calculated.

Technical issues are presented when using atomizer and neutralizer:

- ◆ Atomizer and neutralizer introduce additional air flow using compressed air which will decrease RH inside test ducts. This means that RH is no more regulatable if air flow rate provided by neutralizer is high.
- ◆ If test purpose is at small filtration velocity, lower than 2cm/s, neutralizer is not usable. The minimum air flow rate produced by neutralizer is exceed required air flow, the upstream fan and downstream fan inside test rig will stop consequently and particles will propagate backward due to overpressure.
- ◆ The salt particles will deposit on nozzles, might reduce production of particles or even clog entirely the nozzles. Regularly cleaning of nozzles is essential to maintaining functionality of components and even avoiding further corrosion.

### 3.51 Description of test rig



Figure 51 Test rig connected with neutralizer and atomizer

In Figure 51 shows configuration for proceeding efficiency test: atomizer TSI 3079A is connected to neutralizer EAN 581, which provides discharged particles in the test rig before the mixing plenum. A saturator is shown clearly in figure, it is essential for RH control. Since water in saturator consumes rapidly during test, a suction pipe is inserted in bottle of distilled water. The suction is powered by small recirculation pump on right side of saturator tower, which also aspirate the compressed air to be humidified. The velocity of such pump needs to be adequately adjusted to enable the function; the adjustment is done by regulating electrical power in electronic control module (Figure 52).

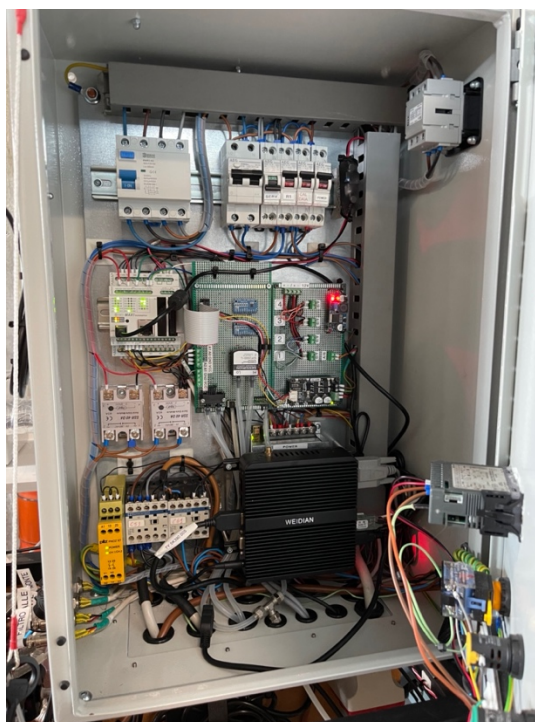


Figure 52 Electronic control modules

Apart from saturator, the basic working principle of this test rig is same as the first test rig for efficiency test. For controlling the RH, the compressed air is used in the inlet at 2°C and 3% RH approximately. The cold and dry inlet air is then ramified into 2 branches, one of them is humidified by passing through saturator. Two branches of supply air flow are mixed again before aerosol inlet, the fraction of humidified air flow can be regulated by adjusting three-way valve (Figure 53 right) which connected to 2 branches of supply air flow and mixed air as inlet of mixing plenum. In this way RH control of air flow is done and reading of RH is provided to the user by hygrometer installed in upstream of filter section. A switch for RH control by activating recirculation pump of saturator.



Figure 53 Handlebar for regulating opening of three-way valve for RH control (left) three-way



valve behind the handle bar (right)

The temperature control is also needed when specific temperature of test air flow is required. Since compressed air is at 2°C when it's produced, it will be heated up by exchanging heat along supply tube, so the temperature is strongly depending on environmental condition. In case of room temperature at 25°C, the temperature of test air flow is read by thermal couple as 22°C at the inlet of test rig. The temperature control is done by heaters installed before the saturator and before the mixing plenum, which is electrically controlled by PID. Once heaters are activated, RH value will consequently decrease.

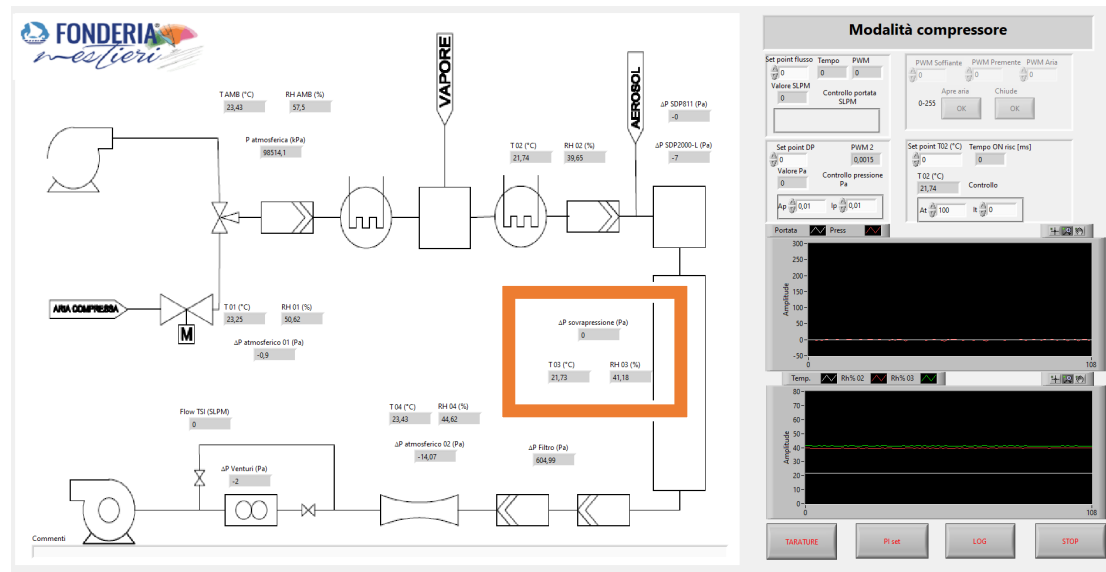


Figure 54 Control interface of test rig

In Figure 54 shows diagram of components of test rig on the left part: two operation mode is selectable, using compressed air as inlet air for RH control or using upstream fan as the first test rig. However, this diagram not correctly representing every component: 1) three-way valve is mixing humidified air flow from saturator instead on diagram the saturator is not presenting. 2) The 'VAPORE' block is no more presenting in newest vision of test rig because it has been substituted by saturator. Except those problems, the reading of sensors at several section of test rig is correctly represented: 1) T01 and RH01 provides readings at inlet of compressed air 2) T02 and RH02 provides readings after saturator and heater 3) T03 and RH03 provides readings of test air flow at filter test section, after mixing plenum, which is highlighted in diagram.

The right part in Figure 54 shows useful information to user: the upper part allow user to input parameters for controlling air flow rate, overpressure, and target temperature. Ap and Ip are parameters for PID control. The lower part consists of two graphs: 1) upper graph shows continuous reading of TSI flow meter at downstream and the overpressure at filter test section 2) lower graph shows continuous reading for RH value: red line is RH02, green line is RH03, white line is RH AMB for environmental condition.

The stability and speed of air flowrate control and overpressure control is depending on



parameters of PID: the  $I_p$  (derivative gain) should be at 0.5 for fast changing of desired overpressure and flow rate, and it should be set to 0.01 again when overpressure is stabilized for minimizing the oscillation.

The RH control is stabilized when red line (RH02) and green line (RH03) tends to be parallel straight line. They might not be superimposed because a constant difference of RH is introduced by atomizer and neutralizer. If handlebar of three-way valve is regulated, red line will have a transient curvature firstly, and green line will react consequently. The target RH is reached when green line is stabilized at fixed value. An example shown in Figure 55.

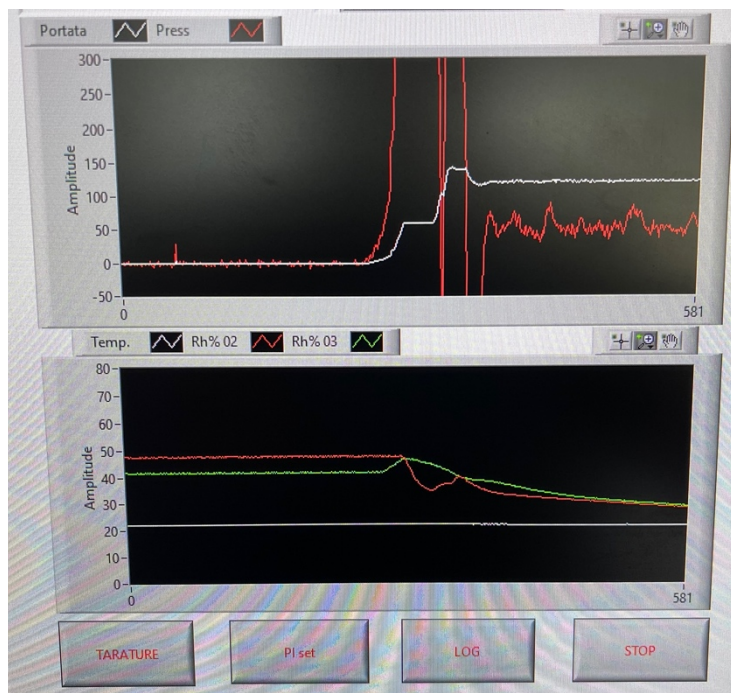


Figure 55 Graphs for overpressure, flow rate and RH control during test

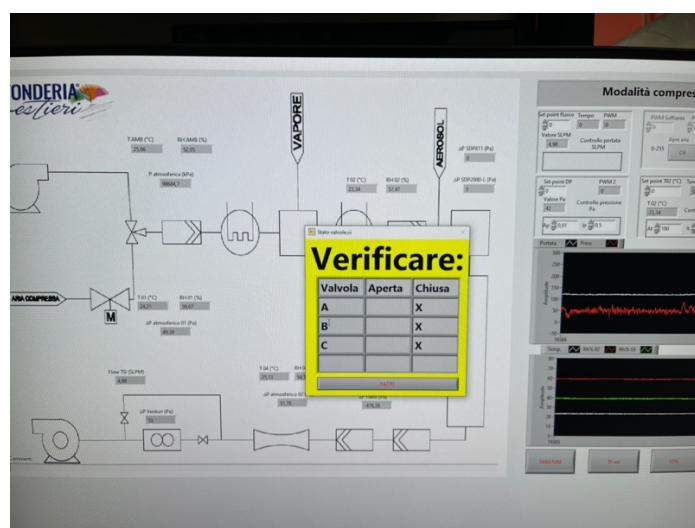


Figure 56 Check mechanical valves opening for compressed air mode



Before starting of test rig, it is required to check mechanical valve opening, which is shown on Figure 56. Valve A is pressure relief valve for ramification of air flow from compressor upstream. Valve B is opened in compressor mode, using upstream air flow provided by compressor in environmental condition. Valve C is a throttle valve for regulating air flow before downstream fan. The valve setting is required to check after selection of the operational mode, otherwise correct functionality will not be reached. In case of compressed air mode, all valves should be closed because upstream fan is not activated.



Figure 57 9mm aerosol sampling nozzle

The aerosol sample nozzle diameter is important for isokinetic sampling. The 5mm nozzle installed in test rig is substituted by 9mm nozzle so that PSD detected by OPS3330 is improved because with 5mm nozzle, large particles is not detected by particle counter which means that sampling error has occurred. After being installed 9mm sampling nozzle shown in Figure 57, the large particles in the range 3-10 micrometer are presenting.



### 3.52 Atomizer

The PSD of produced particle is depending on concentration of solution. 20% KCl produces particles with CMD higher than that produced by 2% KCl. For efficiency test, it is essential to have particle produced with range 0.3-10 micrometer.

Another important point for having particles within range for test is that number concentration is enough high for stable sampling, but it cannot exceed overload limit of optical counter. The number concentration can be adjusted by regulation outlet aerosol air flow of atomizer. (Figure 58) For efficiency test TSI 3079A is produced for moderate number concentration, the flow meter is set to 100-150 nl/h to have enough particles in all the size bins without overloading OPS3330 (Figure 59).



Figure 58 Flow meter for regulating aerosol output (TSI 3079A)

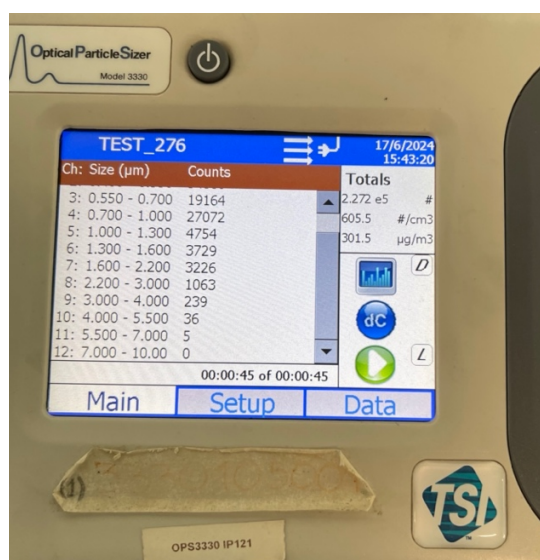


Figure 59 Particles produced by TSI 3079A at 100nl/h (1.67 SLPM)



The number concentration detected is affected by volume flow rate of test air: at lower flow rate particle counters read more particles than higher flow rate, this might be caused by mixing of air flow and aerosol in mixing plenum.

At 121 SLPM, detected number of particles using OPS3330 changes as adjusting aerosol outlet flow rate of atomizer listed in Table 10, values are average of 26 cycles for each level of aerosol flow rate:

Aerosol flow rate [nl/h]	Total number of particles in 45s [#]	Number concentration [#/cm <sup>3</sup> ]	Mass concentration [#/cm <sup>3</sup> ]
200	1.4e6	3166	520
150	1.0e6	1712	218
100	5.1e5	900	100

Table 10 Number of particles detected in changes of aerosol flow rate of atomizer (20% KCl)

The ideal number concentration of particles for efficiency test is within 300-400#/cm<sup>3</sup> or within 1% #/cm<sup>3</sup> of 350#/cm<sup>3</sup>. However, such condition is hard to maintain during tests because aerosol detected is sensitive to perturbation of test air flow.

Another atomizer Topas ATM 230 is not suitable for efficiency test because number concentration of produced aerosol is too high for OPS3330, but it is ideal for loading test.

### 3.53 Neutralizer EAN 581

Solid particles produced by atomizer carry electrostatic charges. It is difficult to study charge number on each particle. In order to minimize unknown effect due to columbic force produced by charged particles on filter media, it is necessary to neutralize the particles as much as possible so that particle capture efficiency results minimum. The method is using neutralizer, which works based on the principle of corona discharge. The working parameters of neutralizer is voltage and current level of ionization head. Two operation modes of EAN 581: alternative current mode (AC=CV) and constant current mode (DC=CC). In AC mode, voltage level of ionization head is adjustable, and current level will adopt automatically. In DC mode, controllable parameter is current level. In case of study, AC mode is used. The parameters of voltage level set point need to be tuned since aerosol charge distribution is unknown.



Figure 60 EAN 581 in operation

In Figure 60 shows 4 adjusting knobs of neutralizer: from left to right 1) Set point for negative voltage 2) Set point for positive voltage 3) Open/Close of neutralizer 4) Pressure level of inlet compressed air. Neutralization of particles needs proper inlet sheath air flow to be mixed with aerosol air flow for adjusting aerodynamic behavior of particles being neutralized. The inlet air flow is compressed air supplied in 4 bars, the working diagram shown in Figure 61.

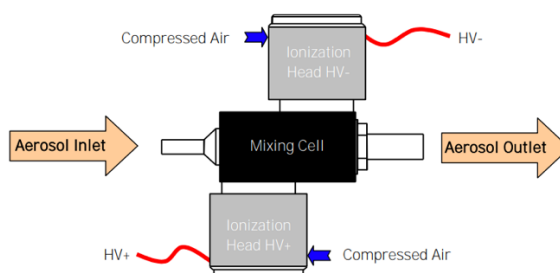


Figure 61 Mixing chamber configuration for neutralization of EAN 581



The sheath flow rate is adjustable by regulating inlet pressure, the relationship between them is provided by working manual in Figure 61:

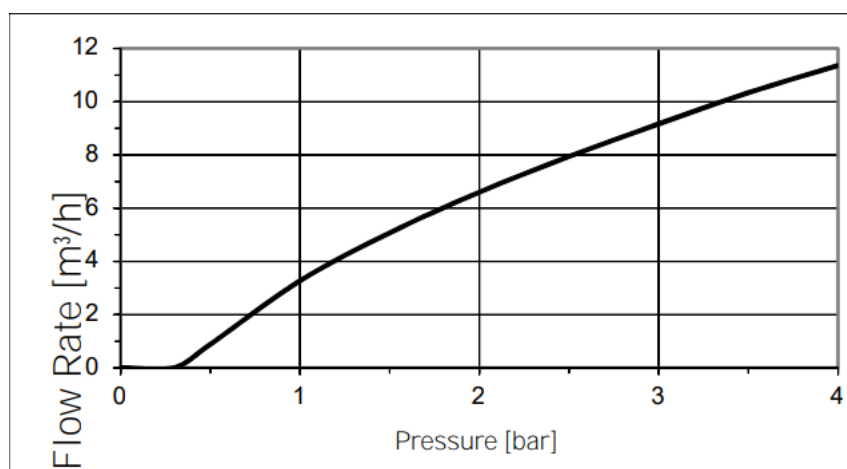


Figure 62 Mixed flow rate in relationship with inlet pressure of EAN 581

The minimum inlet pressure is 0.5 bar, for minimizing the effect on RH of test air flow by introducing neutralized air flow, the operating inlet pressure for test is set at 0.8 bar. It's worth noting that RH of test air flow is not controllable if inlet pressure is exceeding 1.5 bar because additional compressed air flow rate is too high.

A technical issue for using EAN 581 is that after activating neutralizer, particles larger than 3 micrometers are no more detected (Figure 63). This might be due to effect of mixing of air flow. However for efficiency testing, the important range of particle size is 0.3-3 micrometers since efficiency for particles larger than such range is typically about 100%, at least for media tested in the case of study.



Figure 63 Particles detected by OPS3330 after activating the EAN 581



### 3.54 Operating parameters of neutralization

The voltage level of positive and negative ionization head is the operating parameters to be tuned. It depends on number concentration of atomized particles, air flow rate, viscosity of air and RH. Theoretically higher number of particles to be neutralized means higher voltage level is need but exact relationship is still not clear.

The experimental set up for tuning is to test the efficiency of electrostatic fibrous filter media under several voltage levels (Table 11), at fixed flowrate of sheath flow and aerosol flow. The electrostatic media is to highlight the electrostatic effect on particle removing. The experimental results are then reported and compared later in result and discussion section; the minimum efficiency indicates that particles are neutralized.

Test number	Positive voltage [kV]	Negative voltage [kV]
1	0	0
2	1.4	1
3	2.4	2
4	3.4	3
5	4.4	4
6	5.4	5

Table 11 Experimental set up for tuning neutralization parameters

The tests are done in CV mode, the voltage level is set at slightly positive respect to electrostatic balance. Sheath air flow is at 2m<sup>3</sup>/h (33 l/min), aerosol flow is at 120nl/h (2 l/min). The order of tests is start from lower voltage level and increase stepwise 1kV up to 5kV, for avoiding spark generation during test. The voltage level higher than breakdown voltage of air will generate sparks which could damage the neutralizer. +5.4kV and -5.0kV are typical values indicated in test certificate of EAN 581 for avoiding spark.



### 3.55 Tested fibrous flat sheet media



Figure 64 Left) Ahlstrom media for loading test Right) Technostat FA6900NW electrostatic media for tuning neutralizer

The efficiency tests for both materials are done at 23°C and RH42.5% for consistency of experimental set up. Test results for clean filter media is reported in next section. Loading test on Ahlstrom is not done due to technical issue of SMPS. Since that reliable test results of loading test should be combined with continuous reading of PSD during test.



## 4. Results and discussion

### 4.1 Pressure drop of nanofiber media

#### 4.11 Test results

Pressure data measured by TEXTEST at filtration velocity of 1cm/s to 15cm/s.

##### 1) PAN (Polyacrylonitrile)

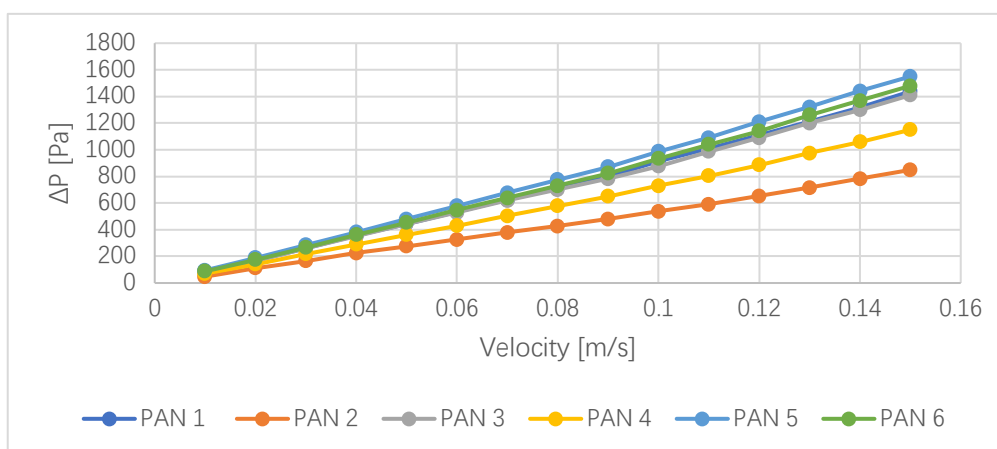


Figure 65 Air resistance test result PAN

##### 2) PAN0.4CNF (Polyacrylonitrile + Cellulose nanofibrils)

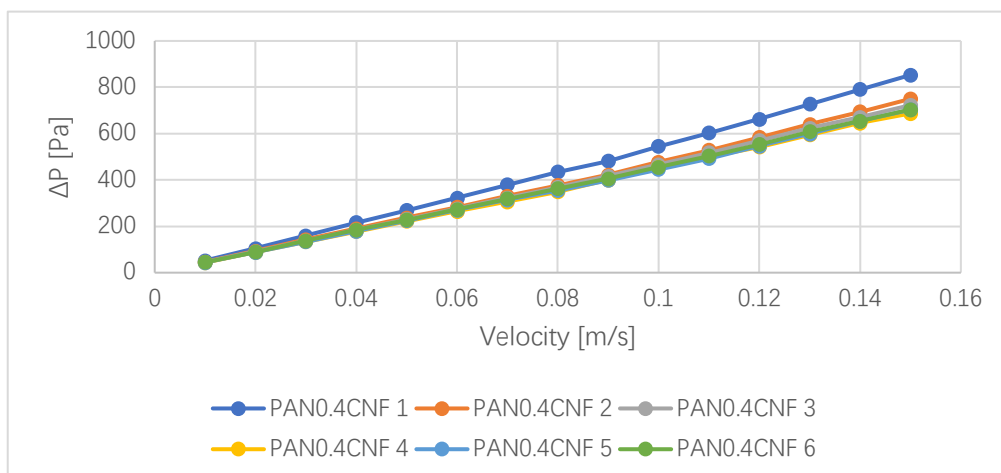


Figure 66 Air resistance test results PAN0.4CNF



### 3) PAN15CNC (Polyacrylonitrile + Caster oil + Cellulose nanocrystals)

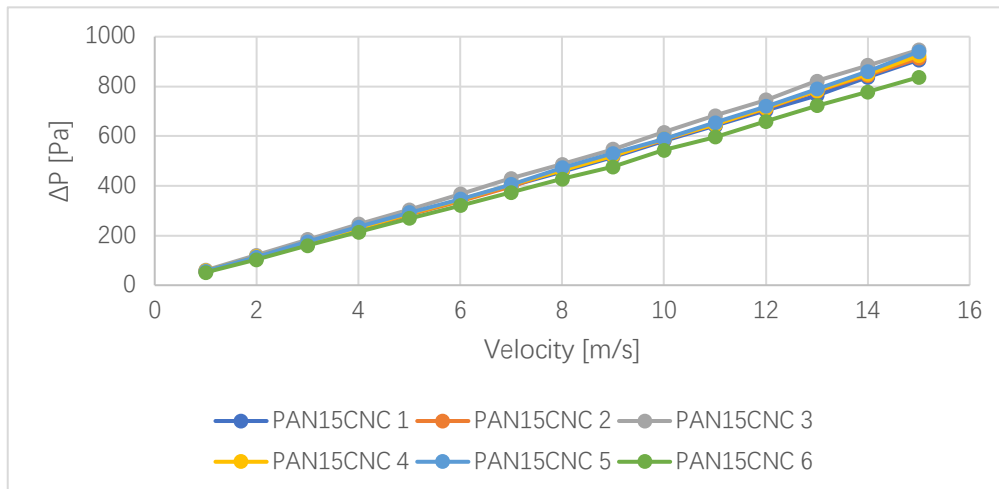


Figure 67 Air resistance test results PAN15CNC

### 4) PANCO (Polyacrylonitrile + Caster oil)

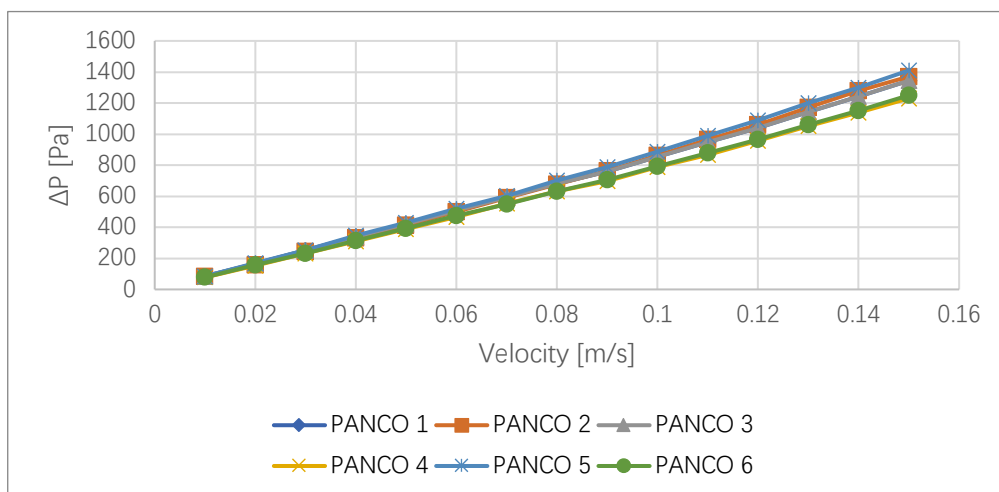


Figure 68 Air resistance test results PANCO



5) PANCO0.4CNF (Polyacrylonitrile + Caster oil + Cellulose nanofibrils)

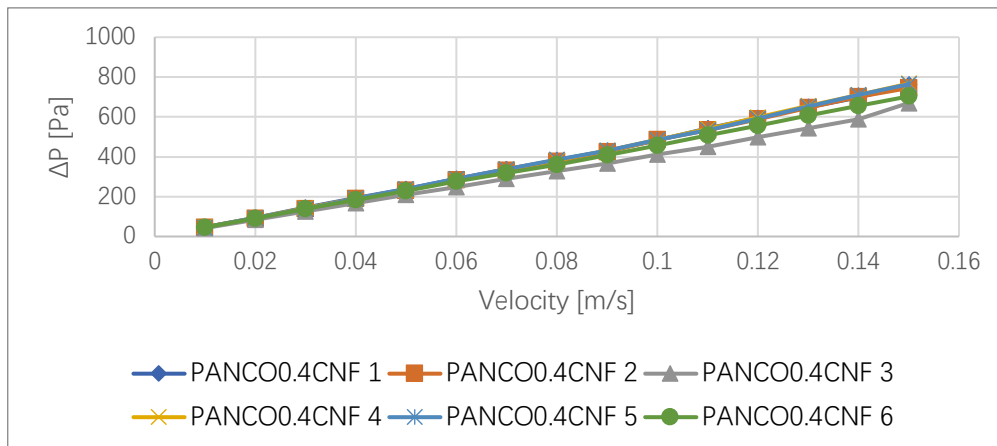


Figure 69 Air resistance test results PANCO0.4CNF

6) PANCO15CNC (Polyacrylonitrile + Castor oil + Cellulose nanocrystals)

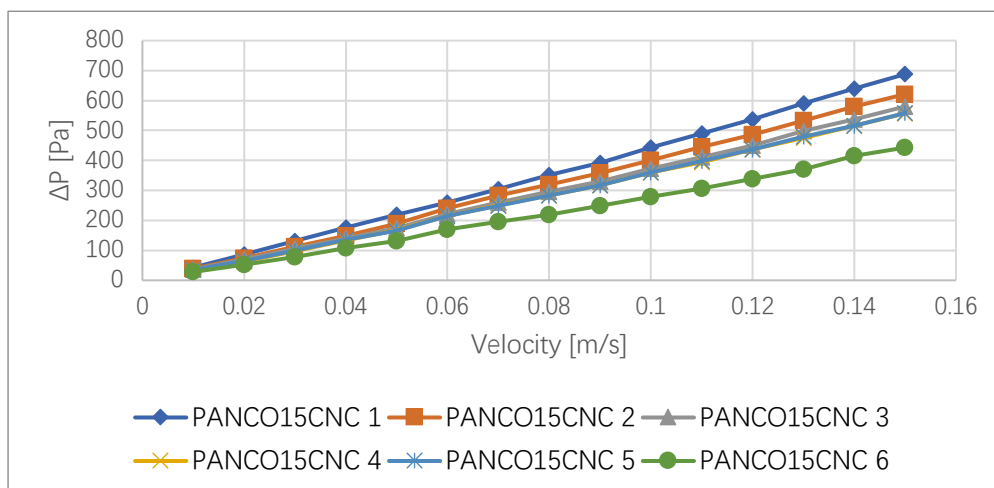


Figure 70 Air resistance test results PANCO15CNC



## 4.12 Discussion

The tested results of 36 samples, generally shows linearly increasing of pressure drop as increases of filtration velocity, which is in accordance as predicted by Darcy's law for clean fibrous filter media. However, there are some data points with slight deviation from linear trend is observed. This could be explained by realistic fibrous media with polydisperse fiber sizes, random orientation, or inhomogeneity, which are out of simplified assumptions of theory.

Slope of pressure drop increasing resulting differently for six types of media. This is because of fiber diameters, thickness and solidity are not same. However, for same type media, some samples are deviate pretty much from others. As shown in Figure 65, PAN 2 and PAN 4 results differently while other four samples have approximately same slope of trend. Same phenomenon is present for PANCO15CNC 6 in Figure 70 and PAN0.4CNF 1 in Figure 66. This could be explained by inhomogeneity of fiber distribution along surfaces, some part of area might consist of less fiber or layer of media is too thin induces lower resistance and vice versa.

For better comparison of 6 types of samples, average values of samples are reported together in Figure 71.

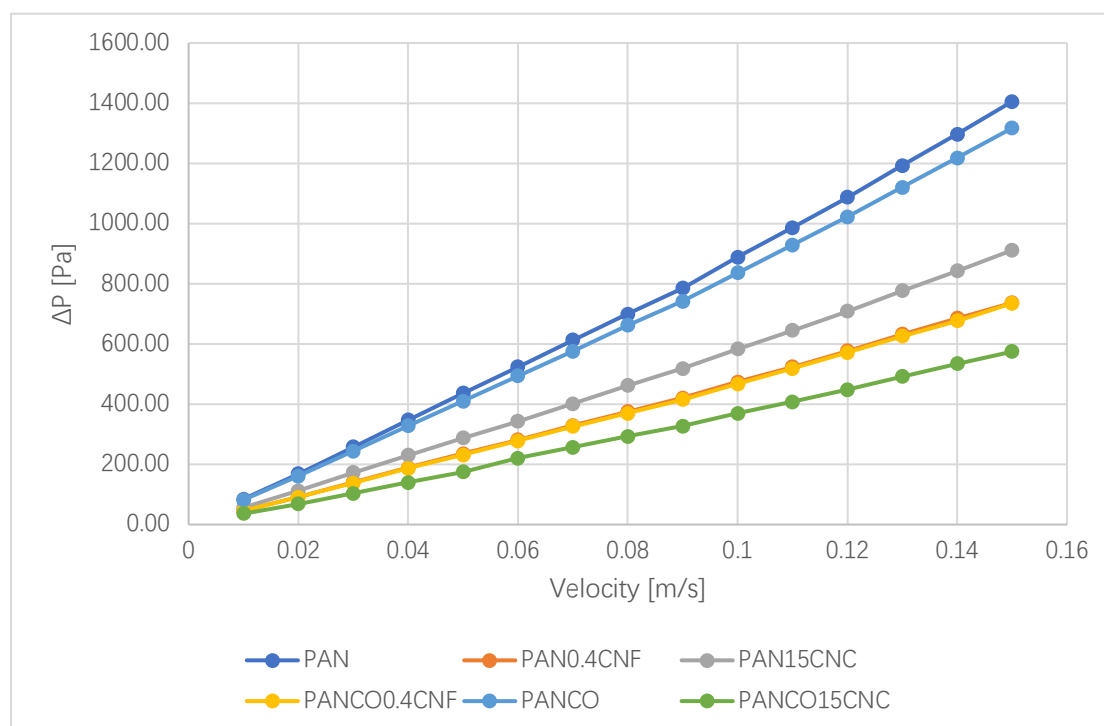


Figure 71 Comparison of 6 types of samples



## 4.13 Theoretical model

For comprehensive verification of test results, two theoretical models are used for prediction of fibrous filter media. Empirical model proposed by Davies[19]:

$$\Delta p = \frac{\mu U_0 t f(\alpha)}{d_f^2} \text{ with } f(\alpha) = 64\alpha^{1.5}(1 + 56\alpha^3)$$

For  $0.006 < \alpha < 0.3$  and laminar flow, where  $d_f$  is average diameter of fiber,  $\alpha$  is average solidity of media,  $\mu$  is viscosity of transport fluid,  $U_0$  is average filtration velocity,  $t$  is thickness of media.

Second model considered slip effect due to large Knudsen number, proposed by Brown[21] based on Kuwabara flow:

$$\Delta p = \frac{16\alpha(1 + 1.996Kn)}{d_f^2 [Ku + 1.996Kn \left( -0.5 \ln \alpha - 0.25 + \frac{\alpha^2}{4} \right)]} \mu U_0 t$$

With  $Kn = \frac{2\lambda}{d_f}$ ,  $\lambda$  is mean free path of air molecules, Ku is the Kuwabara hydrodynamic factor which accounts for effect of neighboring fibers on flow around single fibers:

$$Ku = -0.5 \ln \alpha - 0.75 - 0.25\alpha^2 + \alpha$$

	$d_f$ [nm]	$t$ [um]	$\alpha$ [%]
PAN	249±50	157±4	7.2±0.8
PANCO	321±56	154±3	6.2±0.9
PAN15CNC	353±63	147±6	6.8±0.9
PANCO15CNC	379±65	144±2	5.9±0.6
PAN0.4CNF	310±67	152±10	2.8±0.5
PANCO0.4CNF	378±56	133±4	5.5±0.2

Table 12 Characteristics of media available for calculation



In standard condition:  $\mu=1.81E-05$  Pa\*s,  $\lambda=66$ nm

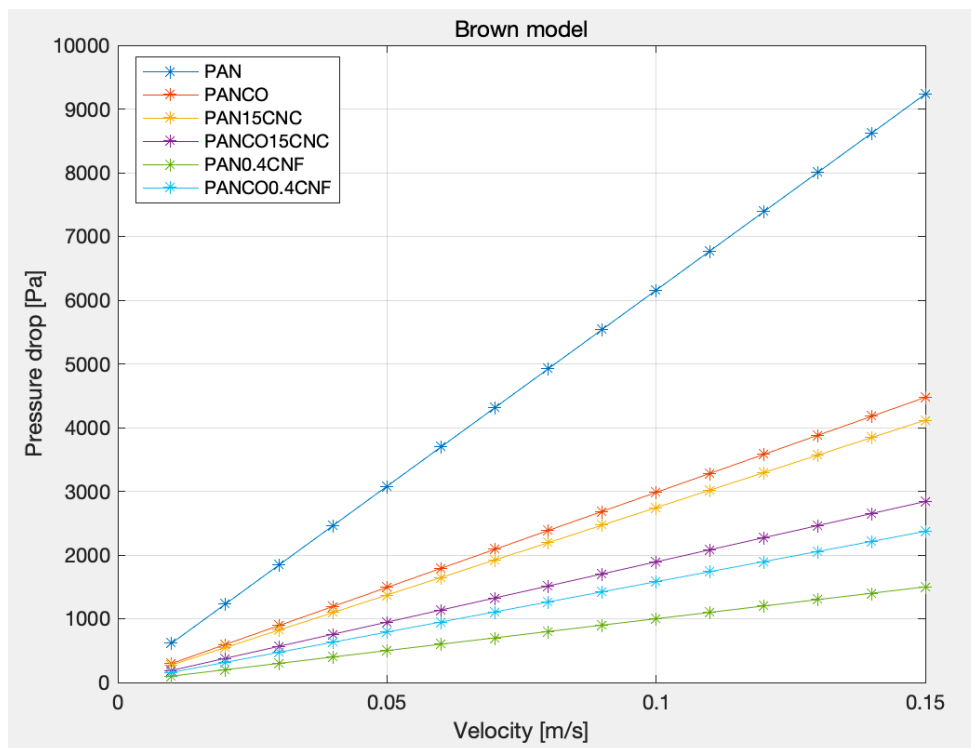


Figure 72 Brown model considering slip effect

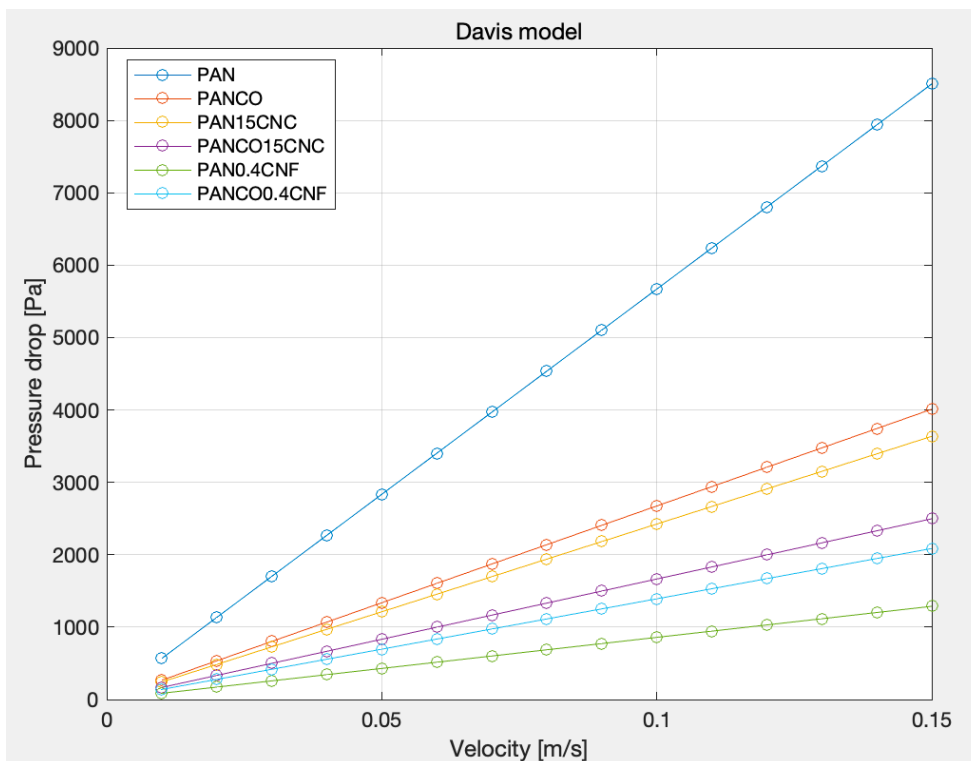


Figure 73 Davies model



Comparison of pressure drops between 2 models and experimental results at 10cm/s is listed in Table 13. It is concluded that both Davies model and Brown model over estimated pressure drop in values, for each type of media, compared to experimental results. But trends of pressure drop increases almost confirmed with test results: trend of PAN media has highest slope, because of finest fibers and greater fiber packing density. Second higher slope is of PANCO, with slightly decreasing packing density and larger fiber. Third is PAN15CNC, being similar solidity compared to PANCO but fiber diameter larger. Those are also true in experimental results. For other three types of media, being similar their fiber diameters and packing density, their pressure drops slope results similarly for both experimental and theoretical models, but orders are not exactly confirmed. The discrepancy might be due to realistic nature of fibrous media, and measured solidity and fiber diameters is not accurate.

	PAN	PAN0.4CNF	PAN15CNC	PANCO	PANCO0.4CNF	PANCO15CNC
Davies model	5669	858	2424	2673	1391	1665
Brown model	6157	1000	2744	2983	1581	1893
Experimental	888	474	584	836	468	369

Table 13 Pressure drops [Pa] comparison at velocity 10cm/s

As for comparison between two models, Brown model predicted slightly higher pressure drop respect to Davies model. This is because fiber diameters are not so close to mean free path so slip effect are not relevant in the case. By changing scale of fiber diameter, calculated value shows in Table 14, as fiber diameters of PAN decreases, Davies model predicts higher pressure drop than Brown model, means that slip effect reduces significantly drag force.

$d_f$ [nm]	2.49	24.9	249	2490	24900
Davies model	85038	850	8.50	0.085	0.00085
Brown model	74519	769	9.23	0.117	0.00124

Table 14 Comparison of pressure drop [kPa] calculated using 2 models by changing fiber diameter of PAN, at fixed velocity = 15cm/s



## 4.2 Particle removal efficiency

Samples with pressure drop increases closer to average value is selected for representing each category to do efficiency tests. Chosen samples are listed:

- ◆ PAN 6
- ◆ PANCO0.4CNF 2
- ◆ PAN15CNC 3
- ◆ PAN0.4CNF 3
- ◆ PANCO 3
- ◆ PANCO15CNC 3

### 4.21 OPS3330

Selected samples are tested using OPS3330 first, following standard method, at fixed filtration velocity 10cm/s for particle size range 0.3-10 micrometer, results are listed as follow:

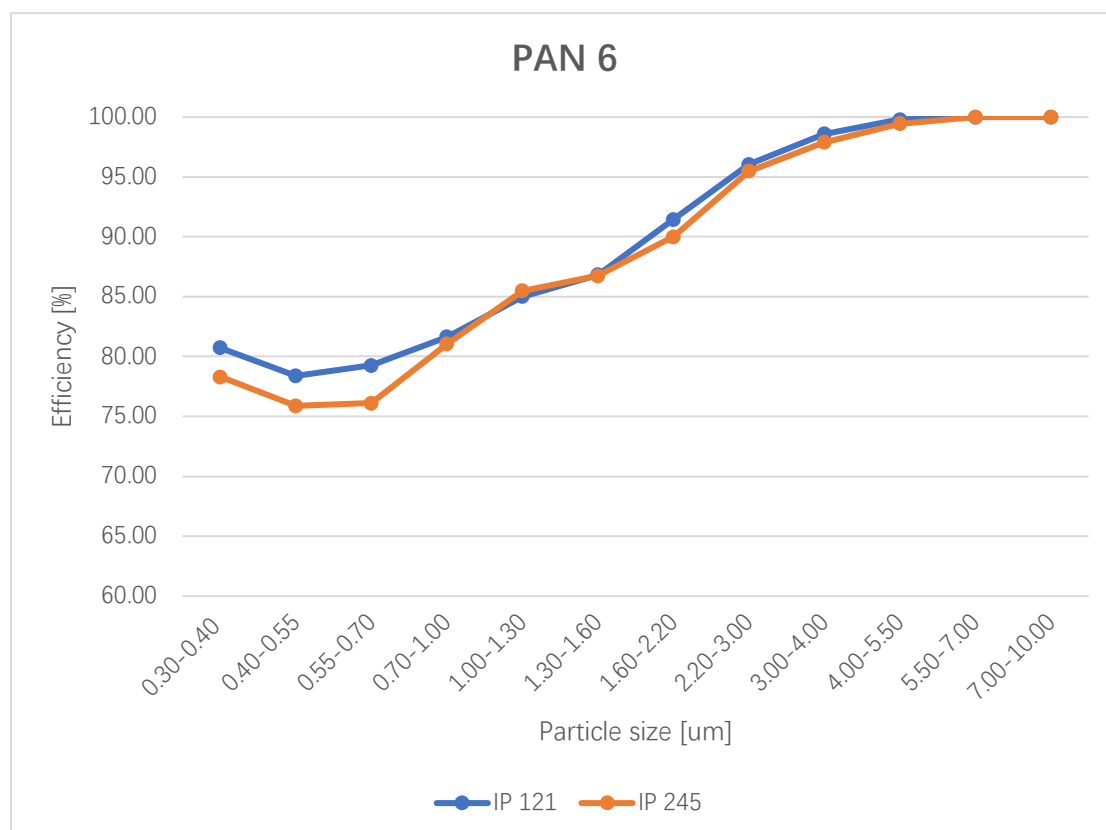


Figure 74 PAN 6 fractional efficiency tested using two OPS3330



Figure 74 shows that two models of OPS3330 test similar efficiency with slight deviation, which is caused by uncertainties of experiments and accuracy of two spectrometers might result slight difference.

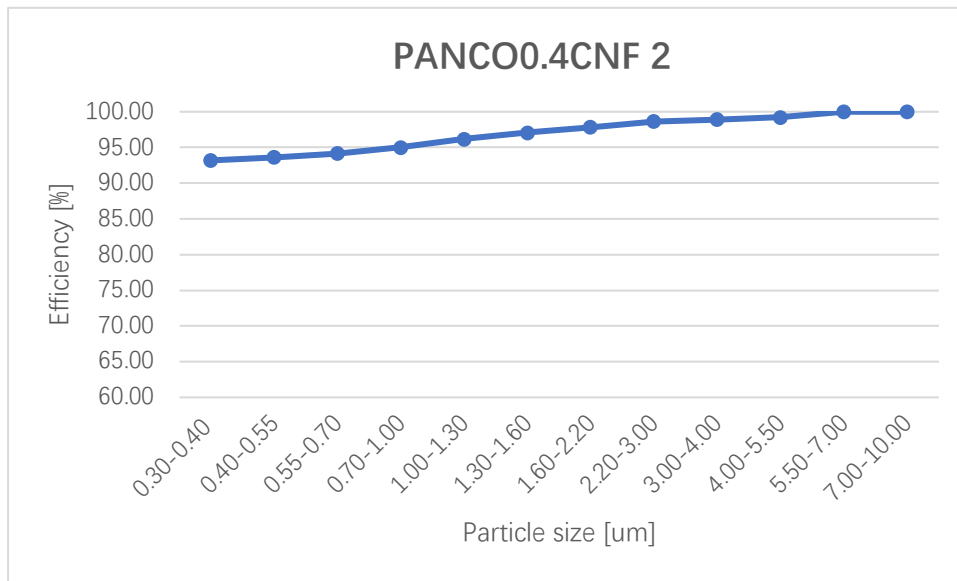


Figure 75 PANCO0.4CNF 2 fractional efficiency

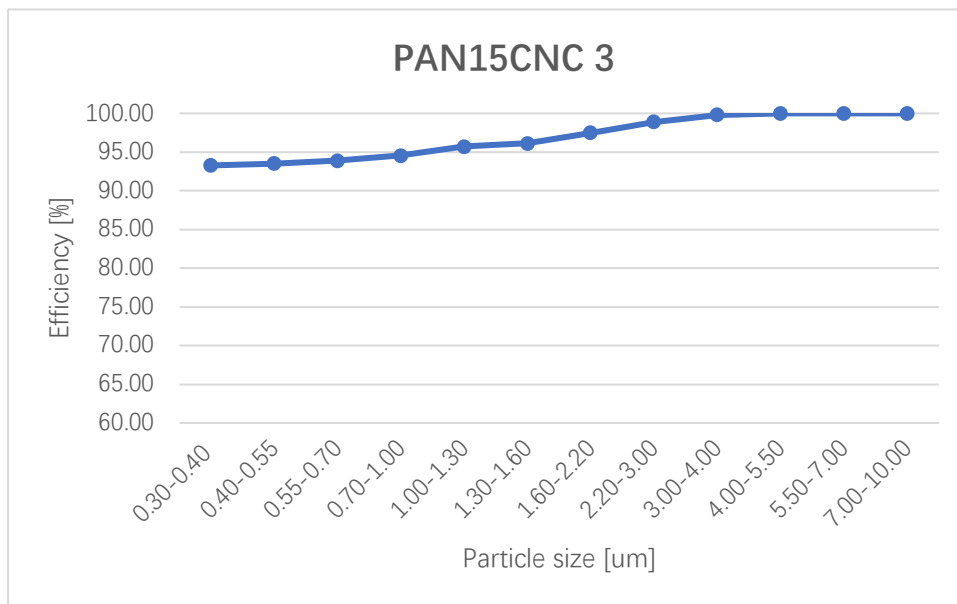


Figure 76 PAN15CNC 3 fractional efficiency

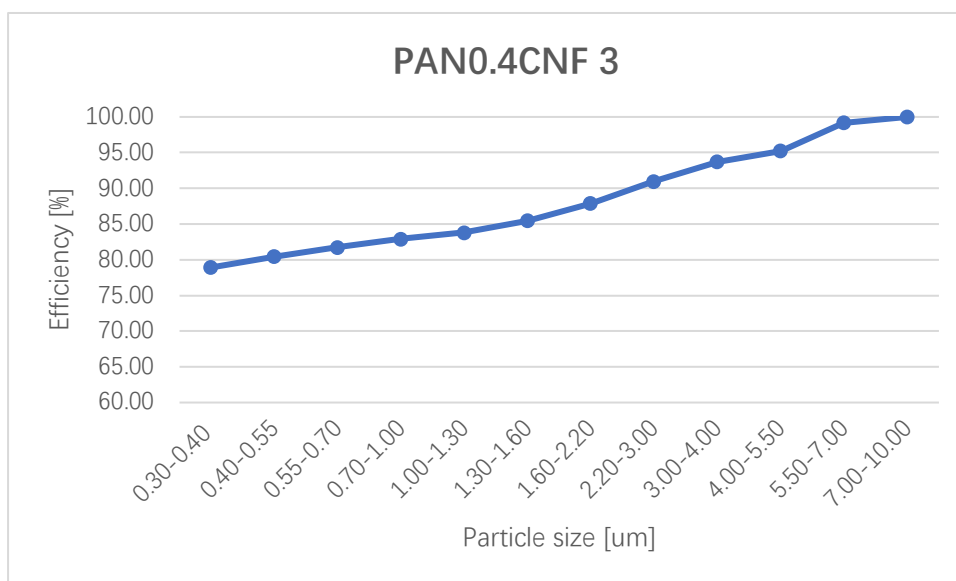


Figure 77 PAN0.4CNF 3 fractional efficiency

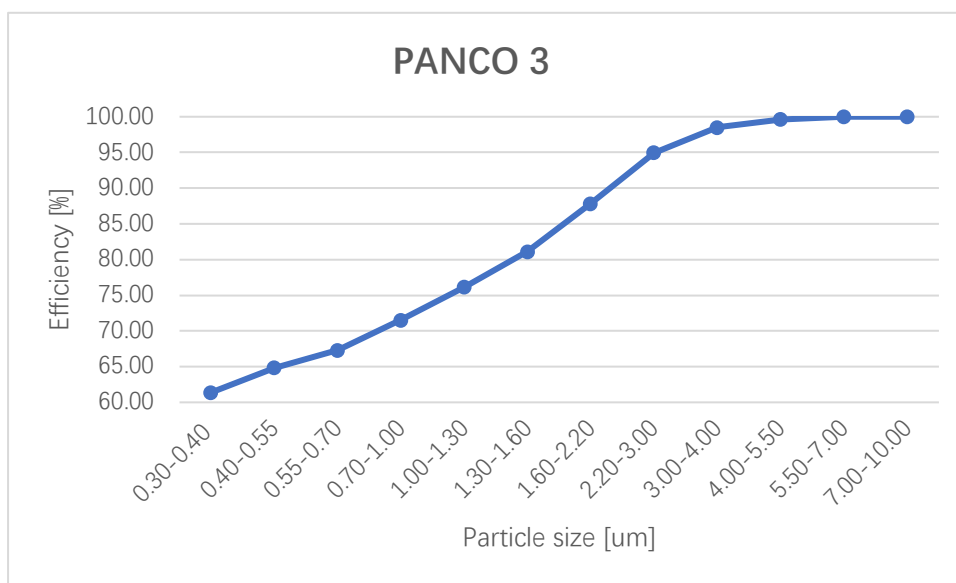


Figure 78 PANCO 3 fractional efficiency

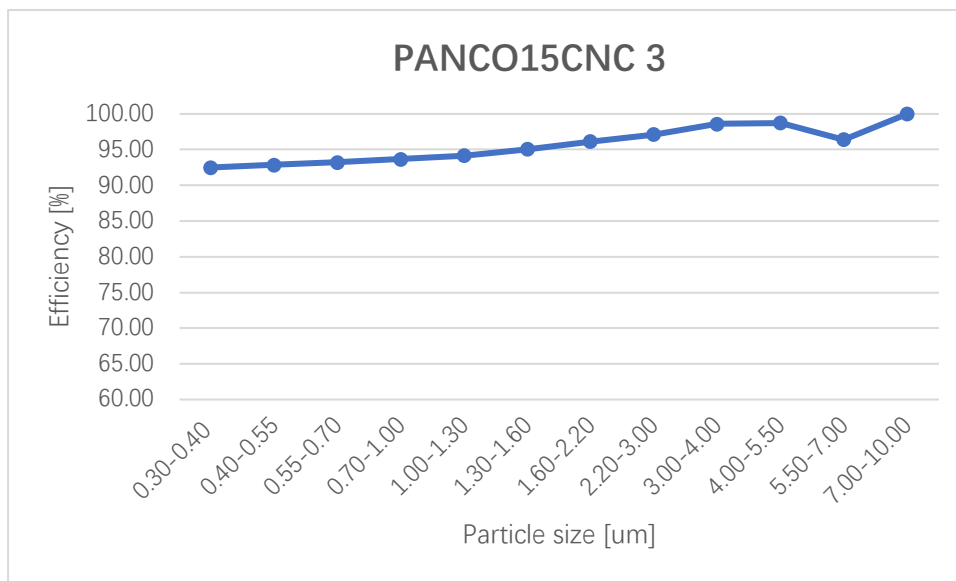


Figure 79 PANCO15CNC 3 fractional efficiency

Overall comparison of fractional efficiencies of 6 type of media plotted:

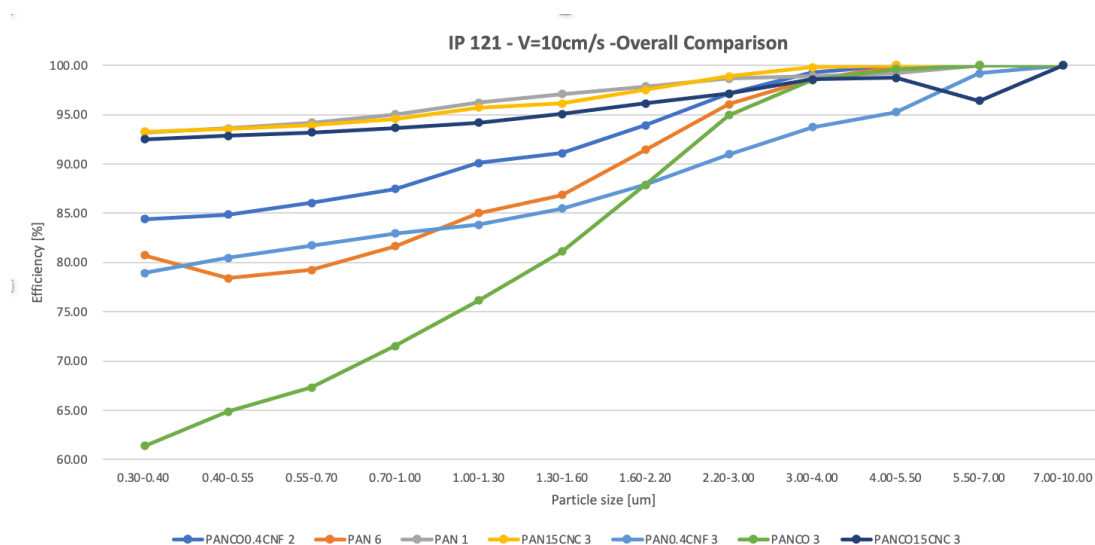


Figure 80 Overall comparison of fractional efficiencies for particle size range 0.3-10 micrometers

Figure 80 shows that six types of media both showing high fractional efficiencies, this means that electrospinning technology effectively produces media with good performance. However, from results at this size range, it is hard to identify most penetrating particle size (MPPS) and minimum efficiencies which are critical parameters for comprehensively studying behavior of media. Especially for studying filtration performance for ultrafine particles. So, efficiency tests also are done with LAS3340A which provides wider spectrum of fractional efficiency.



## 4.22 LAS3340A vs OPS3330

Following same experimental set up, results of two spectrometers are compared to validate each other by comparing fractional efficiencies at superimposed size range. Efficiency tests are repeated several times until uncertainties for all particle size range within 10%, by increasing cycle time for sampling. So errors introduced by experimental procedure are minimized.

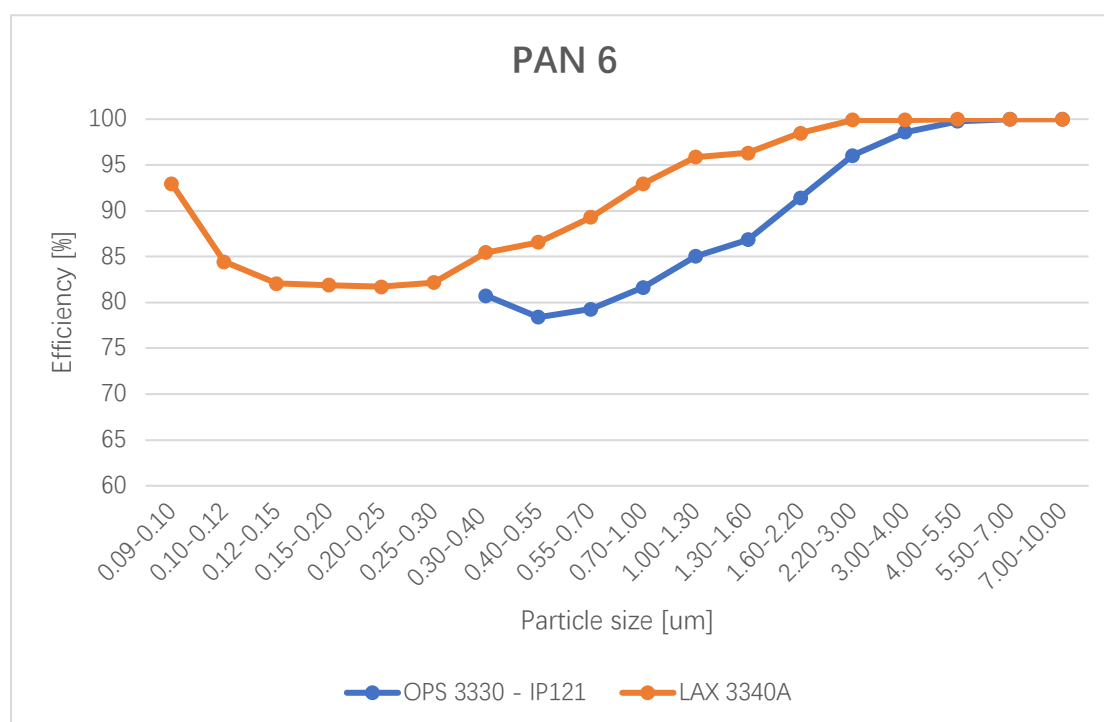


Figure 81 Fractional efficiency tested PAN 6

From Figure 81, it is noted that fractional efficiencies tested at all particles size range by LAX3340A is increased respected to result obtained before with OPS3330. There is a time difference of 3 months between two tests. The explanation could be that sample are aged under environmental effects. Sample might already be clogged by background particles, or fiber structure aged, or tested surface are displaced between two tests. For checking possible malfunctioning of spectrometers, sample are tested again with OPS3330, results are compared in Figure 82. The new results shows that some changes happened to samples.

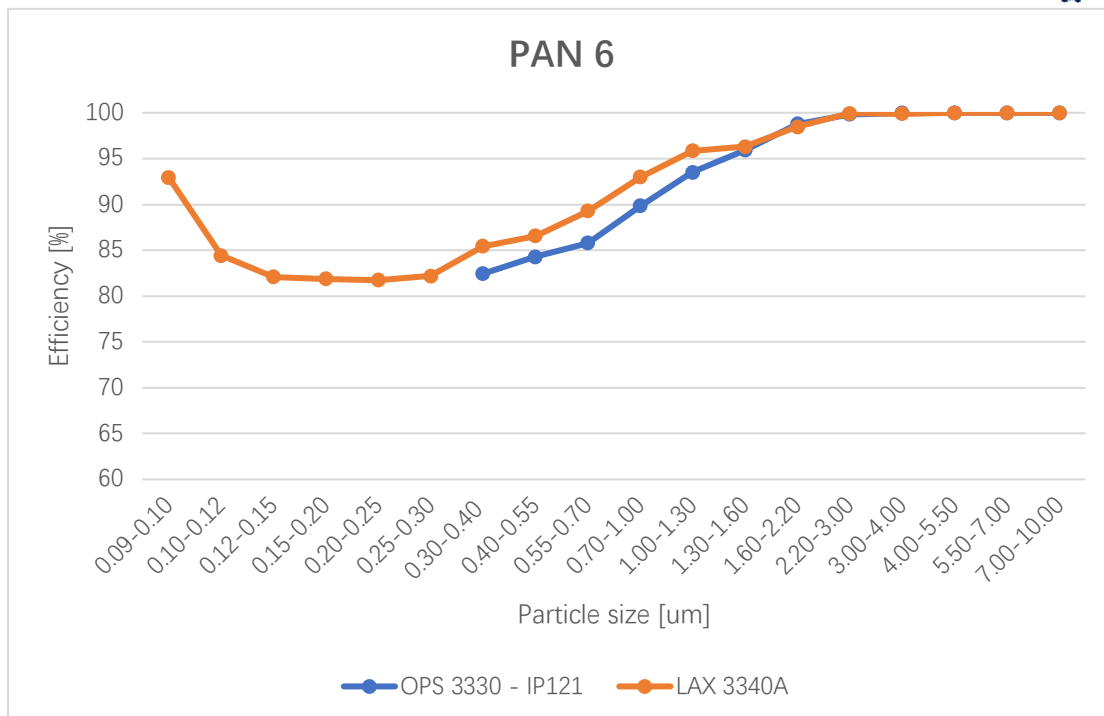


Figure 82 Fractional efficiency test PAN 6: OPS3330 test repeated

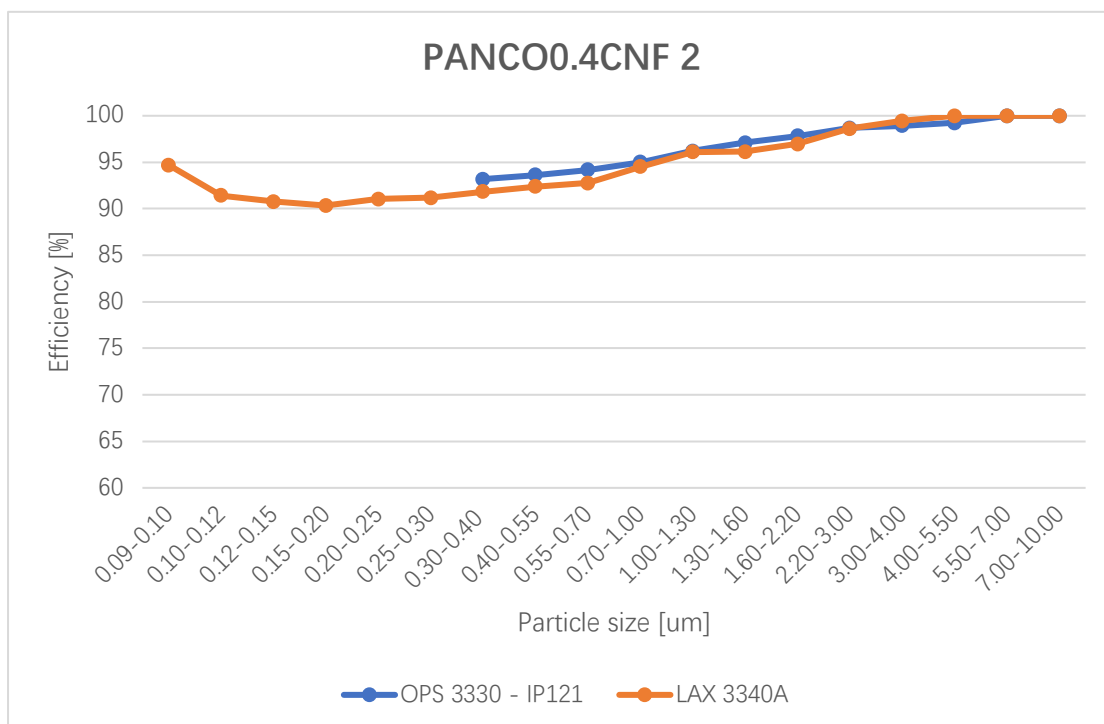


Figure 83 Fractional efficiencies tested PANCO0.4CNF 2

Comparing results of Figure 81, Figure 83 and Figure 84 ,same efficiency change not presents for PANCO0.4CNF 2 and PANI5CNC 3, with initially higher fraction efficiencies.

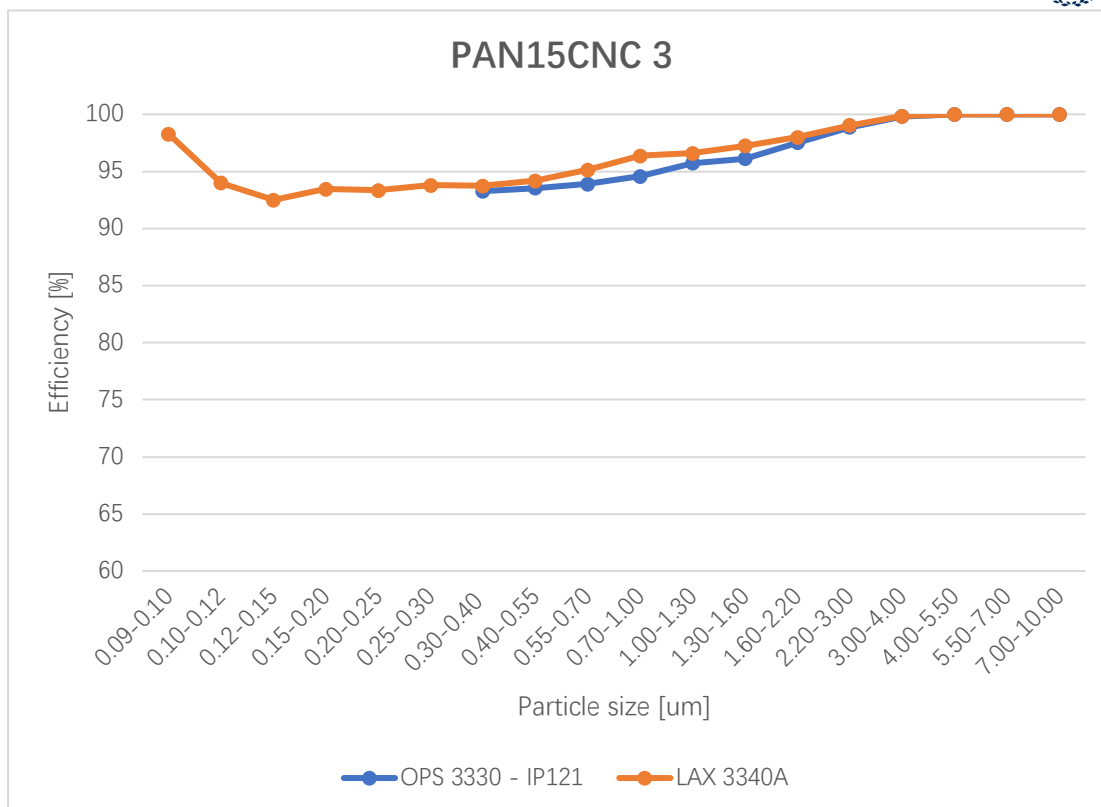


Figure 84 Fractional efficiency tested by two spectrometers PAN15CNC 3

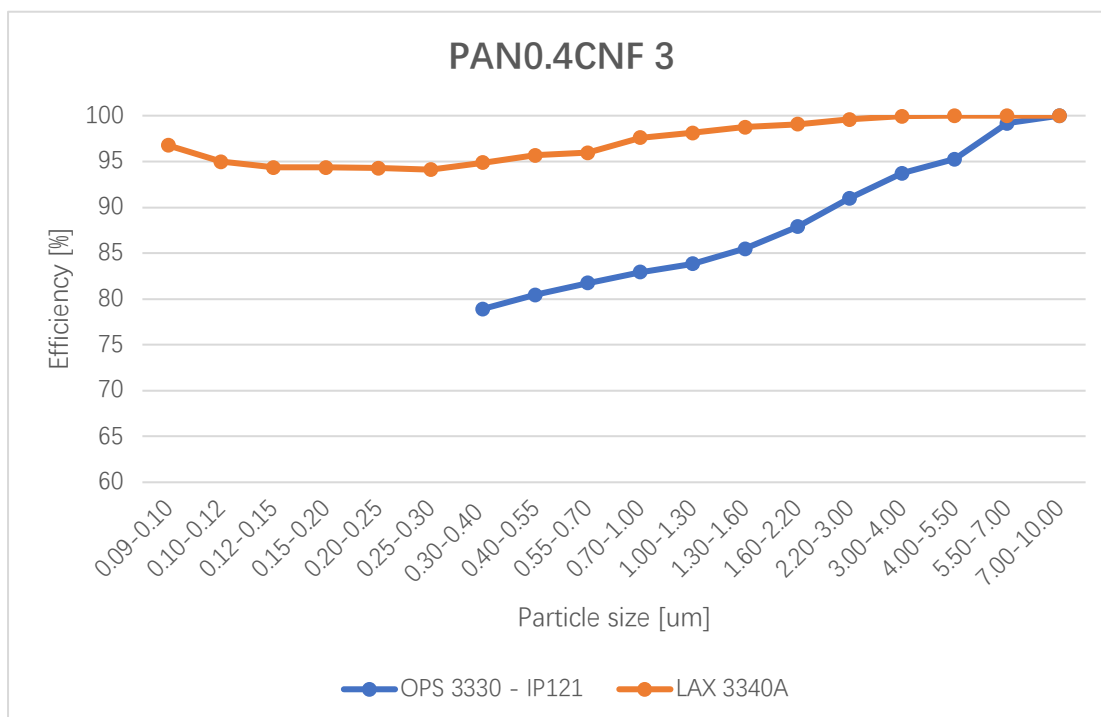


Figure 85 Fractional efficiency tested by two spectrometers PAN0.4CNF 3

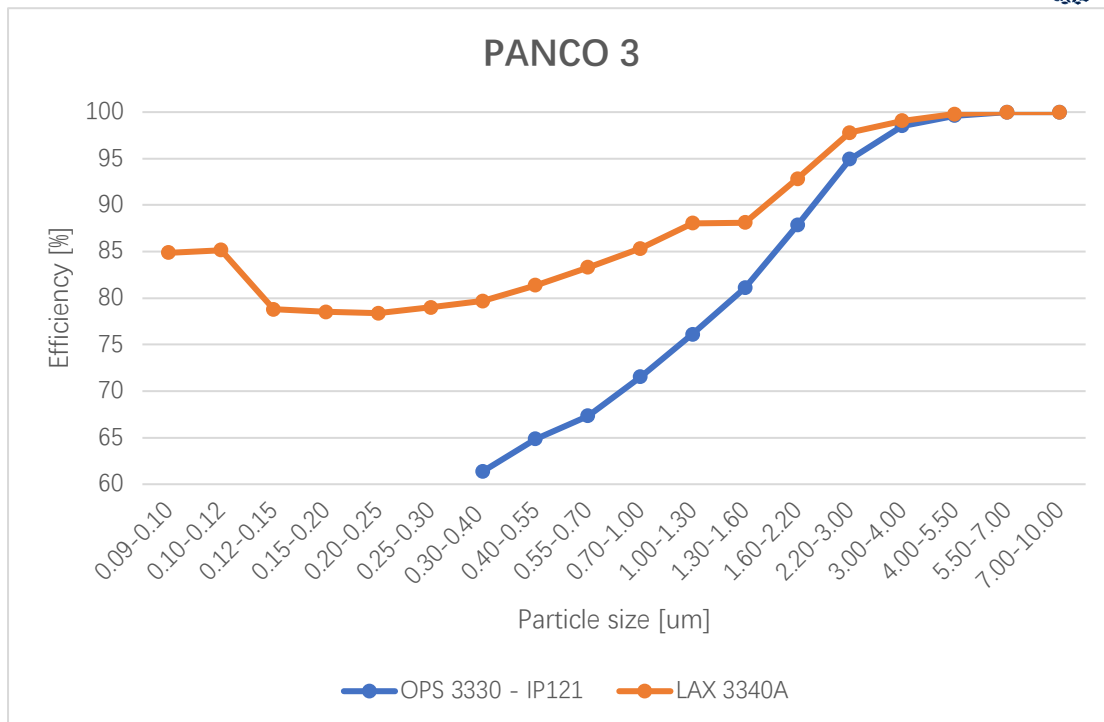


Figure 86 Fractional efficiency tested by two spectrometers PANCO 3

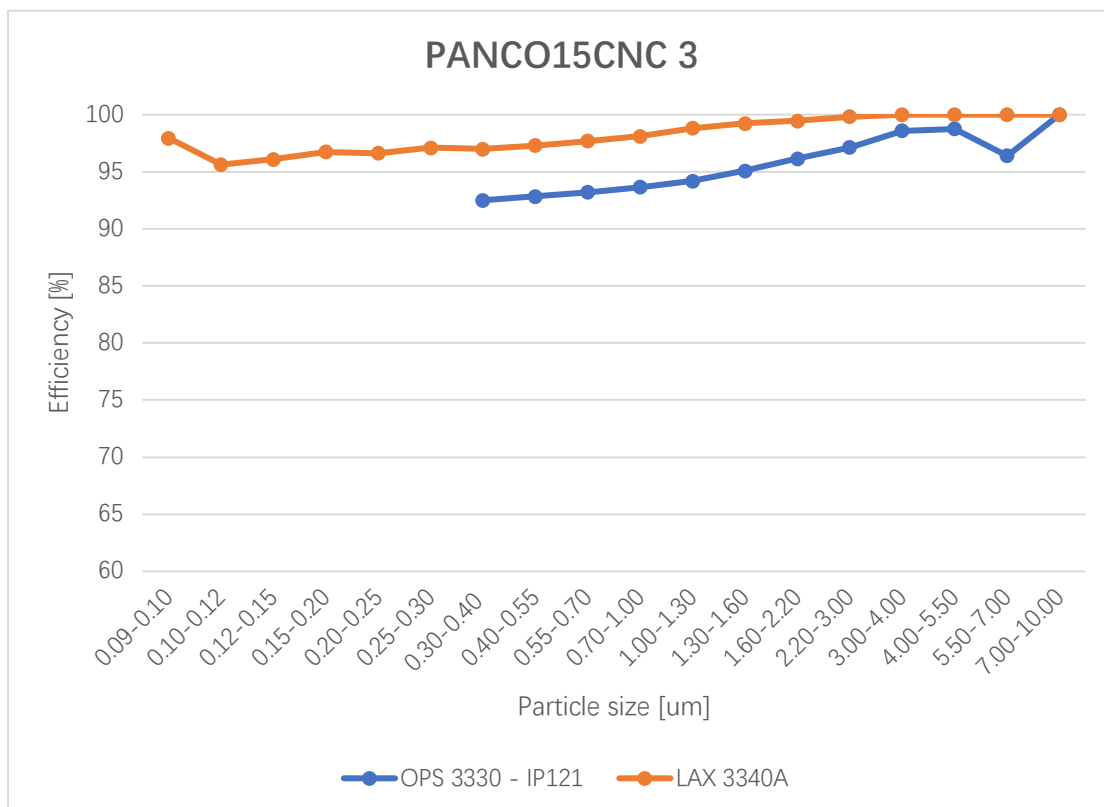


Figure 87 Fractional efficiency tested by two spectrometers PANCO15CNC 3



Same problem as PAN6 is also presented in last 3 test results (Figure 85, Figure 86, Figure 87), so tests are repeated for those media with OPS3330.

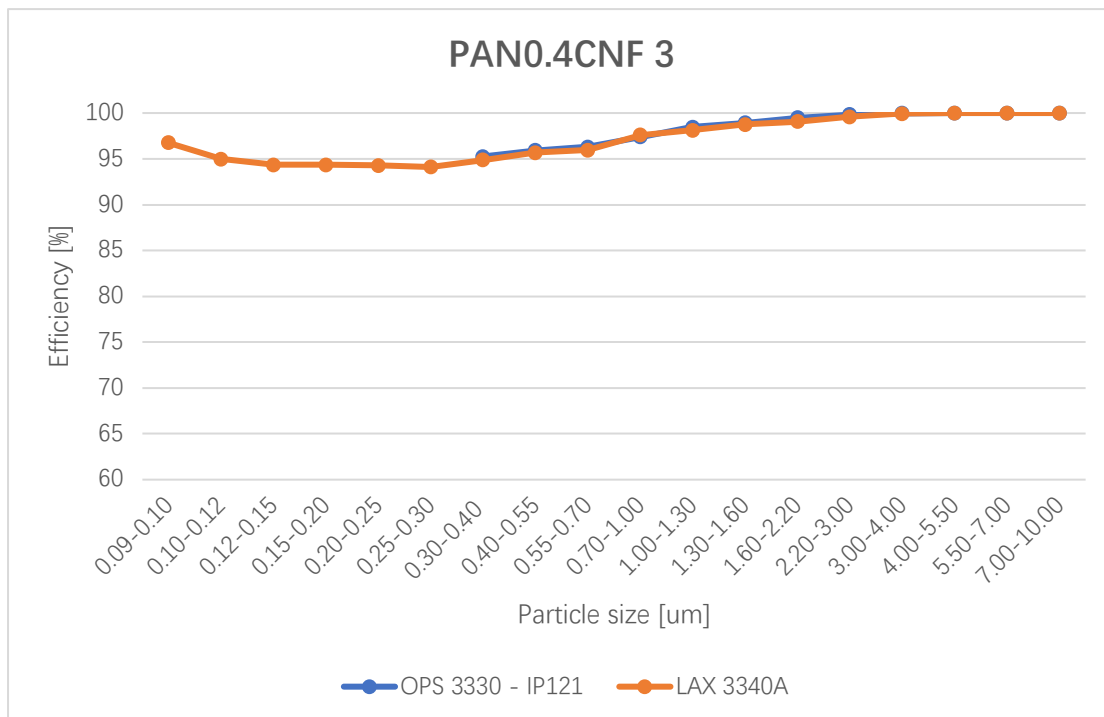


Figure 88 Fractional efficiency test PAN0.4CNF 3: OPS3330 test repeated

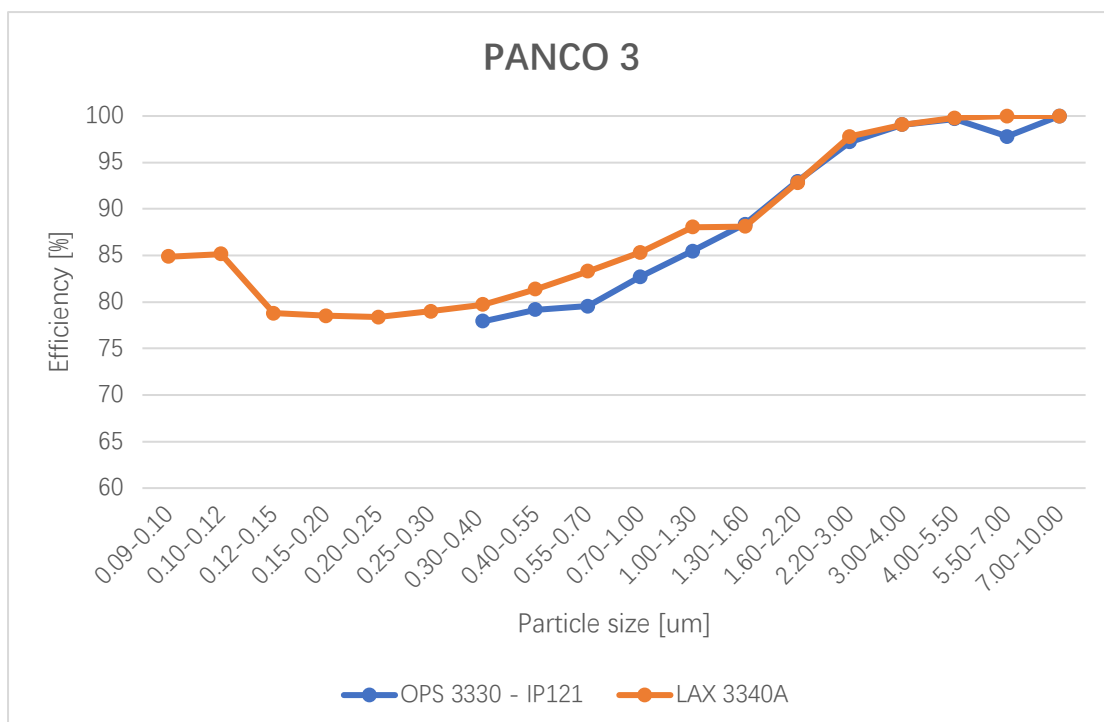


Figure 89 Fractional efficiency test PANCO 3: OPS3330 test repeated

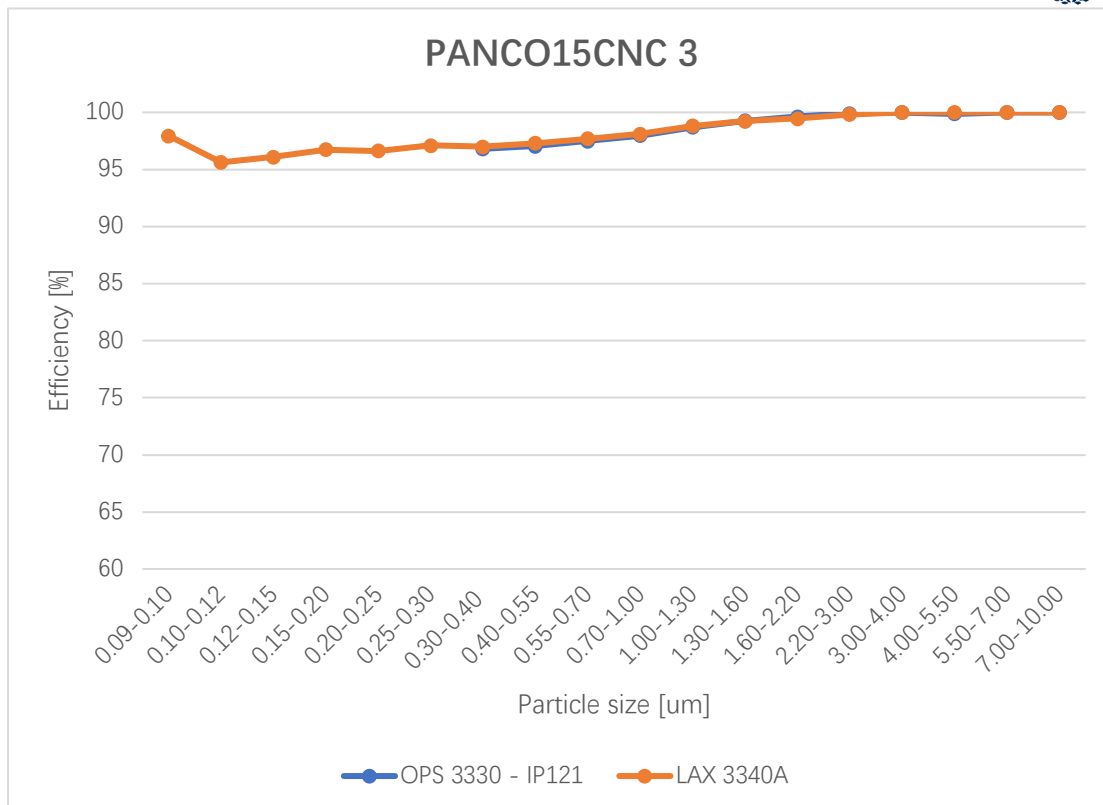


Figure 90 Fractional efficiency test PANCO15CNC 3: OPS3330 test repeated

Repeated test results (Figure 88, Figure 89, Figure 90) shows tested fractional efficiencies are increased for those media, most probable reason is displacement of sample area, thus efficiencies changes due to inhomogeneity of spatial distribution of fibers. Since only 4 media out of 6 are noted with this phenomenon, if media are aged, same efficiency increases should be also happened to other 2 media.

From results of LAS 3340A, MPPS and minimum efficiency for each type of media are approximately obtained by identifying lowest point of curves on each graph, particle size is geometric mean value of corresponding size range. Experimental results (Table 15) are then compared with theoretical values calculated with average characteristics of each type of media.



	PAN6	PANCO0.4CNF2	PAN15CNC3	PAN0.4CNF3	PANCO3	PANCO15CNC3
MPPS [nm]	220	170	130	270	220	110
Minimum efficiency [%]	81.73	90.35	92.51	94.11	78.39	95.62

Table 15 Experimental results of MPPS and minimum efficiency

## 4.23 MPPS and minimum efficiency

For predicting MPPS and minimum efficiency and validating experimental results. Now analytical expressions derived by Lee and Liu[22] are used for calculating those two parameters.

$$d_{p,min} = 0.885 \left[ \left( \frac{Ku}{1-\alpha} \right) \left( \frac{\sqrt{\lambda}kT}{\mu} \right) \left( \frac{d_f^2}{U_0} \right) \right]^{\frac{2}{9}}$$

For  $0.075 < (\lambda/D_p) < 1.3$ ,  $\lambda$  and  $D_p$  are mean free path and particle diameter respectively,  $k$  is Boltzmann constant.

$$E_{min} = 1.44 \left[ \left( \frac{1-\alpha}{Ku} \right)^5 \left( \frac{\sqrt{\lambda}kT}{\mu} \right)^4 \left( \frac{1}{U_0^4 d_f^{10}} \right) \right]^{\frac{1}{9}}$$

For single fiber efficiency.

Those formulas are based on assumptions:

- ◆ Only diffusion and interception collection are considered, inertial impaction are negligible for this case at low velocity, electrostatic forces do not present
- ◆ Solidity is relatively small
- ◆ Interception parameter  $R=d_p/d_f$  is relatively small compared to 1

Despite that accuracy of the expressions are found to be lower in later studies, considering interaction between interception and diffusing particles.



And minimum media efficiency is calculated with predicted minimum single fiber efficiency:

$$\eta = 1 - P = 1 - \exp\left(-E_{min}\alpha \frac{4}{\pi(1-\alpha)d_f} t\right)$$

Where P is penetration.

Results are reported as scatter plot (Figure 91).

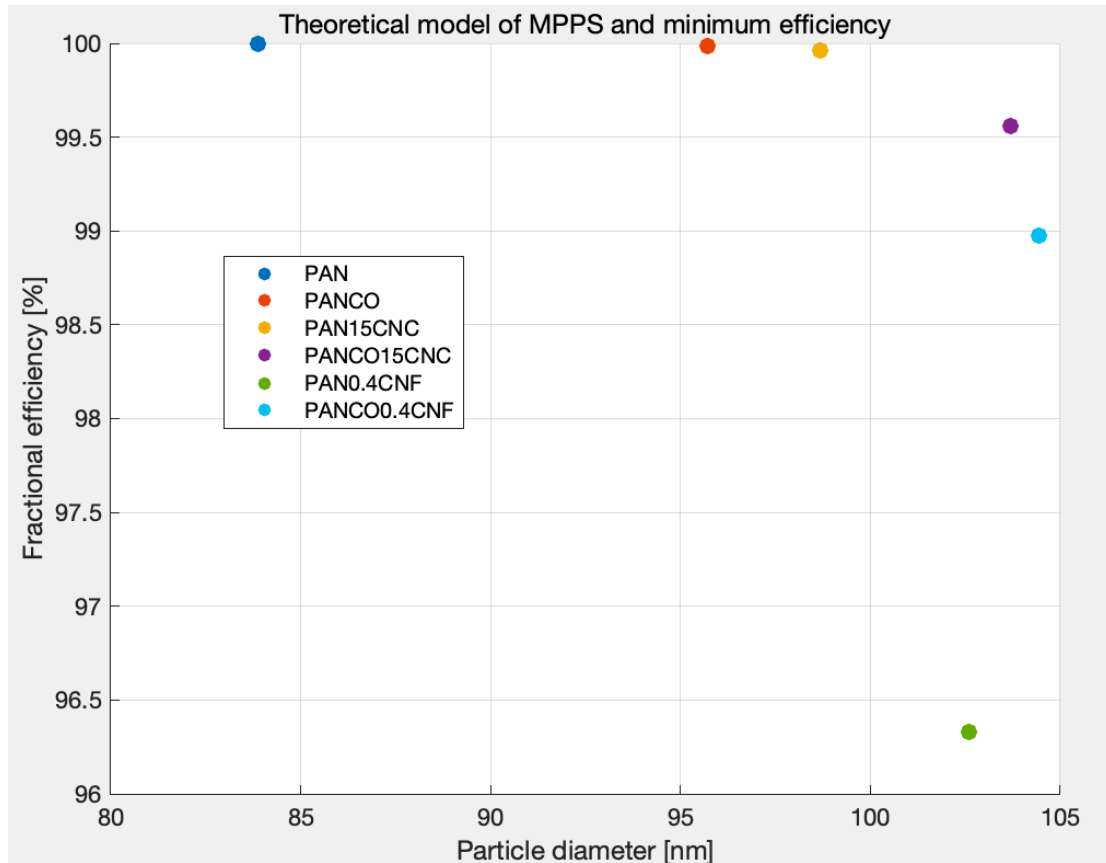


Figure 91 Calculated MPPS and minimum media efficiency of 6 types of media



Calculated results and experimental results are listed in Table 16 for better visualization.

	PAN	PANCO0.4CNF	PAN15CNC	PAN0.4CNF	PANCO	PANCO15CNC
Theoretical						
MPPS [nm]	84	104	99	103	96	103
Minimum efficiency [%]	100	98.98	99.96	96.33	99.99	99.56
Experimental						
MPPS [nm]	220	170	130	270	220	110
Minimum efficiency [%]	81.73	90.35	92.51	94.11	78.39	95.62

Table 16 Comparison between experimental and theoretical MPPS and Minimum efficiency



## 4.24 Discussion

It is noted that for PAN15CNC and PANCO15CNC, calculated values predict well the real behavior of media, but for other media shows larger discrepancy. Overall, calculated MPPS are lower respect to experimental results, with higher minimum media efficiencies. This means theoretical model overestimates filtration efficiency. Referring to previous comparison of theoretical air resistances with test results (Table 13), analytical solutions predict also higher pressure drops introduced by media. Considering filtration velocity is 10cm/s, quality factors Q at MPPS can be calculated to better compare overall filtration performance. For experimental minimum efficiency refers to results of LAS 3340A.

$$Q = -\ln(1 - \eta)/\Delta p$$

Q [1/Pa]	Davies model	Brown model	Experimental
PAN	0.0033	0.0031	0.0018
PANCO	0.0033	0.0030	0.0018
PAN15CNC	0.0032	0.0029	0.0042
PANCO15CNC	0.0033	0.0029	0.0084
PAN0.4CNF	0.0038	0.0033	0.0061
PANCO0.4CNF	0.0033	0.0029	0.0048

Table 17 Quality Factors of six type of media: analytical solution to experimental results

As predicted by analytical models (Table 17), six type of media having almost same quality regarding filtration, because in theory realistic characteristics of media are not considered. However experimental results show a variety in performance of tested media. PAN and PANCO showing lowest quality, while PANCO15CNC has highest quality which is 3 times more than that of formers.

### 4.3 Loading test

Firstly, tests are done using standard flat sheet media provided with 8130A for checking normal functionality of machine. Those media have comparable efficiency for filtrating ultrafine particle with nanofiber samples tested previously, the penetration values are about 10%. Nanofiber samples are tested at 90nm resulting penetration from 5% to 20%, for 75nm particles, those value would further decrease because of enhanced diffusion capture. Loading tests are conducted under 14cm/s which slightly higher than 10cm/s for efficiency test. Another effect regarding comparison the efficiency of standard media with nanofiber samples, higher velocity could increase penetration slightly because of residence time for diffusing particle being captured is shorter.

Figure 92 shows an example of sample tested after loading test, it is clear to see white area showing that particle cake is formed. And small crack is presented, means media is broken under high pressure drop induced by particle cake.



Figure 92 Loaded standard flat sheet media

Test results are recorded includes penetration value and pressure drop at each time step of measuring during loading test, they are plotted as function of loaded mass, which is calculated by tester firmware with formula:



$$W = M * \frac{F}{1000} * T$$

Where W is mass loaded in mg, F is flowrate in l/min, M is mass concentration of aerosol in  $mg/m^3$  measured through gravimetric test, T is time in min.

## 4.31 Loading curve

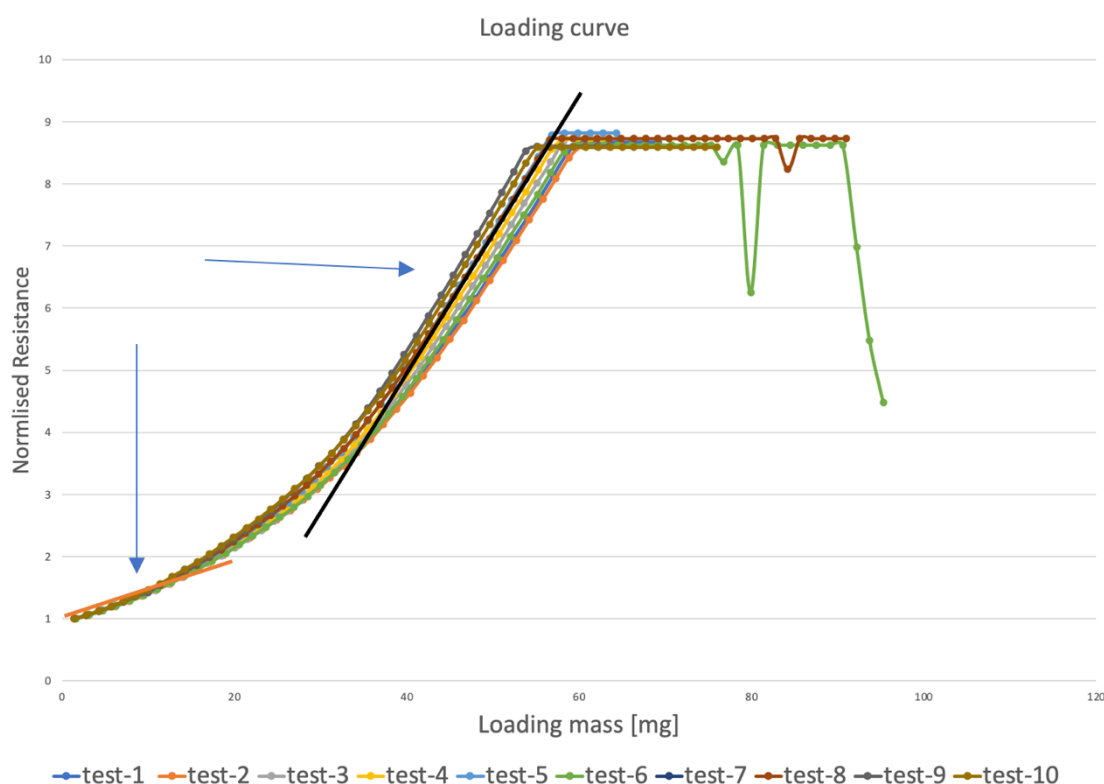


Figure 93 Loading curve tested on standard media

In Figure 93 shown results of normalized resistance as function of loaded mass. Pressure drops detected are normalized respect to initial resistance of tested media. It is clearly noted two linear regimes in graph. First with shorter range indicates depth loading phase, in which air resistance increase linearly with lower rate. Second phase is noted as surface loading phase, in this phase pressure drop is increasing faster with mass loaded. At end of this phase, air resistance keeps increasing but pressure transducer not able to detect it being maximum reading range is reached. Tests are stopped until media are broken, so that air resistance will decrease while increasing the penetration.

Between surface loading and depth loading, there is a transient regime, in which penetration of media keeps decreasing but it is very close to 0%, means that media is almost fully clogged, and particle cake start to form. At surface loading phase, air resistance is due to media itself and particle cake.



All ten tests are done under same setting, but there is still a variation of curves. It seems that slight changes of loading behavior are happened during transition phase, this might be explained by variation of particles production. And slope of depth regime and surface regime are approximately same for all tests. Depth loading behavior depends on filtration characteristics, which is well studied using filtration theory. Thus, for same type of media, at same filtration velocity, with same particle size distribution upstream, the depth loading behavior is predictable to be same. This can be verified by Figure 94, showing normalized penetration decreases as mass loaded. From graph, efficiency is reach 100% approximately at 30mg loaded mass, which could represent end of depth loading phase. Penetration decreasing curve fits well with each other shows good homogeneity of standard media.

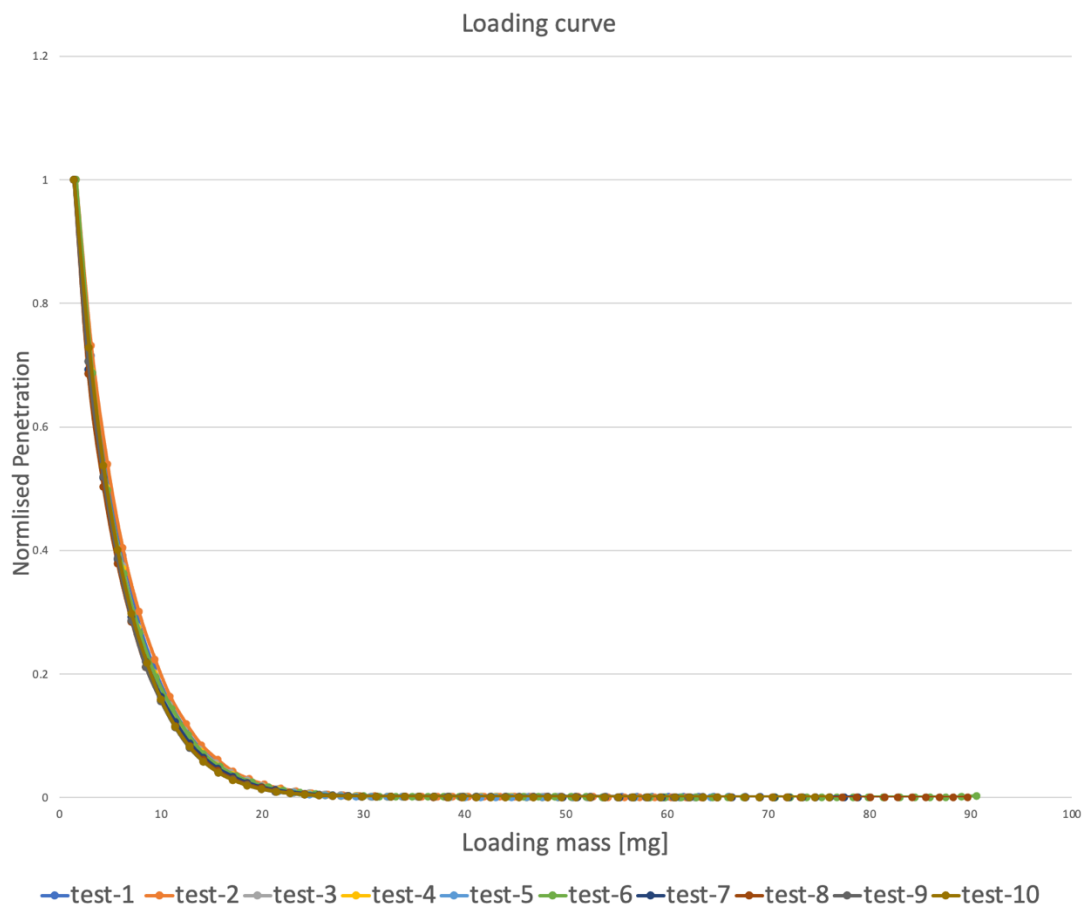


Figure 94 Normalized penetration as function of mass loading

For transient phase between depth and surface loading, however, there is no distinct threshold defined. As approximation, surface loading is considered for normalized pressure being higher than 5.

As for loading test, since layer efficiency of media is already reaching 100%, means that media characteristics no more affecting particle capture. So, surface loading should be as function of particles and air flow. The condition of air flow is controlled to be same; RH is verified being around 30% for all test, and particle size distribution for all tests are verified within indicated range. For all those aspect, slope of surface loading should be same for all tests.



Assuming surface loading is started at normalized pressure drop equal to 5, it is calculated a confidence interval for loaded mass at that pressure drop for assessing variability of surface loading results due to inherent uncertainty introduced by experiments.

test	1	2	3	4	5	6	7	8	9	10
Mass [mg]	38.5	39	42	42.4	41.1	40.5	39.7	41.8	40.5	39.7

Table 18 Loaded mass at start of surface loading, normalized pressure=5

Considering 95% confidence level, loaded mass at certain normalized pressure during surface loading can be calculated with uncertainty, assuming slope of surface loading results of each test are equal. At  $\Delta p/\Delta p_0=5$ , loaded mass= $40.5\pm 3.3$ mg (Table 18).

### 4.32 Linear regression of surface loading

For correlate surface loading behavior at this specific experimental condition, linear regression is used to predict particle cake growth rate by experimental data for  $\Delta p/\Delta p_0>5$ .

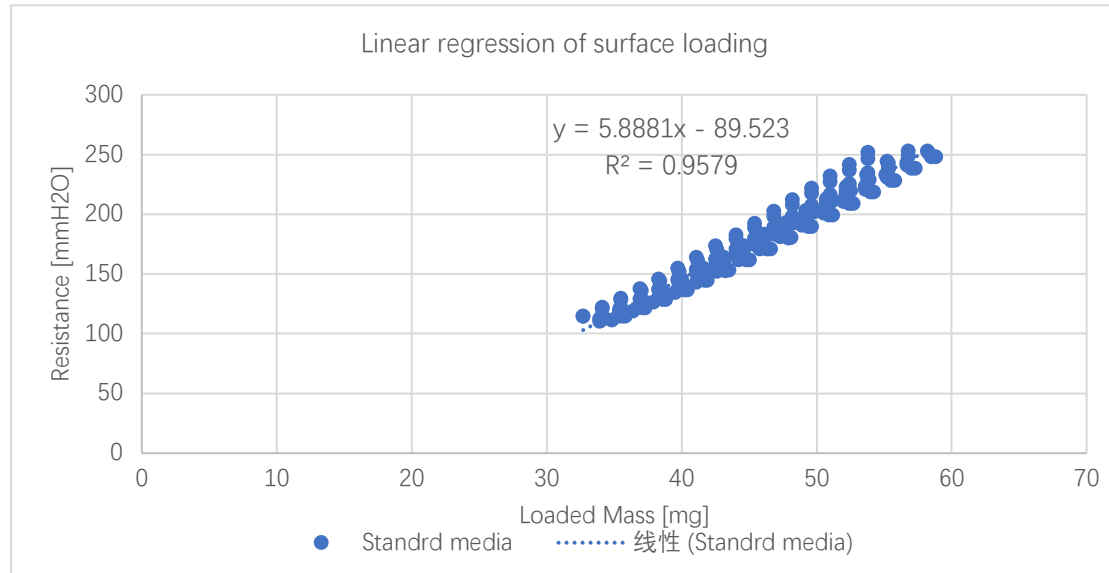


Figure 95 Linear regression of standard media: surface loading behavior

In Figure 95, experimental data with detected pressure drop are plotted for linear regression, reducing errors introduced by previous phases. Liner relationship of pressure drop as mass loading under experimental condition RH=30%, filtration velocity=14cm/s, CMD=78nm, GSD=1.95, is obtained, noting that constant -89.523 depends on previous loading phases:

$$\Delta p = 5.8881W - 89.523 [mmH2O]$$



### 4.33 Comparison of two media

For validate conclusion that at this experimental condition, surface loading behavior is constant, regardless type of media. Another FCR media is tested 3 times, compared to 3 tests results of standard media within same day, so the variation of loading behavior between each test is minimum.

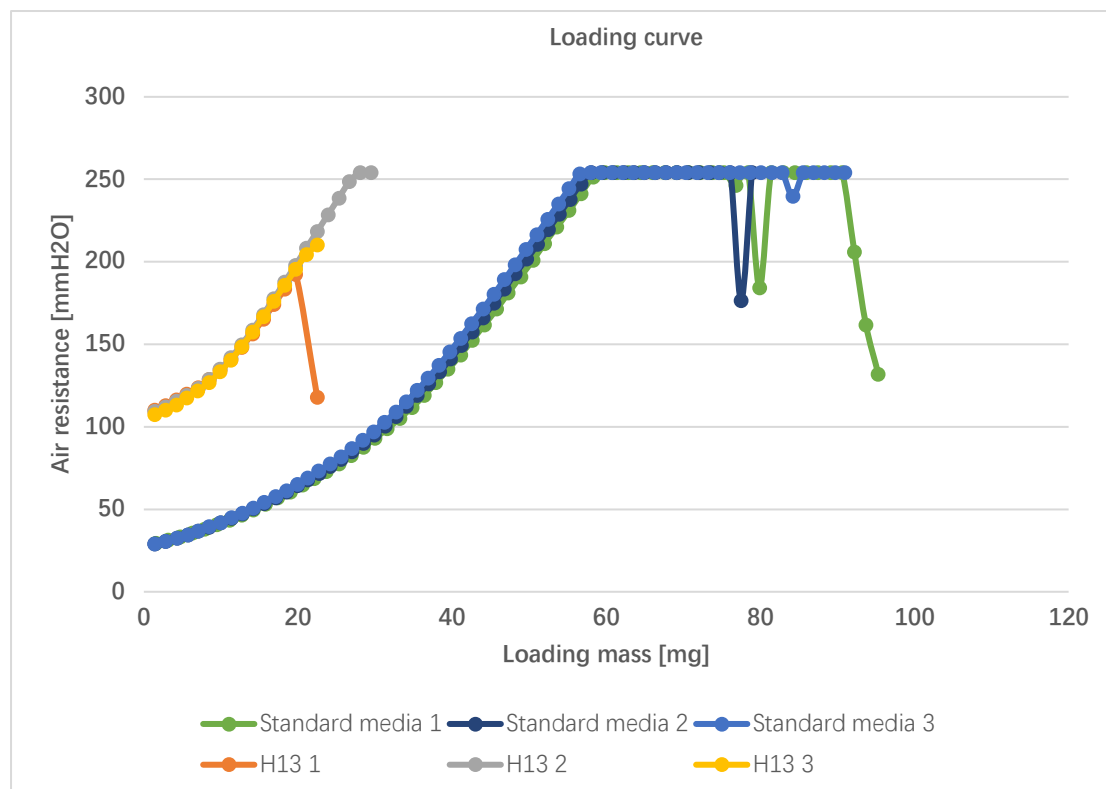


Figure 96 Loading tests on two types of media

Results shown in Figure 96 do not use normalized pressure drops noting that depth loading behavior of two media is different. H13 media has very low initial penetration, 0.7%, thus depth loading phase is much shorter than standard media. It is clearer comparing normalized penetration decreasing curve of two media in Figure 97.

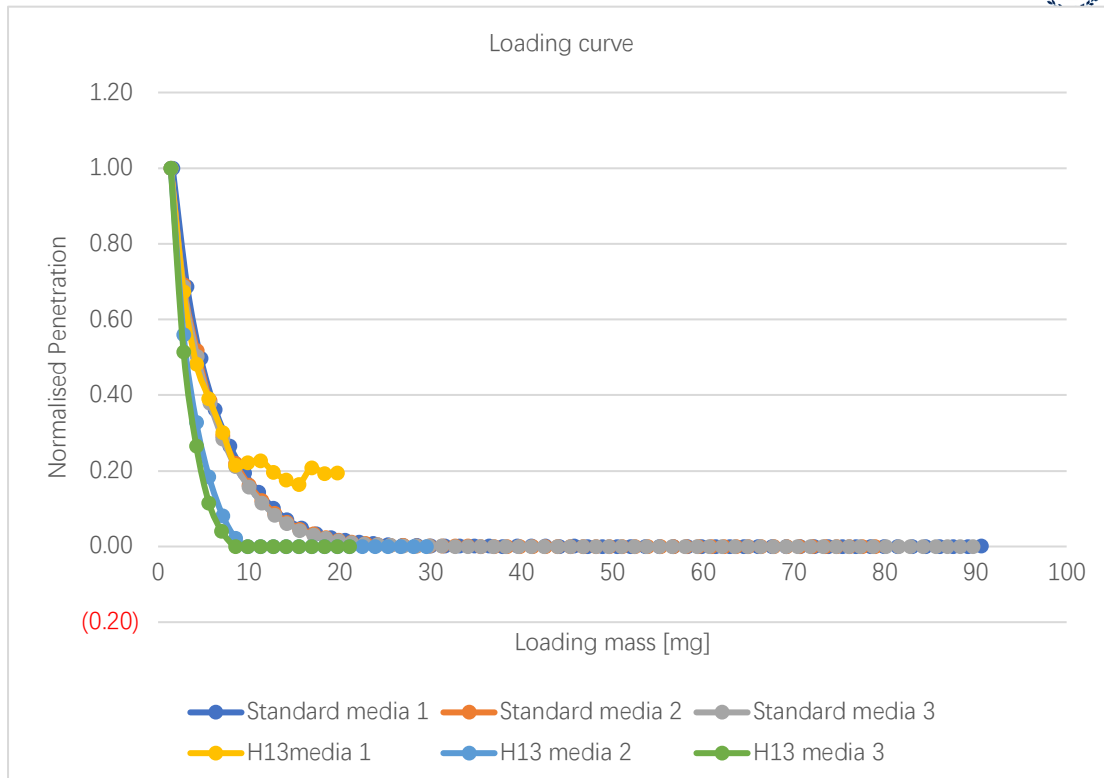


Figure 97 Normalized penetration curves of two media

From graph, the penetration of H13 media decrease faster than standard media during depth loading.

For comparing behaviors of surface loading of two media, same approach to set starting point of surface loading is apply to H13 media, selecting  $\Delta p/\Delta p_0=1.3$ .

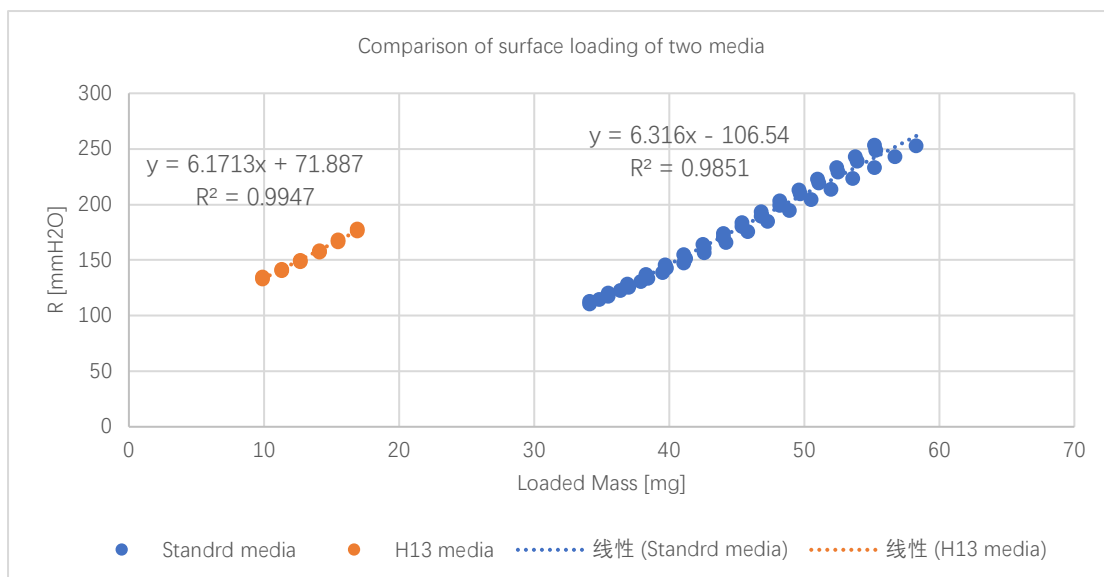


Figure 98 Comparison surface loading of two media



From Figure 98, the slopes of two media are almost equal, which verifies that surface loading behavior does not depend on media. Instead, it varies slightly for variations on environmental conditions, and upstream particle size distribution. Figure 99 shows loaded H13 media.

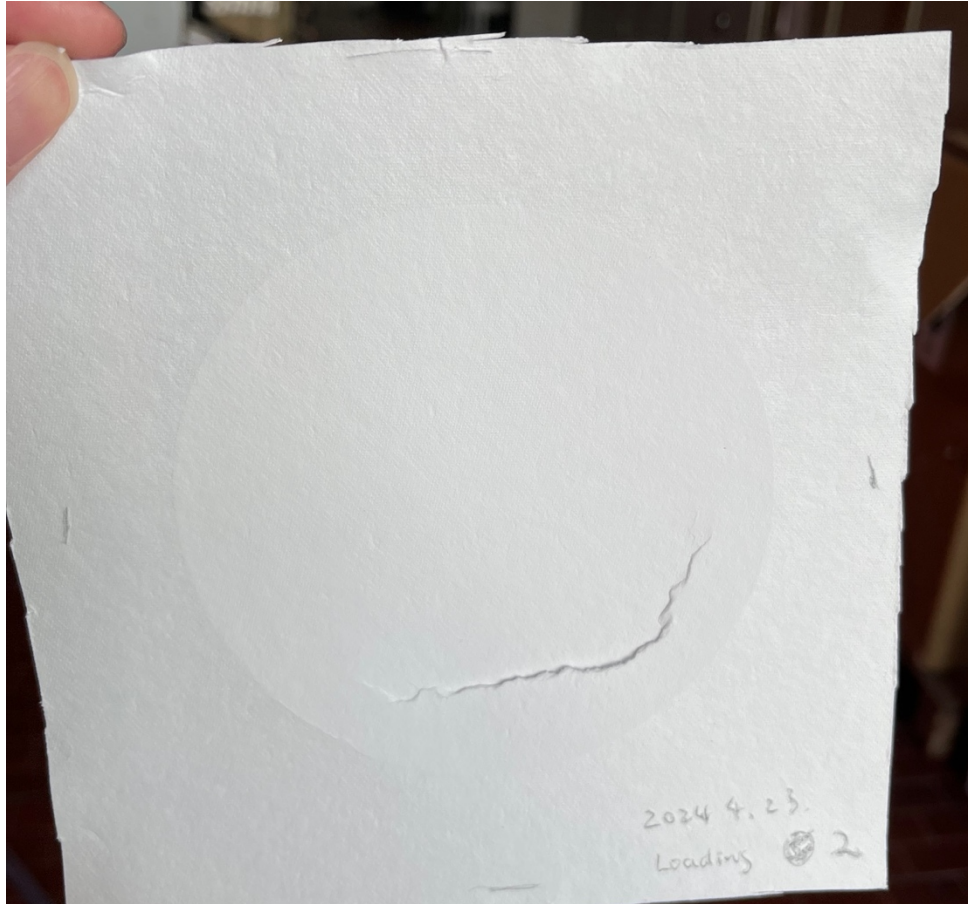


Figure 99 Loaded FCR media sample

As conclusion of loading test part, surface loading probably plays crucial role on predicting filter clogging. From loading curves tested of two media, it is noted that in depth loading regime, pressure drops increase relatively slowly, and duration of this phase is relatively short. But still, it cannot conclude that depth loading is not important for predict overall loading phase because varies type of media behaves differently, and it additively affects final pressure drop of loading process. It is necessary to do same loading tests on nanofiber media, to know exactly how media clogged by ultrafine particles on both loading regimes.

From another aspect, initial penetration of standard media and nanofiber samples are close, thus depth loading for latter is reasonably considered similar as tested results. And knowing relationship between pressure increase and loaded mass on surface loading under specific experimental condition, allows predicting loading behavior of nanofiber samples in approximated way.



## 4.4 Filter media tested with RH controlled

### 4.41 Characterization of clean Ahlstrom media

Air resistance tests and fractional efficiency tests are done on 3 samples of Ahlstrom media prepared with 160mm perforated plates at targeted temperature and RH. Test of air resistance is done on test rig and TEXTEST for comparison.

#### 1) Air resistance

Sample	TEXTTEST	Test rig
1	105 Pa	155 Pa
2	110 Pa	160 Pa
3	109 Pa	160 Pa

Table 19 Air resistances of 3 sample of clean Ahlstrom media tested on test rig and TEXTTEST

The results in Table 19 shows different accuracy of pressure reading of test rig and TEXTTEST, but precision is same. The overpressure inside test ducts is set at 50Pa, same as setting for efficiency test.

#### 2) Fractional efficiency

The test procedure is same as described previously using first test rig except for RH controlled at 42.5% and at controlled temperature at 23°C. The results are represented in Figure 100. After efficiency test, the pressure drop of 3 samples increases 3 Pa means that loading effect is presenting for solid particles but is negligible for limited time.

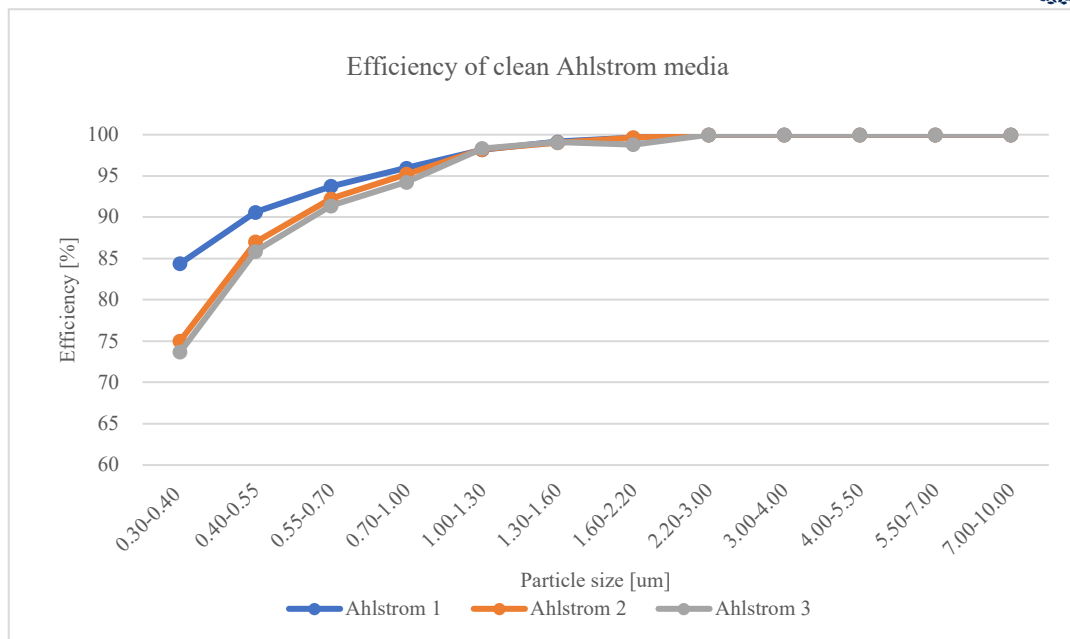


Figure 100 Clean Ahlstrom media efficiency

## 4.42 Parameter tuning for neutralization

The correlation ratio assessment is done before each test for avoiding anomalies when operates neutralizer. The correlation ratio results similarly for each voltage level.

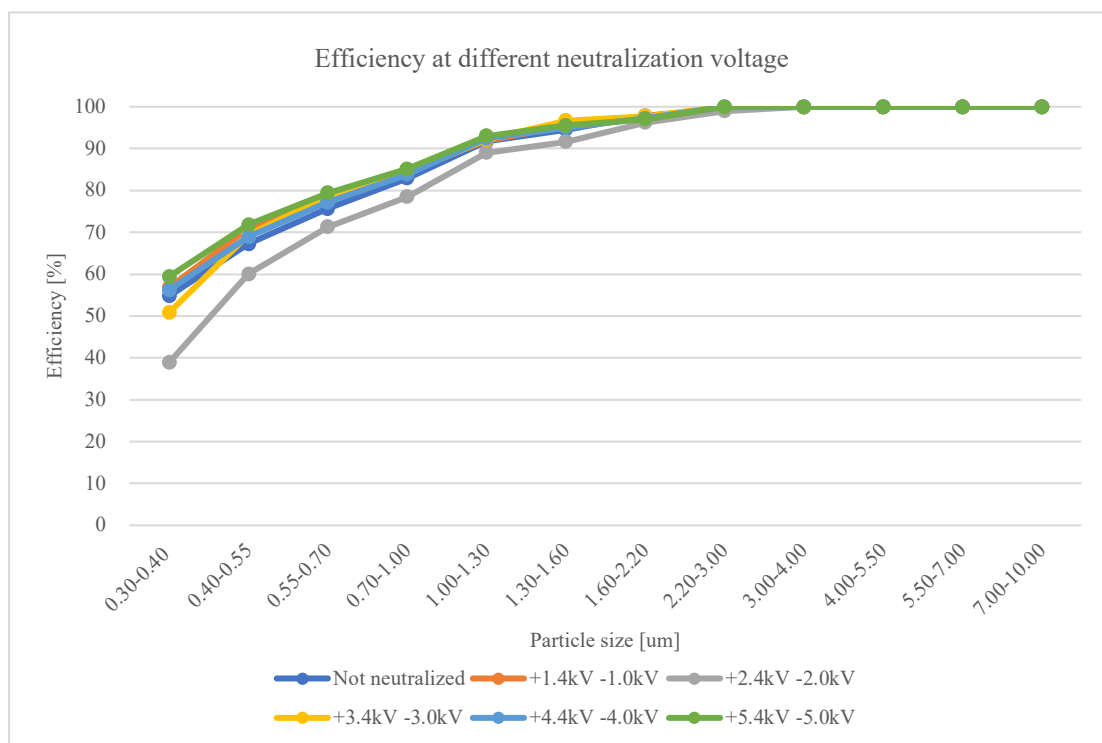


Figure 101 Efficiency for each voltage level of neutralizer



The results in Figure 101 shows minimum efficiency is reached when set point of voltage in neutralizer is +2.4kV -2.0kV, which means that particles are discharged. Fractional efficiencies in all size range are firstly decreasing as increases of voltage from 0kV to 2kV, then decreasing as voltage increases from 3kV to 5kV. Except for minimum efficiencies at +2.4kV -2.0kV, other efficiencies are quite close to not neutralized case, which means that if particles charge distribution are not neutralized, electrostatic force will have similar effect on particle removal efficiency regardless the charge state of particles.

Those parameters could be useful for further study of loading behavior of filter media at same air condition for minimizing electrostatic effect, so that RH can be controlled as single variable.



## 5. Conclusion

Designing new fibrous media for providing better engineering solution on air filtration, it would aspect that improving of filtration efficiency is advantageous for less increases on pressure drop across the filter media. Theoretically air resistance of nanofiber media can take advantage of slip effect as fiber diameters decreases, because that large Knudsen number would result lower pressure drop increases due to finer fibers. In this case of study, fiber diameters of tested nanofiber samples are within range from  $200\mu m$  to  $400\mu m$ , through calculation using two analytical models, one considering slip effect while another not. Predicted pressure drop at different filtration velocities are similar in both cases, however considering slip effect results slightly higher pressure drops in this fiber diameter range if compare calculation results of two models.

In experimental tests regarding air resistance of nanofiber media samples, pressure drops are tested much lower than analytical prediction. The differences might be caused by considering average fiber diameters and solidities of samples instead of a distribution of such parameters, the calculation accuracy could be improved on this aspect. Another reason could be spatial inhomogeneity of samples, or random orientation of fiber, which are out of theoretical assumption, and presents inherent difficulties for precise assessment. However, the difference resulting so large means that measurement of solidity and fiber diameter might not be accurate. Further studies could be focus on this aspect by apply peeling method indicated by ASTM standard to measure fiber characteristics layer wise, instead of measuring those parameters only in first layer.

For particle removal efficiency of tested samples, test results are also influenced by spatial inhomogeneity and fiber orientation of sample media. This could be an explanation to the differences observed when comparing first test results of OPS3330 with that of LAS 3340A, because that sample area of media could be displaced between two set of tests. Maintaining same position and test samples again with OPS3330, those differences are corrected.

MPPS of tested samples are out of range of detection using OPS3330, thus smaller than  $0.3\mu m$ . LAS 3340A is mandatory for studying MPPS and minimum efficiency of nanofiber samples. Analytical calculations are performed to calculate MPPS and minimum efficiency using measured fiber diameters and solidities of samples. Again, differences between experimental results and analytical solution are high.

For more comprehensive view of quality of nanofiber media, quality factors are computed considering both air resistances and minimum efficiencies of nanofiber samples, for experimental results and analytical solutions. Analytical quality factors of tested nanofiber samples are close for each type of samples. Instead, experimental quality factors showing larger differences between types of samples. PANCO15CNC showing highest quality factor which is 3 times higher than lowest quality factors of PAN and PANCO. Overall analytical solutions predict quality factors in the same scale of experimental results, by overestimating air



resistances and efficiency. So, the errors are more likely related to inaccuracy of measurements of fiber diameters and solidities.

Loading tests are performed with masks test machine, the approach for penetration reading using photometers is fast, but gravimetric tests are required to know the mass concentration of upstream particles. Besides, precisely knowing particle size distribution charging filter media is essential to have meaningful test results. SMPS reveals stable production of aerosol particles, count median diameters of produced particle size distribution along tests are checked within range indicated by standard. Instead, geometric standard deviation over the upper threshold indicated by standard during test, this might be caused by consumption of solution. To reduce this effect, salt solution should be strictly handled according to user manual, and constantly maintenance on aerosol generator is needed.

As results of loading test, although tests are not done with nanofiber samples directly, tested standard media which have comparable penetration value at ultrafine particle size range to nanofiber samples, this could lead to similar behaviors of depth loading phase. And surface loading phase is only influenced by particle properties and environmental conditions. Overall, similar pressure drop increase as function of loaded mass might be predictable for nanofiber samples using available test results and obtained linear relationship of surface loading behavior. For acceptable accuracy of prediction, much more experiments on different type of media is needed.

Further study for loading test could be study loading behavior of various type of filter media using test rig with RH control. At different RH, the loading behaviors can be correlated providing broader insight regarding loading process of filter media.



## References

- [1] D. E. Schraufnagel, “The health effects of ultrafine particles,” *Experimental and Molecular Medicine*, vol. 52, no. 3. 2020. doi: 10.1038/s12276-020-0403-3.
- [2] C. Chen, B. Zhao, W. Zhou, X. Jiang, and Z. Tan, “A methodology for predicting particle penetration factor through cracks of windows and doors for actual engineering application,” *Build Environ*, vol. 47, no. 1, pp. 339–348, Jan. 2012, doi: 10.1016/J.BUILDENV.2011.07.004.
- [3] C. Chen, B. Zhao, and X. Yang, “Preventing the entry of outdoor particles with the indoor positive pressure control method: Analysis of influencing factors and cost,” *Build Environ*, vol. 46, no. 5, pp. 1167–1173, May 2011, doi: 10.1016/J.BUILDENV.2010.12.003.
- [4] L. Morawska *et al.*, “Airborne particles in indoor environment of homes, schools, offices and aged care facilities: The main routes of exposure,” *Environ Int*, vol. 108, pp. 75–83, Nov. 2017, doi: 10.1016/J.ENVINT.2017.07.025.
- [5] WHO, “WHO global air quality guidelines 2021,” 2021.
- [6] W. C. Hinds, *Aerosol technology: properties, behaviour, and measurement of airborne particles.*, 2nd ed. WILEY INTERSCIENCE, 1999.
- [7] ASHARE 52.2, “Method of Testing General Ventilation Air-Cleaning Devices for Removal Efficiency by Particle Size,” 2017, [Online]. Available: [www.ashrae.org/technology](http://www.ashrae.org/technology). Accessed: 2024.05.01
- [8] ISO EN, “ISO EN 16890-1:2016 ‘Air filters for general ventilation — Part 1: Technical specifications, requirements and classification system based upon particulate matter efficiency (ePM).’” 2016.
- [9] ISO EN, “ISO EN 16890-2:2016 ‘Air filters for general ventilation — Part 2: Measurement of fractional efficiency and air flow resistance.’” 2016.
- [10] Office of the Federal Register, “N. A. and R. A. 40 CFR Appendix J to Part 50 - Reference Method for the Determination of Particulate Matter as PM10 in the Atmosphere. Govinfo.Gov 73–78 (1999)”.
- [11] Office of the Federal Register, “N. A. and R. A. 40 CFR Appendix L to Part 50 - Reference Method for the Determination of Fine Particulate Matter as PM2.5 in the Atmosphere (2001)”.
- [12] Office of the Federal Register, “ENVIRONMENTAL PROTECTION AGENCY 40 CFR Parts 53 and 58 Revised Requirements for Designation of Reference and



- Equivalent Methods for PM<sub>2.5</sub> and Ambient Air Quality Surveillance for Particulate Matter.”
- [13] P. Tronville, V. Gentile, and J. Marval, “Guidelines for measuring and reporting particle removal efficiency in fibrous media,” *Nature Communications*, vol. 14, no. 1. Nature Research, Dec. 01, 2023. doi: 10.1038/s41467-023-41154-4.
- [14] TSI, “OPTICAL PARTICLE SIZER SPECTROMETER MODEL 3330 OPERATION AND SERVICE MANUAL P/N 6004403, REVISION G,” 2016.
- [15] L. Edelman, “Air filtration: Air filter media - an industry evolves,” *Filtration and Separation*, vol. 45, no. 9, pp. 24–26, Nov. 2008, doi: 10.1016/S0015-1882(08)70368-9.
- [16] “Introduction and fiber-processing methods.” [Online]. Available: <http://ebookcentral.proquest.com/lib/polito-ebooks/detail.action?docID=4459584>. Accessed: 2024.05.09
- [17] “2 Nanofibers 2.1 Benefits of nanofibers.” [Online]. Available: <http://ebookcentral.proquest.com/lib/polito-ebooks/detail.action?docID=4459584>. Accessed: 2024.05.09
- [18] “Introduction and fiber-processing methods.” [Online]. Available: <http://ebookcentral.proquest.com/lib/polito-ebooks/detail.action?docID=4459584>. Accessed: 2024.05.09
- [19] C.N. Davies, *Air Filtration*. London: Academic Press, 1973.
- [20] J. Wang and P. Tronville, “Toward standardized test methods to determine the effectiveness of filtration media against airborne nanoparticles,” *Journal of Nanoparticle Research*, vol. 16, no. 6, 2014, doi: 10.1007/s11051-014-2417-z.
- [21] R. C. Brown, *An Integrated Approach to the Theory and Applications of Fibrous Filters.*, Air Filtration. Pergamon, 1993.
- [22] K. W. Lee and B. Y. H. Liu, “On the Minimum Efficiency and the Most Penetrating Particle Size for Fibrous Filters,” *J Air Pollut Control Assoc*, vol. 30, no. 4, pp. 377–381, 1980, doi: 10.1080/00022470.1980.10464592.
- [23] K. W. Lee and B. Y. H. Liu, “Theoretical Study of Aerosol Filtration by Fibrous Filters,” *Aerosol Science and Technology*, vol. 1, no. 2, pp. 147–161, Jan. 1982, doi: 10.1080/02786828208958584.
- [24] G. Kasper, S. Schollmeier, and J. Meyer, “Structure and density of deposits formed on filter fibers by inertial particle deposition and bounce,” *J Aerosol Sci*, vol. 41, no. 12, pp. 1167–1182, Dec. 2010, doi: 10.1016/J.JAEROSCI.2010.08.006.



- [25] C. Wang and Y. Otani, "Removal of Nanoparticles from Gas Streams by Fibrous Filters: A Review," *Ind Eng Chem Res*, vol. 52, no. 1, pp. 5–17, Jan. 2013, doi: 10.1021/ie300574m.
- [26] A. C. Payatakes and L. Gradoń, "Dendritic deposition of aerosol particles in fibrous media by inertial impaction and interception," *Chem Eng Sci*, vol. 35, no. 5, pp. 1083–1096, 1980, doi: 10.1016/0009-2509(80)85097-4.
- [27] D. A. Japuntich, "Clogging of fibrous filters with mono disperse aerosols," 1991.
- [28] G. Berry, I. Beckman, and H. Cho, "A comprehensive review of particle loading models of fibrous air filters," *Journal of Aerosol Science*, vol. 167. Elsevier Ltd, Jan. 01, 2023. doi: 10.1016/j.jaerosci.2022.106078.
- [29] TEXTTEST AG Switzerland, "FX 3300 LabAir IV working manual." [Online]. Available: [www.texttest.ch](http://www.texttest.ch) Accessed: 2024.03.23
- [30] TSI, "42 CFR PART 84 STANDARD." [Online]. Available: [www.tsi.com](http://www.tsi.com)
- [31] John H. Seinfeld and Spyros N.Pandis, *Atmospheric Chemistry and Physics: From Air Pollution to Climate Change*. John Wiley & Sons, 2012.
- [32] ISO EN, "ISO 16890-2 AIR FILTERS FOR GENERAL VENTILATION: DETERMINING FRACTIONAL EFFICIENCY," 2016. [Online]. Available: <https://vimeo.com/207607041>. Accessed: 2024.05.12
- [33] TSI, "LASER AEROSOL SPECTROMETER MODEL 3340A OPERATION AND SERVICE MANUAL."
- [34] ATI (Air Techniques International), "Laskin Nozzle Generators TDA-4B and TDA-4Blite Operation and Maintenance Manual."
- [35] TSI, "CERTITEST ® AUTOMATED FILTER TESTER MODEL 8130A." [Online]. Available: [www.tsi.com](http://www.tsi.com) Accessed: 2024.04.01
- [36] TSI, "CERTITEST ® AUTOMATED FILTER TESTER MODEL 8130A OPERATION AND SERVICE MANUAL P/N 6010824, REVISION A," 2017.
- [37] TSI, "ELECTROSTATIC CLASSIFIER MODEL 3082 SCANNING MOBILITY PARTICLE SIZER™ (SMPS™) SPECTROMETER MODEL 3938 OPERATION AND SERVICE MANUAL P/N 6006760, REVISION C," 2016.